

ORIGIN AND METAMORPHISM OF PART OF THE
HERMON GROUP NEAR BANCROFT, ONTARIO

ORIGIN AND METAMORPHISM OF PART OF THE
HERMON GROUP NEAR BANCROFT, ONTARIO

By

David S. Jennings, B. A.

A Thesis

Submitted to the School of Graduate Studies

in Partial Fulfilment of the Requirements

for the Degree

Doctor of Philosophy

McMaster University

November, 1969

DOCTOR OF PHILOSOPHY (1969)
(Geology)

McMaster University,
Hamilton, Ontario.

TITLE: Origin and Metamorphism of Part of the Hermon Group Near
Bancroft, Ontario

AUTHOR: David S. Jennings, B. A. (Lehigh University)

SUPERVISOR: Professor Denis M. Shaw

NUMBER OF PAGES: xv, 225.

SCOPE AND CONTENTS:

A detailed geological and petrochemical study of an upper amphibolite grade, "Grenville Series" sequence is presented. Integrated structural, stratigraphic and geochemical data have led to the conclusion that this sequence accumulated as an interbanded volcanic and sedimentary prism either in an Upper Proterozoic geosyncline or volcanotectonic depression.

Metamorphic phase assemblages, in general, approach equilibrium. Assemblages showing disequilibrium, "frozen", reactions are discussed in detail. Experimental data on all the phase assemblages suggests the most probable range of metamorphic conditions to be 625° to 690° and 5.5 to 7 kilobars total pressure. The

effects of retrograde metamorphism on the prograde assemblages
are documented.

ABSTRACT

A 70 sq. mi. tract of upper amphibolite facies amphibolites, gneisses, leptites and marbles has been mapped in detail to establish an origin and model of accumulation for these rocks, as well as to document their metamorphic history as part of a progressive metamorphic sequence in the Bancroft-Madoc area of the Grenville Age Province in Ontario. Structural mapping has defined one period of prograde mineral growth contemporaneous with deformation. This deformational episode is thought to be older than the period 800-1,000 m. y. usually ascribed to the Grenville orogenic event.

Stratigraphic relations and whole rock analytical data have shown the amphibolites, gneisses and leptites to have been derived from basaltic flows, pelitic sediments interbanded with intermediate tuffaceous rocks, and arkosic clastic debris. These units may have been deposited either in an Upper Proterozoic geosyncline of broad regional extent or in a more local volcano-tectonic depression. Rocks of the map area accumulated near a structural high within or marginal to this basin of deposition.

Prograde metamorphism in the study area is of upper amphibolite facies rank. Application of data on synthetic systems implies a range in metamorphic conditions from 625° to 690°C and 5.5 to 7 kilobars total pressure. Several staurolite decomposition equilibria are considered in detail as is the decomposition of muscovite in the presence of quartz. Different calc-silicate reactions occurring in adjacent compositional bands in the same outcrop shed light on the roles of fluid phase compositions and partial fluid pressures on carbonate equilibria. Coexisting calcite-dolomite pairs are used to estimate minimal temperatures of metamorphism. A host of reactions are written to describe the effects of a pervasive, greenschist, retrograde metamorphism on each major rock type. The cause and extent of this event are, at present, uncertain.

ACKNOWLEDGEMENTS

Sincere thanks for his supervision, continued interest and critical audience through all stages of this study are extended to Denis Shaw. I am indebted (perhaps to an unknown extent) to my wife, Alice, for her prowess as a draftsman, rock crusher, clerk, cartographer, bull cook and part-time field assistant. Without her help in these many capacities, this study would have been interminable.

My supervisory committee members, Drs. H. P. Schwarcz, R. H. McNutt, G. R. Purdy and W. B. Clarke proffered much welcome advice. Thanks are given to Len and Don Falkiner for thin section preparation, Frank Tebay for X-ray diffraction assistance, Kenneth Ramlal for the new silicate analyses in this thesis and to John Muysson for his instruction in atomic absorption techniques. Frances Campbell, Dianne Jordan and Paul Fletcher performed most of the spectrographic work. Able field assistance was provided by Gobi Grossman and Mati Raudsepp. Ian Mason generously made available sundry norm programs. Dr. D. F. Hewitt of the Ontario Department of Mines

made his air photos of the study area available. Jack Whorwood provided much needed photographic counsel and Joyce Barrett kindly typed the manuscript. Discussions with many graduate students too numerous to name individually, resulted in many refinements of the ideas presented as well as refinements in my dart game. To all these persons, I am grateful.

For financial support of this study, I would like to acknowledge the National Research Council and various departmental grants. Finally, I wish to thank the reader for his tolerance of these overlong platitudes.

TABLE OF CONTENTS (continued)	Page
5.2 Quartzo-Feldspathic Gneisses	79
5.3 Leptites	99
5.4 Conclusions	110
6. METAMORPHISM	112
6.1 Regional Metamorphism in the Bancroft-Madoc Area	112
6.2 Metamorphism in the Mapped Area	118
6.2.1 Prograde Metamorphism	118
Amphibolites	118
Quartzo-Feldspathic Gneisses	127
Leptites	153
Carbonate Metasediments	157
6.2.2 Retrograde Metamorphism	175
Amphibolites	175
Quartzo-Feldspathic Gneisses	181
Leptites	182
Carbonate Metasediments	188
Interpretation	188
6.2.3 Summary	192
7. TECTONIC SYNTHESIS	194
7.1 Tectonic History of the Bancroft-Madoc Area	194
7.2 Tectonic History of Mapped Area	197
BIBLIOGRAPHY	204
APPENDIX	
1. ANALYTICAL METHODS	220

LIST OF TABLES

	Page
5.1 Compositions of amphibolites, basalts and possible amphibolite protoliths	46-48
5.2 Compositions of average continental crust, average graywacke, average granite and calculated anatectic residua	59-60
5.3 Whole rock analyses, norms, modes, and calculated data for the Hermon Group amphibolites	65-70
5.4 Element ratios and trace element abundance data for various rock types and the Hermon Group amphibolites	76
5.5 Analyses, norms, modes and calculated data for the Hermon Group quartzo-feldspathic gneisses	81-86
5.6 Average compositions of the various quartzo-feldspathic gneiss types and compositionally similar rocks	90-91
5.7 Element ratios for various rock types including the Hermon Group quartzo-feldspathic gneisses	97
5.8 Analyses, norms, modes and calculated data for Hermon Group leptites	103-105
5.9 Composition of leptites and possible leptite protoliths	106
5.10 Trace element ratios for various rock types including the Hermon Group leptites	109
6.1 Amphibolite phase assemblages	121
6.2 Phase assemblages in quartzo-feldspathic gneiss	129-131
6.3 Leptite phase assemblages	155
6.4 Partial analyses of Mg-calcites	161

LIST OF TABLES	Page
6.5 Calc-silicate phase assemblages	165
6.6 Retrograde reactions in amphibolite	177-178
6.7 Retrograde reactions in sub-aluminous and aluminous gneisses	183
6.8 Retrograde reactions in the hornblende and clinopyroxene gneisses	185
6.9 Retrograde reactions in leptites	186

LIST OF FIGURES

	Page
1.1 Remnant superficial rocks in the Grenville Province	2
1.2 Location of study area	4
2.1 Lithologic maps; A, general; B, outcrops	in pocket
2.2 Quartz-sillimanite-plagioclase-muscovite nodules in Silent Lake granite	15
2.3 Foliated, quartz-sillimanite-plagioclase-muscovite veins in Silent Lake granite	15
2.4 Boudinaged quartz-sillimanite-plagioclase-muscovite vein in Silent Lake granite	17
2.5 Boudinage structure in Silent Lake granite	17
2.6 Nodular feldspathic gneiss pod	19
3.2 Hypothetical relationship of the Mayo and Hermon Groups	22
3.3 Calcic inclusions in amphibolite	31
3.4 Boudinage of calcareous interband in amphibolite	31
4.1 Style of mesoscopic folds in Sg	36
4.2 Structural compilation map	in pocket
4.3 Petrofabrics diagrams	in pocket
4.4 Foliation and cross section map of Silent Lake stock	39
5.1 Total iron versus K_2O for various rock types	53
5.2 Moine-de la Roche projection of various rock types	55
5.3 Sample location map	in pocket

LIST OF FIGURES (continued)	Page
5.4 Norms of basalts and amphibolites projected onto base of haplobasalt tetrahedron	71
5.5 Modified K�hler-Raaz diagram showing compositional fields for igneous rocks and the analysed Hermon rocks	73
5.6 Modified K�hler-Raaz diagram showing compositional fields for sedimentary rocks and the analysed Hermon rocks	74
5.7 Potassium-rubidium covariance in the Hermon Group amphibolites	78
5.8 Exploded normative tetrahedron showing compositional relations between Hermon Group quartzo-feldspathic gneisses and various common rocks	87
5.9 Normative tetrahedron showing compositional fields of quartzo-feldspathic gneisses	88
5.10 Moine-de la Roche projection of average compositions of quartzo-feldspathic gneiss varieties and leptites showing similarities to common rocks	92
5.11 Haplogranite system showing normative plots of Hermon Group leptites and extrusive igneous rocks	108
6.1 Approximate disposition of regional metamorphic isograds in the Bancroft-Madoc area	114
6.2 ACKF diagrams for amphibolites	122
6.3 Hornblende-cummingtonite textures	125
6.4 Hornblende-cummingtonite exsolution relations	126
6.5 Compositional quadrilateral showing extent of miscibility gap between calcic and Mg-Fe clinoamphiboles	126

LIST OF FIGURES (continued)	Page
6. 6 ACKF and AFM diagrams for quartzo-feldspathic gneisses	132
6. 7 Staurolite and quartz relicts in plagioclase and cordierite	137
6. 8 Fibrolitic sillimanite intergrown with biotite	139
6. 9 AKFM diagram for assemblage (2)	139
6. 10 Texturally zoned garnet	141
6. 11 Two generations of biotite in staurolite-bearing gneiss	141
6. 12 AKFM diagram for assemblage (3)	142
6. 13 Garnet rimmed by and intergrown with fibrolitic sillimanite	142
6. 14 AKFM diagram for assemblage (4)	144
6. 15 AKFM diagram for assemblage (5)	144
6. 16 Staurolite stability relations	148
6. 17 Metamorphic grid for the study area	151
6. 18 ACKF diagram for leptites	156
6. 19 Location of analysed Mg-Calcites	158
6. 20 Dolomite exsolution lamellae in Mg-Calcite	159
6. 21 The Mg-calcite solvus limb expressed as the function $\log \text{MgCO}_3 = 1.75 \times 10^{-3} T^{\circ}\text{C} - 0.223$	162
6. 22 Calc-silicate phase relations in CaO-MgO-SiO_2 space	166
6. 23 Calc-silicate reaction textures	169
6. 24 Calc-silicate reaction textures	170

LIST OF FIGURES (continued)	Page
6.25 Textural relations for assemblages in the same outcrop	171
6.26 Schematic topology of calc-silicate equilibria in T-X space	173
6.27 Schematic topology of reactions in PT space	174
6.28 Hornblende altering to chlorite	179
6.29 Textures supporting reaction 3 of Table 6.6	179
6.30 Microfractured section showing development of retro- grade hornblende	180
6.31 Biotite breaking down to chlorite	184
6.32 Biotite reacting to muscovite and biotite	184
6.33 Chlorite and muscovite forming at the expense of biotite	187
6.34 Recrystallization of biotite and muscovite	187
6.35 Schematic topology of a generalized retrograde reaction	190
7.1 Summary of tectonic events in Bancroft-Madoc area	196
7.2 Cross section showing inferred, original stratigraphic relations in Bancroft-Madoc area	200
7.3 Summary of tectonic events in map area	203

1. INTRODUCTION

1.1. Purpose of Study

Ever since the initial studies and definition of the Grenville Series by Sir William Logan, the origin and geologic history of this complex lithologic sequence has been of utmost interest to students of the Grenville Age Province. Detailed field and geochronologic studies undertaken largely over the last 60 years have served to more rigidly define the Grenville Series of Logan as a series of volcano-sedimentary remnants probably of Upper Proterozoic age unconformably overlying an older granitic basement in turn being invaded by younger plutonic masses. The disposition of these remnants throughout the exposed portion of the Grenville Age Province is shown in Figure 1.1. One of the largest and perhaps best known of these remnants is the Ottawa River Remnant (Lumbers, 1967a) of which the present study area is a small part.

Study of this particular remnant has been facilitated by its easy accessibility, economic potential and wide range of metamorphic conditions throughout a wide spectrum of rock types. It is the only remnant studied thus far which displays metamorphic zoning from the

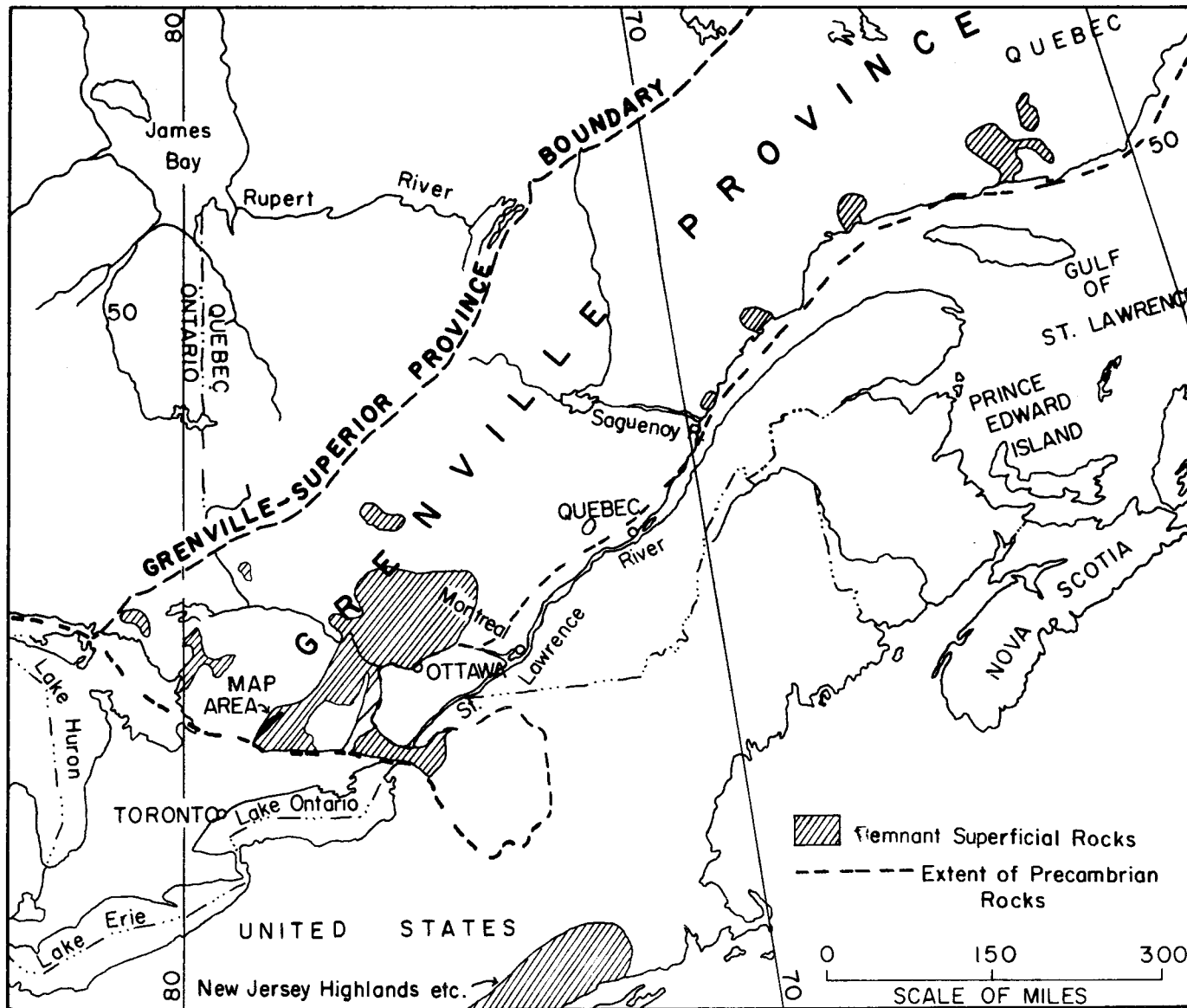


Figure 1.1: Remnant Superficial Rocks in the Grenville Age Province

greenschist to granulite facies of regional metamorphism in a stratigraphic sequence characterized by abundant metasedimentary carbonate rocks. By virtue of its extreme lithologic and metamorphic variability, this remnant affords a unique opportunity to study a nearly unmetamorphosed superficial sequence and its changes with progressive metamorphism.

With these features in mind, a belt of upper amphibolite facies rocks of basic, intermediate and acidic character was selected to study the origin, metamorphism and tectonic history of part of this remnant. The belt chosen straddles the junction of Peterborough, Haliburton and Hastings counties in the townships of Anstruther, Chandos, Cardiff and Faraday southwest of the village of Bancroft, Ontario (Figure 1.2).

1.2. Previous Work

Much of the study area has been mapped previously by the Ontario Department of Mines (Hewitt, 1959 and Shaw, 1962) and by the Geological Survey of Canada (Adams and Barlow, 1910). The small scale mapping of Adams and Barlow (1910) pointed out the variety of supracrustal rock types present in the map area and the salient features of the plutonic rocks intrusive into them. However, neither their work

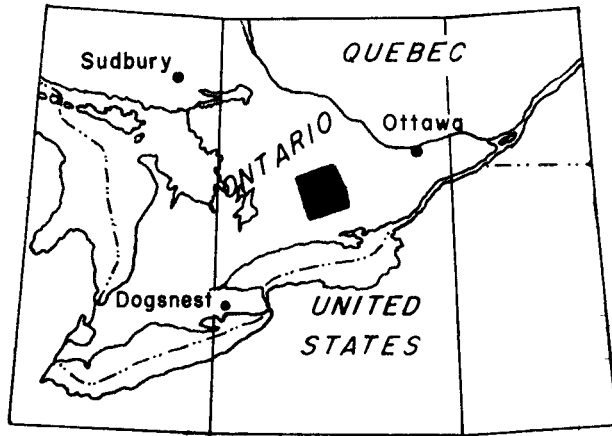
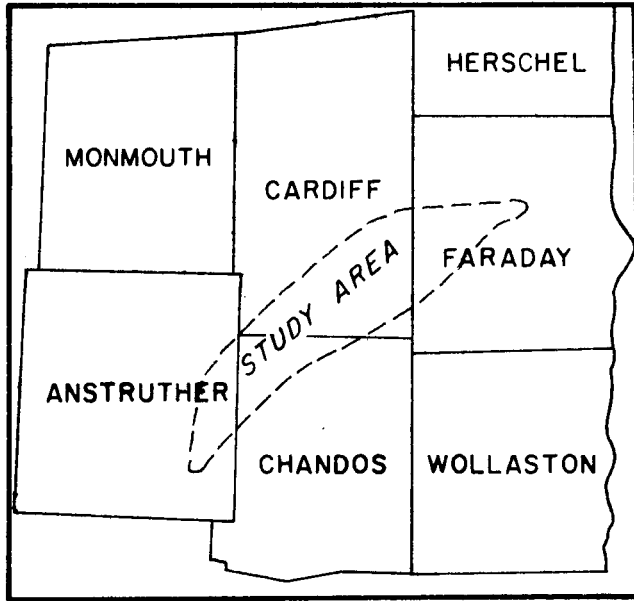


Figure 1.2 Location of Study Area

nor the mapping of Hewitt (1959) in Cardiff and Faraday townships proved sufficiently detailed to delimit a coherent stratigraphy throughout the entire study area. A mappable stratigraphy was found by Shaw (1962) in northwestern Chandos township which formed the basis for further mapping in Anstruther, Cardiff and Faraday townships.

Various compilations of the geology of the Bancroft-Madoc area have included the study area in whole or in part. Among these are the extensive works of Lurnbers (1964, 1967a) and an earlier compilation by Hewitt and Satterly (1957). Samples of amphibolite units in northwestern Chandos township have been analysed and discussed by Kudo (1962) and van de Kamp (1964). Amphibolite samples from the map area as a whole form part of a discussion of amphibolite origins in the Bancroft-Madoc area (van de Kamp, 1968). Krogh (1964) has sampled and dated the Anstruther-Burleigh batholith which forms the southern margin of the map area by Rb-Sr whole rock methods.

1.3. Methods of Investigation

The study area in Anstruther, Cardiff and Faraday townships was mapped by pace and compass methods at a scale of 4 inches to 1 mile with appropriate overlap into Chandos township mapped earlier by Shaw (1962). Representative samples of all lithologic units

were collected from this 70 square mile area where exposure allowed. A grid system of sampling was not feasible in the area because of inadequate exposure. Specimens showing the largest number of phases in an assemblage were also taken in the belief that they contained the most information on the metamorphic history of the area. These specimens as well as those showing compositional banding on a centimeter scale were chosen to augment the representative collections for petrographic study. From this suite of samples over 400 stained thin sections and 25 polished thin sections were studied in an effort to document the metamorphic history of the area. Whole rock analysis of 35 representative samples for both major and minor elements was undertaken to establish a mode of origin for each common, supracrustal rock type in the map area.

2. GENERAL GEOLOGY OF THE MAPPED AREA

For convenience, the general geology of the study area will be discussed in two parts. Rocks of the supracrustal sequence will be described first, followed by a discussion of igneous rocks intrusive into them. To avoid confusion, the term "supracrustal" is applied to metamorphic rocks of metasedimentary or metavolcanic origin which comprise the bulk of the Ottawa River Remnant.

2.1. Supracrustal Rocks

Four lithologies comprise the supracrustal sequence in the study area, amphibolite, quartzo-feldspathic gneiss, leptite and marble. The distribution of these rock types is shown on the lithologic map of the area (Figure 2.1 in pocket).

2.1.1. Amphibolites

Amphibolite, the most abundant rock type, forms thick map units which extend across the length of the map area. These units are essentially massive, dark grayish green hornblende-plagioclase rocks showing only minor compositional banding and limited interbanding with other lithologies. The thick amphibolite unit nearest the northwestern

margin of the map area shows the best examples of compositional banding. In exposures along Highway 28, this banding, usually in excess of several tens of centimeters, is seen to result from slightly variable proportions of predominantly hornblende, plagioclase, epidote and clinopyroxene. This banding is not a pronounced feature and bears no resemblance to rocks like the Connemara "striped" amphibolites (Evans and Leake, 1960).

Northwest of the shear zone cutting this amphibolite, calc-silicate and gneissic rocks become more abundant as interbands in this amphibolite. It is possible that the amphibolite horizons on either side of this shear zone are unrelated. The other major amphibolite unit near the southeastern margin of the map area is more homogeneous and is remarkably massive. This unit sometimes shows abundant sulfide segregations and generally shows more epidote-clinopyroxene-plagioclase pods than the previous unit. These pods can be interpreted either as volcanic fragmentals or as boudins of competent calcic interbands and will be discussed more fully in Chapter 3.

Thin amphibolite or mafic gneiss units are often found in outcrops of quartzo-feldspathic gneiss and marble. When interbanded with gneiss, they commonly show complex phase assemblages often including clinopyroxene and K-feldspar in addition to the necessary hornblende and plagioclase. Their occurrence as thin interlayers in

gneiss with distinctly different phase assemblages serves to distinguish them from the thicker, more massive amphibolite units described above. This distinction is heightened by the analytical data presented in Chapter 5. Thin amphibolite layers in the marbles of the study area are often termed "feather amphibolites" because of the deliquescent arrangement of poikiloblastic crystals of hornblende in the plane of gneissosity (Adams and Barlow, 1910; Shaw, 1962 and van de Kamp, 1968). Particularly good examples of this variety of amphibolite can be found in the marbles immediately adjacent to the southeastern margin of the Tallan Lake Sill in Anstruther and Chandos townships (Figure 2.1).

2.1.2. Quartzo-Feldspathic Gneisses

Fine to medium grained gray gneisses are quantitatively the next most important supracrustal rock type found in the map area. The majority of these gneisses occur in close association with leptyte in a thick horizon through the central portion of this area. Pods or lenses of gneiss in amphibolite are fairly common, however. The mineralogical and chemical variability of these gneisses is extreme as will become apparent later (Chapters 5 and 6), yet the majority retain the appearance and field characteristics of typical Grenville "paragneisses" (Engel and Engel, 1953, 1958; Buddington and Leonard, 1962 and Chesworth, 1967). The term "quartzo-feldspathic gneiss" is

purely descriptive covering a wide variety of gneissic types. Its utility as a field term is retained throughout the text.

Compositional banding is prevalent within these rocks commonly extending to the thin section level. Very few examples of relict sedimentary structures have been found in the course of mapping. The few, known instances of graded bedding and cross stratification will be treated in subsequent sections.

The quartzo-feldspathic gneisses are not migmatized except in the immediate vicinity of granitic intrusives. Their banded character accentuates mesoscopic fold structures in gneissosity making such structures more easily recognizable in this rock type. It should be noted that only mesoscopic folds have been observed in the supracrustal rocks.

2.1.3. Leptites

Leptite, as used in the present investigation, connotes a pink, fine grained, quartz-feldspar-mica rock of granitic composition having a poorly developed tectonite fabric and an enigmatic origin. This definition is at odds with some commonly used (e. g. Magnusson, 1936, p. 334) but it provides a non-genetic, working description of one of the important rock units in the study area.

The close association of leptite and quartzo-feldspathic gneiss has been previously noted, but the details of this association

warrant further comment. In many parts of the map area, leptite is seen to grade laterally into quartzo-feldspathic gneiss parallel to gneissosity. This lateral interdigitation gives rise to wedgelike leptite outcrop patterns in map view (Figure 2.1).

Little direct evidence of the past history of the leptites is seen in the field. Only one occurrence of interbanded quartzite and leptite has been mapped in northwestern Chandos township. Because of this lack of genetic criteria and the generally granitic character of the leptites in outcrop, previous workers have incorrectly mapped the distribution of granite and leptite in the vicinity of granitic intrusives, particularly the Silent Lake stock (Adams and Barlow, 1910 and Hewitt, 1959).

2.1.4. Marbles

Both calcitic and dolomitic marbles are common to the carbonate envelope of the map area. These two varieties may occur as discreet lithologic horizons or as two carbonate marbles. Both types are white, medium to coarsely crystalline and frequently contain interbanded calc-silicate pods and bands. Calc-silicate units are particularly well developed in Anstruther township northwest of the Tallan Lake Sill. In this general region, several pods of very coarsely crystalline tremolite, or actinolite and diopside up to 10 feet by 30 feet

have been found. More commonly, the calc-silicates are found as thin interbands or as knots often weathered into relief above the surface of the dull white weathering marbles.

Excellent examples of feather amphibolite in these marbles are to be found in Anstruther, Chandos and Faraday townships along the southeastern margin of the map area. No examples of this rock type were noted in Cardiff township principally because of the generally poor exposure in the carbonate terrain. Curiously, feather amphibolites are nowhere found in the marbles bordering the map area on the northwest.

Carbonate mylonites are occasionally found in the Pratt's Creek shear zone in Chandos and Anstruther townships northwest of the Tallan Lake Sill. These strongly sheared rocks assume a fine grained, sugary texture and are commonly grey with strongly developed planar and linear fabric elements. Quartz "augen" are occasionally encountered in the mylonites.

2.2. Intrusive Rocks

Four igneous intrusives invade the supracrustal rocks in the study area. The main features of each body will be discussed in the following sections.

2.2.1. Anstruther-Burleigh Batholith

The Anstruther-Burleigh batholith, first named by Adams and Barlow (1910) during their classic investigations of the Haliburton-Bancroft area, extends nearly 25 miles from the Paleozoic cover in northern Smith township into the study area (Adams and Barlow, 1910). The generally fine grained, pink, granitic rocks of this large intrusive possess a characteristic, concentric, internal foliation defining a broad domal structure in, at least, the portion of the body in Anstruther township (Adams and Barlow, 1910). A variety of gneissic inclusions or xenoliths aligned parallel to this foliation are a further diagnostic feature of the pluton. Its concentric foliation and intrusive contacts with the surrounding country rocks attest to a magmatic origin, a conclusion reached earlier by Adams and Barlow (1910, pp. 78-87).

In figure 2.1, a migmatite zone is shown to envelope the granite. The outer limit of this zone marks the furthest recognizable extent of granitic activity in the supracrustal rocks. The boundary between it and the granite proper is rather arbitrary making the point at which granitic material prevails over xenoliths. Much of the migmatite zone is characterized by large, discordant, coarsely crystalline pegmatitic dikes in places producing very minor, coarsely crystalline hornblende-plagioclase-scapolite skarns in the host gneisses.

The margin of the main granitic body is bordered by a thin porphyritic halo up to 100 feet in thickness. In this halo, K-feldspar phenocrysts up to 3-5 cm. in length occur randomly oriented in a somewhat more coarsely crystalline matrix than commonly observed throughout the rest of the body. Within the main granitic mass, several graphic pegmatite dikes were encountered.

2.2.2. Silent Lake Granite

Originally named the Pine Lake granite by Adams and Barlow (1910) and renamed by Hewitt (1959) to accompany a change in the lake name, this fine grained, pink, biotite granite has been of interest since its initial mapping because of numerous horizons of quartz-sillimanite-plagioclase-muscovite nodules immersed within the granite. These nodules occur most commonly in varied sizes as isolated, elliptical nodules whose plane of elongation lies within the plane of penetrative foliation in the granite (Figure 2.2). In addition, zoned quartz-sillimanite-plagioclase-muscovite veins cut the granite and possess the same foliated character as the granite (Figure 2.3). Occasionally these veins are seen to be boudinaged into nodule trains with the original zonation of the veins preserved concentrically within the resultant nodules (Figure 2.4). Evidence that at least some of the nodules have formed by



Figure 2.2 Quartz-sillimanite-plagioclase-muscovite nodules lying within the plane of foliation in the Silent Lake granite. Scale is six inches in length. North shore of Silent Lake.

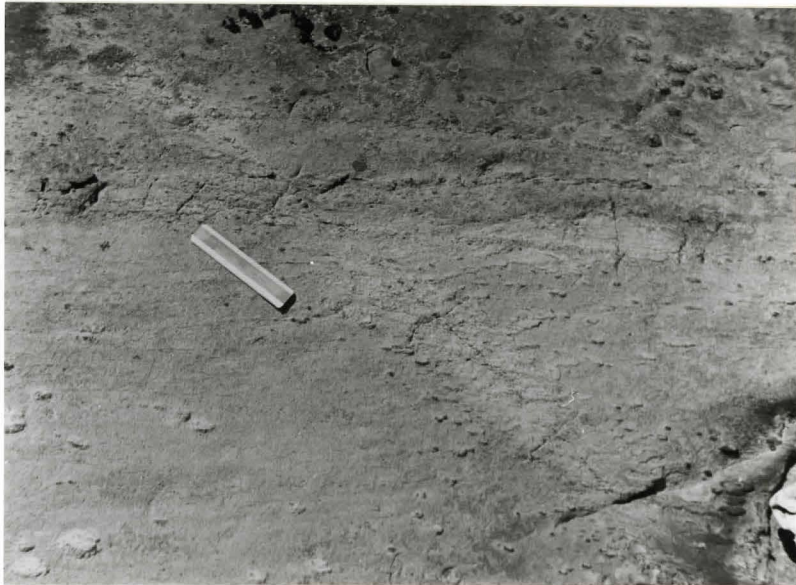


Figure 2.3 Foliated, quartz-sillimanite-plagioclase-muscovite veins cutting the Silent Lake granite. North shore of Silent Lake.

a boudinage mechanism is provided by the presence of boudinage structures in the absence of recognizable vein material (Figure 2.5). An exacting, descriptive account of the nodules and veins is given by Adams and Barlow (1910, pp. 127-139) to which the reader is referred for further details.

Utilizing the observations discussed above in conjunction with the structural data and interpretation of Chapter 4, a preliminary model for the formation of this enigmatic, nodular granite is tendered below. The concentrically developed magmatic flow foliation defining a doubly plunging, recumbent dome within the Silent Lake stock (see Chapter 4) represents the active plane of movement along and across which late stage quartz-sillimanite-plagioclase-muscovite veins were intruded and synchronously boudinaged into their present nodular form. The preferred long axis orientation of the nodules parallels mineral lineation and lies in the plane of foliation in a down-dip direction. Perhaps this linear fabric element defines the transport direction for the upward, diapiric movement of a granitic crystal mush responsible for boudinaging these apparently late stage veins. Veins which are foliated but not boudinaged may represent very late material crystallized out of a residual vapor phase just prior to the consolidation of and cessation of upward movement in the entire granitic mass. The lack of a well developed migmatite zone and the pronounced wrap of

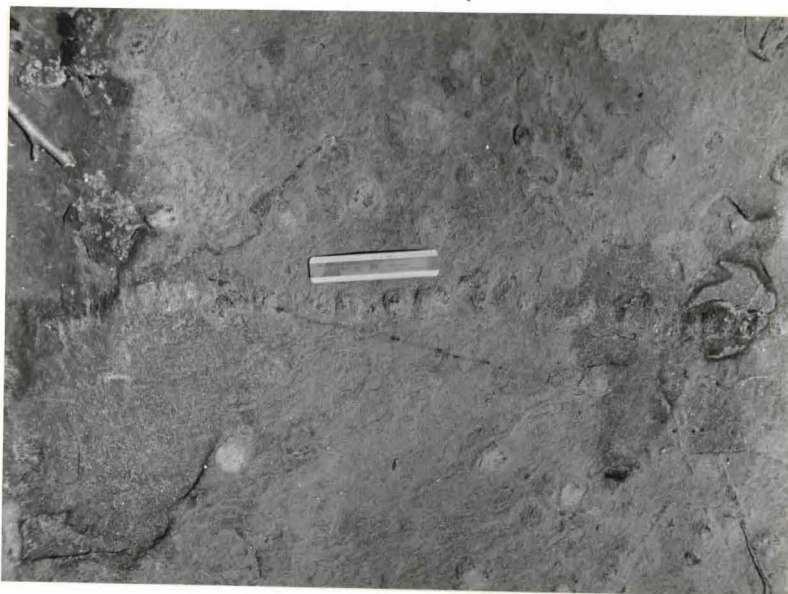


Figure 2.4 Boudinaged quartz-sillimanite-plagioclase-muscovite vein in granite. North shore of Silent Lake.



Figure 2.5 Boudinage structure in granite giving rise to elliptical nodules. Northern margin of Silent Lake stock.

gneissosity in the supracrustal rocks around the stock are compatible with a diapiric mode of intrusion (Figure 2.1).

A similar occurrence of nodules is found in a pegmatite envelope in quartzo-feldspathic gneiss approximately one half mile northeast of the Silent Lake stock (Figure 2.6). In this example a pod of feldspathic gneiss laden with quartz-sillimanite-plagioclase nodules forms the core of a pegmatitic pod which is flattened in the plane of foliation. The nodules are elongated parallel to mineral lineation in the enclosing gneiss but show no evidence of being produced by a boudinage mechanism.

2.2.3 Bow Lake Granite

Since this body has not been mapped in entirety in the present study, the ensuing discussion is in the nature of a reconnaissance. The bulk of the granitic rocks investigated are pegmatitic in character with the exception of minor fine grained patches toward the eastern margin. Isolated migmatitic exposures considerably removed from the main portion of the body imply a rather broad zone of migmatization associated with this intrusive. An interesting occurrence of skarn in a migmatized amphibolite and gneiss unit is found at the southern extremity of the body on Highway 28. Here, blue scapolite, pink potash feldspar, plagioclase, biotite and minor yellow calcite occur as dis-



Figure 2.6 Nodular feldspathic gneiss pod enclosed in pegmatite.
Approximately one half mile northeast of the Silent Lake
stock.

cordant veins and concordant bands in relation to foliation and gneissosity. Interpretation of geological relations in the vicinity of this body are considerably hampered by extensive sand plain cover.

2. 2. 4 Tallan Lake Sill

The outcrop pattern and structure of this metagabbro body have been delimited in Chandos township by Shaw (1962) and Adams and Barlow (1910). This study has mainly extended the outcrop limits of the sill into Anstruther, Cardiff and Faraday townships with little attention being paid to its detailed petrology. These extensions are in all respects similar to the occurrences in Chandos township in that they are fairly coarse grained, well foliated to massive metagabbros with some relict igneous textures in phase assemblages characteristic of the amphibolite facies. In Faraday township, and in scattered occurrences in Anstruther township, acidic horizons are found at the presumed base of the sill in accord with similar relations in Chandos township (Shaw, 1962). Occasionally these acidic rocks show pronounced sulfide mineralization. The sill is highly sheared by the Pratt's Creek shear zone at their mutual intersection near Highway 28.

3. STRATIGRAPHY

3.1. Stratigraphy of the Bancroft-Madoc Area

In order to interpret the stratigraphic relations within the mapped area, it is necessary to review the stratigraphy of the Hastings Lowlands on a regional scale. To date, the only comprehensive study of this nature is that of Lumbers (1967a). While reports of the Ontario Department of Mines on most of this broad area exist, more importance is attached to the integrated structural, stratigraphic and geochronologic interpretations of Lumbers. It should be noted that rock-stratigraphic relations will be emphasized due to the paucity of geochronologic data.

Lithologic units in the Hastings Lowlands in the Bancroft-Madoc area have been divided by Lumbers (1967a) into the Hermon and Mayo Groups encompassing the bulk of metavolcanic and metasedimentary rocks respectively. Each of these groups has been subdivided into several formations whose distinct lithologies allow them to be traced over considerable distances within the Lowlands (Figure 3.1, in pocket). A generalized, hypothetical, east-west cross section showing the relative age relations and depositions of these units is shown in Figure 3.2.

SECTION SHOWING HYPOTHETICAL RELATIONSHIP OF THE MAYO AND HERMON GROUPS

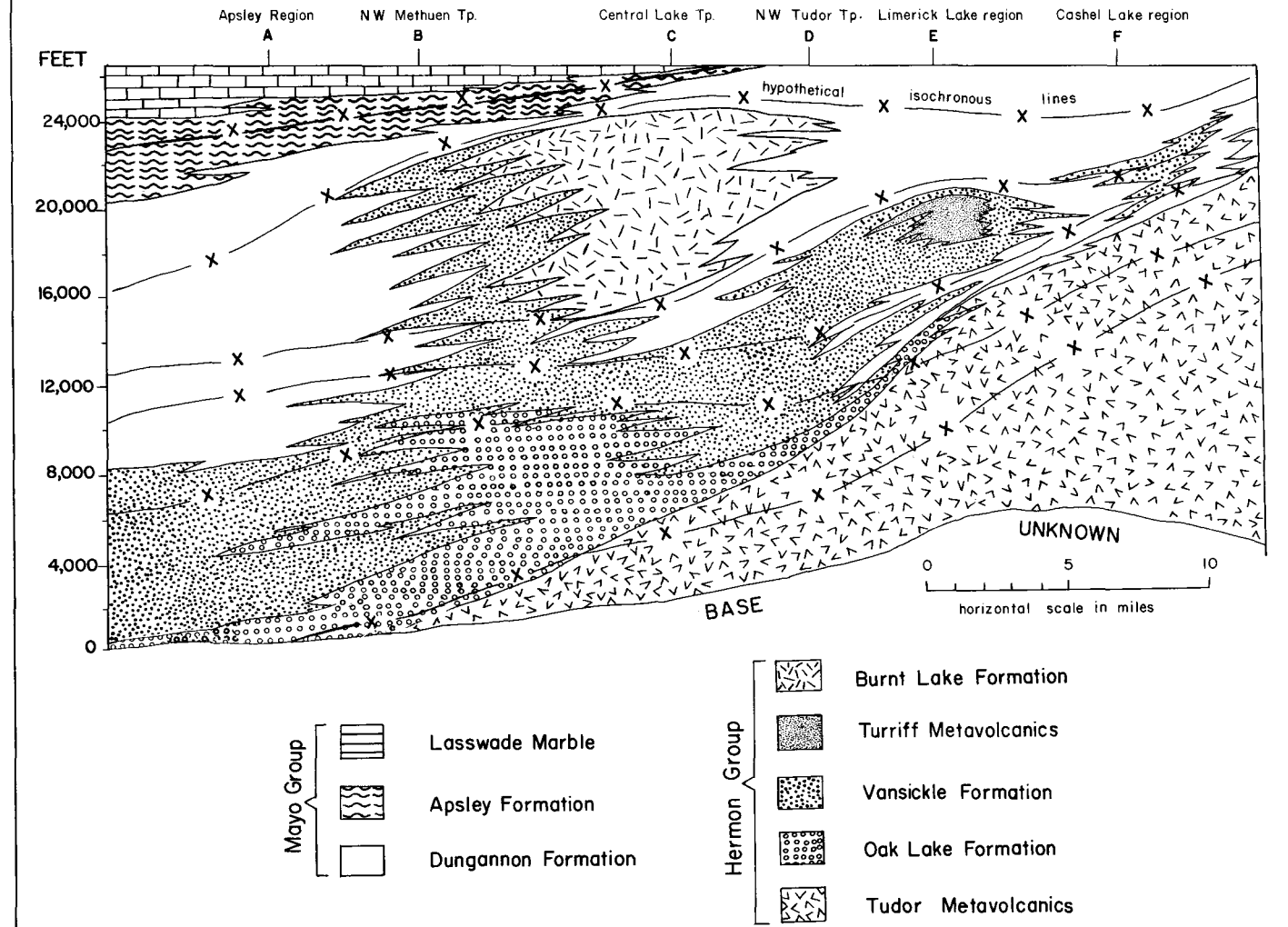


Figure 3.2

After Lumbers (1967)

It has been shown on structural and geochronological grounds that the oldest rocks in the Bancroft-Madoc region occur along the flanks of the Elzevir-Ashby Dome (Lumbers, 1967a; Silver and Lumbers, 1966). This sequence, largely composed of basaltic and andesitic flows and pillow lavas, is termed the Tudor metavolcanics and forms the lowermost formation of the Hermon Group (Lumbers, 1967a). Toward the top of the Tudor metavolcanics, which thin to the north and west of the Elzevir-Ashby Dome, thin bands of felsic metavolcanics are encountered. These bands are correlated with the Oak Lake formation defined by Hewitt (1961) in Methuen Township (Figure 3.1) and are considered to interfinger with and overlie the upper part of the Tudor metavolcanics (Lumbers, 1967a). In general, the upper part of the Oak Lake formation intertongues with quartzo-feldspathic gneisses and feldspathic metagraywackes assigned to the Vansickle formation, named and described by Hewitt (1961) for the type exposures near the village of Vansickle in southeastern Methuen township (Lumbers, 1967a).¹ Stratigraphically above the Vansickle are the Turriff metavolcanics and the Burnt Lake formation, a sequence of mafic metavolcanics and felsic

¹ However, in the eastern portion of the Lowlands, especially Limerick and Cashel townships, the upper portion of the Oak Lake formation intertongues with lowermost Dungannon marble (Lumbers, 1967a).

flows and pyroclastic rocks respectively (Lumbers, 1967a). These two volcanic sequences, found along the flanks of the Ormsby Dome and the major synclinorium to the southeast (Figure 3.1), represent the uppermost formations in the Hermon Group.

From Figure 3.2 it is apparent that the lowermost meta-sediments of the Mayo Group interfinger with the middle and upper portions of the Hermon Group suggesting vulcanicity and sedimentation to be contemporaneous during accumulation of the supracrustal prism. Varying thicknesses of the formations in these groups further suggest differential rates of accumulation from place to place.

The Mayo Group is best exposed in the western and north-western portions of the Bancroft-Madoc area (Figure 3.1). The oldest formation in the group, the Dungannon formation named by Hewitt and James (1956) for the type exposures in Dungannon township, interfingers with all other formations exposed in the Lowlands (Lumbers, 1967a). It consists chiefly of calcitic and dolomitic marbles with interbanded quartzo-feldspathic gneisses and feather amphibolites. The upper portion of the Dungannon intertongues with the lowermost amphibolites and quartzo-feldspathic gneisses of the Apsley formation named for the type exposures near the village of Apsley (Shaw, 1962). Conformably overlying the Apsley formation are the relatively pure marbles of the

Lasswade marble. Named by Shaw (1962) for exposures near the village of Lasswade in southern Chandos township, this marble lies in the cores of synclinal folds throughout Methuen, Chandos, Wollaston, Cardiff and Faraday townships (Figure 3.1). The distinction between marbles of the Dungannon and Lasswade formations is tenuous and further study may necessitate stratigraphic revision.

Structural, stratigraphic and geochronologic evidence led Lumbers (1967a) to postulate an integrated model of accumulation for the supracrustal series in the Hastings Lowlands. The thinning of the Tudor metavolcanics outward from the Elzevir-Ashby Dome, their broad geographical extent, the predominance of basaltic and andesitic flow rocks and the association of pillowed lavas and carbonate metasediments suggest that the Tudor may in fact represent a shield volcanic complex whose base is unknown and whose center lies in eastern Grimsthorpe and western Anglesea townships, the site of greatest accumulation of Tudor lavas. The interfingering of the Oak Lake and Tudor formations and the general thickening of the Oak Lake north and west of the postulated volcanic center may indicate that the metavolcanics underwent continuous differentiation with outpourings of felsic flow and pyroclastic rocks on the flanks of the shield volcanic complex. This complex probably evolved into a strato-volcanic complex in this way with contem-

poraneous denudation of the volcanic piles resulting in the production of feldspathic and minor mafic graywackes of the Vansickle formation.

Vulcanism and clastic sedimentation appear to have been contemporaneous with carbonate sedimentation in the shallow marine basins flanking the strato-volcanic complex resulting in the interfingering of Dungannon, Oak Lake, and Vansickle lithologies. Other meta-volcanic units, such as the Turriff and Burnt Lake formations, appear to represent renewed activity in the volcanic complex following periods of degradation and clastic sedimentation. The accumulation of the Apsley formation and Lasswade marble appears to represent a prolonged period of volcanic quiescence and clastic sedimentation¹ followed by largely chemical sedimentation in the western portion of the sedimentary basin.

3. 2. Stratigraphy of the Mapped and Adjacent Areas

The amphibolites, quartzo-feldspathic gneisses and lepidolites in the map area were initially assigned to the Hermon formation by Hewitt (1959) and Shaw (1962). Named for the type exposures near the village of Hermon in Mayo township (Hewitt and James, 1956), the

¹ It is possible that the Apsley represents metamorphosed intermediate volcanics on purely compositional grounds but this argument is refuted by Simony (1960).

Hermon formation was thought to overlie the Dungannon formation in the flanks of the Detlor anticline (Hewitt and James, 1956). The regional stratigraphic and geochronologic data of Lumbers (1967a) and Silver and Lumbers (1966) demonstrate this to be erroneous for several reasons. First, Hewitt and James (1956) and Evans (1964) included the Tudor metavolcanics and the overlying Oak Lake formation in their Hermon formation in Mayo, Ashby and Denbigh townships (Lumbers, 1967a) and incorrectly interpreted the synclinal structures to the west, north and east of the Elzevir-Ashby Dome as anticlines, e. g. the Detlor anticline. This misinterpretation gave rise to the notion that the Hermon was in fact younger than the Dungannon formation. Preliminary U-Pb data on zircons from the Oak Lake metarhyolites in Mayo Township suggest the Oak Lake to be slightly younger than the underlying Tudor metavolcanics substantiating Lumbers (1967a) contention that in fact the Oak Lake (part of the Hermon Formation as defined by Hewitt and James (1956) and Evans (1964)) is younger than and overlies the Tudor north of the Elzevir-Ashby Dome. Since the lithologies of the Hermon Formation are continuous with and identical to those of the more rigidly defined Hermon Group of Lumbers, it seems advisable to abandon the former term in favour of the latter. Hermon Group lithologies can be traced nearly uninterrupted parallel to the boundary of the Hastings Highlands from Ashby, Mayo and Dungannon townships into the map area (Figure 3.1).

Compositional graded bedding in quartzo-feldspathic gneisses north of Port Hope Lake (Figure 2.1) suggests the Hermon Group lithologies in the map area to be right side up underlying the marbles of the Dungannon Formation. It should be noted that no macroscopic folds could be defined in the vicinity of these exposures which would alter the present interpretation. It thus appears reasonable to correlate the rocks of the map area with the Hermon Group as defined by Lumbers (1967a) because of their stratigraphic position and apparent age.

The lithologic succession in the map area can be sub-divided in a general way into a lower amphibolite, a middle unit of interfingering quartzo-feldspathic gneisses and leptites, an upper amphibolite and an upper leptite (Figure 2.1). These units comprise the Hermon Group which has been divided into discreet formations in other parts of the Bancroft-Madoc area. Because of the complex interrelationships between these units in the map area, no subdivision into formations has been attempted. A marble envelope encloses the Hermon Group within the map area. Marbles along the southeastern margin of the area belong to the Dungannon Formation but the shear zone along the northwestern margin complicates stratigraphic assignment of the marble and amphibolite terrain to the

to the north adjacent to the Harvey-Cardiff Arch and the Hastings Highlands.

Returning to the Hermon Group rocks, the most interesting aspect of their stratigraphy is the interdigitation and gradational relations between certain lithologies. This is particularly evident in the case of the leptites and quartzo-feldspathic gneisses in northwestern Chandos and southeastern Cardiff townships. In these areas obvious leptites grade into quartzo-feldspathic gneiss parallel to gneissosity in a matter of a few hundred feet. Relations of this nature are seldom observed with amphibolite. In general, contacts across gneissosity are sharp and conformable where exposed. Gradational contacts are not unknown, however. The contact between the lower amphibolite and middle quartzo-feldspathic gneiss and leptite unit is gradational over a few tens of feet on the north shore of Silent Lake. The significance of these stratigraphic relations will be treated in a later chapter concerning the origin of each of the major rock units.

Relatively few sedimentary or volcanic structures have been found during the course of mapping. The only occurrence of sedimentary structures other than the above mentioned graded bedding is an example of cross bedding in an outcrop of quartzo-feldspathic gneiss on an abandoned logging road east of Silent Lake. Unfortunately, only the forset beds are preserved making a top determination impossible.

In the upper amphibolite unit in western Anstruther and northwestern Chandos townships and in the lower amphibolite unit south of Lower Paudash Lake in Faraday township, diopsidic and epidotized inclusions are occasionally found in isolated exposures. These inclusions may appear as disconnected, isolated pods in the rock (Figure 3.3) or as discreet boudins in an obvious boudinage structure (Figure 3.4). In all cases visible foliation wraps around these inclusions. The inclusions may be interpreted either as (a) epidotized volcanic fragmentals or bombs similar to those reported by Hewitt (1962) in Wollaston township and Shaw (1962) in Chandos township or (b) as a streaked out boudinage structure of a more competent, calcic interbed. The difference in bulk composition of the inclusions and their unfoliated nature favors the latter of these two alternatives.



Figure 3.3 Calcic inclusions in amphibolite. Exposure immediately west of Highway 28 at southern extremity of map area, Anstruther township.



Figure 3.4 Boudinage of calcareous interband in amphibolite south of Lower Paudash Lake, Faraday township.

4. STRUCTURAL GEOLOGY

4.1. Structure of the Bancroft-Madoc Area

The gross structural features of the Bancroft-Madoc area have been named and documented by Lumbers (1967a). In general, this area is dominated by five structural highs, the Harvey-Cardiff Arch, the Hastings Highlands, the Kasshabog Arch, the Ormsby Dome and the Elzevir-Ashby Dome (Figure 3.1). The Harvey-Cardiff Arch and the Hastings Highlands bound the Bancroft-Madoc area on the north and northwest, the Elzevir-Ashby Dome forms the boundary on the east. The supracrustal sequence lying between these highs is divided into two major, unnamed synclinoria by the Kasshabog Arch and Ormsby Dome. Crossfolding within and across these generally north-easterly trending structures follows a northwest-southeast trend producing the complex fold pattern characteristic of the region. It should be emphasized that this fold pattern in no way reflects a single deformational or metamorphic event but rather is the end product of at least two major periods of dynamo-thermal metamorphism and intrusion followed by a late stage period of regional uplift (Lumbers, 1967a). The study area

lies on the north-west limb of the major synclinorium between the Harvey-Cardiff Arch and the Kasshabog Arch.

Hewitt and James (1956) divided the Bancroft-Madoc area on a structural basis into the Hastings Highlands and the Hastings Basin. According to them the Highlands, a center of plutonic activity and "ultrametamorphism", are separated from the lower grade rocks of the Basin by a generally complex, poorly defined, southerly dipping fault system which is supposed to parallel the Highland margin. This system, commonly known as the Highland boundary fault system, in general, does not displace lithologic contacts over most of its length as shown by maps of Cardiff, Faraday, Dungannon and Mayo townships (Hewitt, 1959; Hewitt and James, 1956). Its extension and significance west and southwest of Bancroft at present is unclear. The work of Lumbers (1967a; 1968) strongly refutes Hewitt's notion of the Hastings Basin as originally conceived. Hewitt considered the low grade Tudor metavolcanics to be the youngest rocks in the region occupying the core of a structural basin, but Lumbers (1967a) finds the converse to be the case in that the Tudor rocks are the oldest in the Bancroft-Madoc area. Thus, following Best (1966), it is recommended that the term Hastings Basin be dropped in favor of the purely topographic term Hastings Lowlands.

4.2. Structure of the Mapped Area

A structural analysis of the mapped area is undertaken in this section to define the number of deformational episodes and periods of mineral growth which bear on its physical and chemical history. The geometry of the Hermon Group rocks will also be deduced.

The rocks studied are characterized by a strongly penetrative foliation and mineral lineation as well as mesoscopic folds in gneissic layering. Foliation transverse to gneissosity is seen only in fold hinges where it is evident that this foliation is axial planar. Folding is tightly isoclinal with gneissosity folded around southeasterly trending, steeply plunging axes. No megascopic folds have been delineated in the course of mapping.

4.2.1 Macroscopic Geometric Analysis

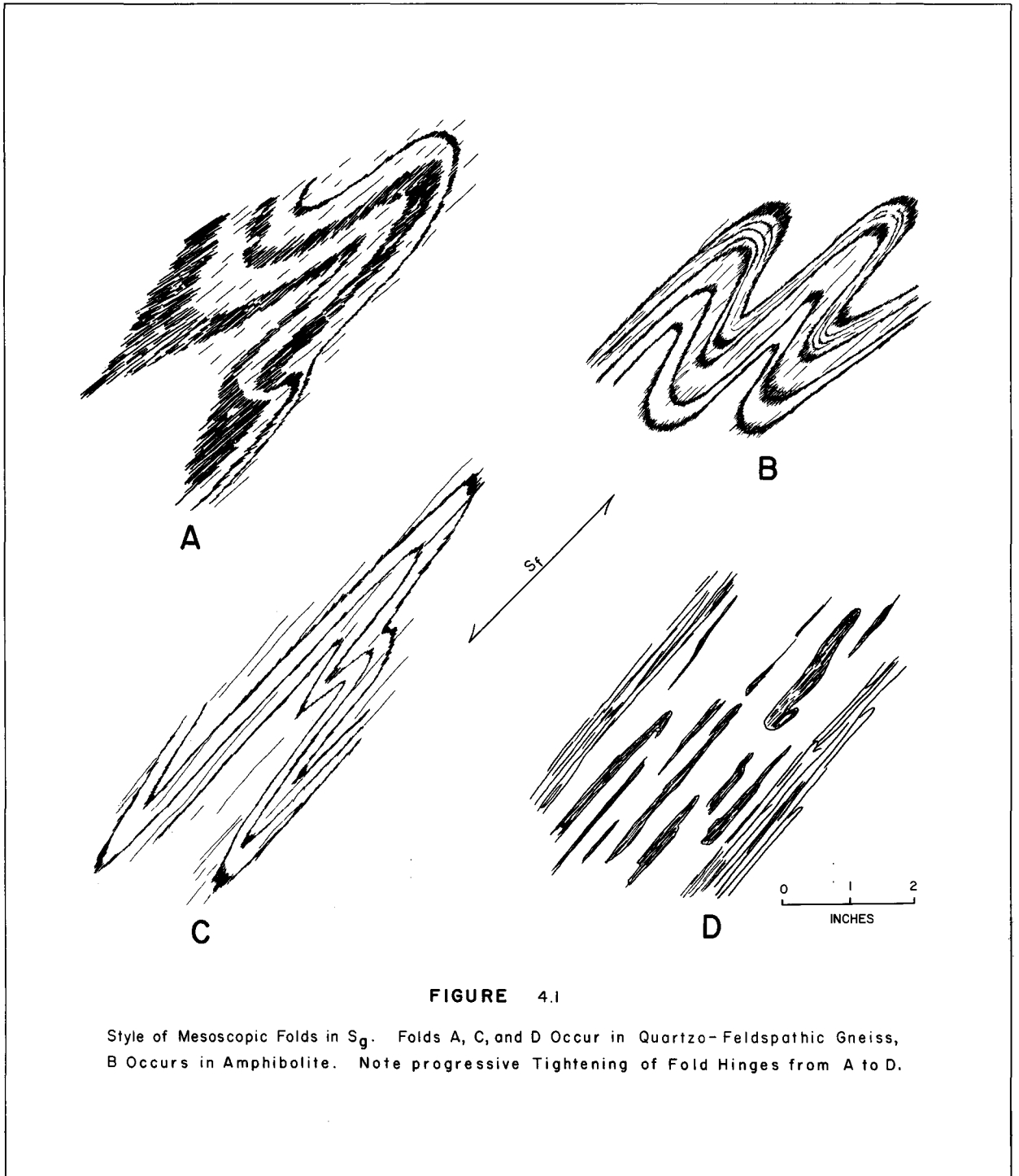
Structural fabric elements used in this study include gneissic layering (Sg), foliation (Sf), axial traces and axial surfaces in Sg, fold axes and mineral lineations (L). Sg denotes either compositional banding or lithologic layering which may or may not be equivalent to original bedding. Sf is the planar fabric element produced and defined by the preferred orientation of inequant minerals in a tectonite. Lineation, L, is the preferred long axis dimension or elongation direction of

tectonite minerals. All fabric data has been plotted on the lower hemisphere equal area projection and only diagrams containing more than 100 data points have been contoured. Diagrams are contoured according to the percentage of points per unit area of the net (Schmidt Method).

4.2.2. Mesoscopic Character of Folds in Sg

Folds in lithologic layering are cylindrical and similar in all examples studied. Between examples varying degrees of tightening are found along the hinge zones (Figure 4.1). All folds are close to tight following the recommendations of Fleuty (1964). Sf parallels the axial surfaces of folds and Sg in fold limbs. The general parallelism of Sf and Sg is not entirely due to the tight style of folding, for gneissosity has been disrupted and transposed parallel to the axial surfaces of folds in some lithologies of high ductility contrast. Transposition occurs through continued tightening of folds similar to those of Figure 4.1 A and B producing tight isoclines as shown by Figure 4.1C. Further tightening results in the disruption of gneissosity with the production of "rootless" folds similar to Figure 4.1D.

Mineral lineations are common to all lithologies in the map area. These lineations are expressed by streaked, linear segregations of various minerals including hornblende, sillimanite, potassium feld-



spar and quartz lying in the plane of foliation. Occasionally lineations coarsen to form mineral rodding up to an inch in diameter. Within folds in lithologic layering it is apparent that fold axes and mineral lineations are parallel and that L is simply the trace of Sg on Sf. Linear mineral segregations developed in Sg parallel to fold axes also constitute L. Axial fabric elements, including fold axes, mineral lineations and rodding, trend east to southeast and are steeply plunging in this direction. Nowhere are these elements seen in the field to be folded or cut by a later generation of S surfaces.

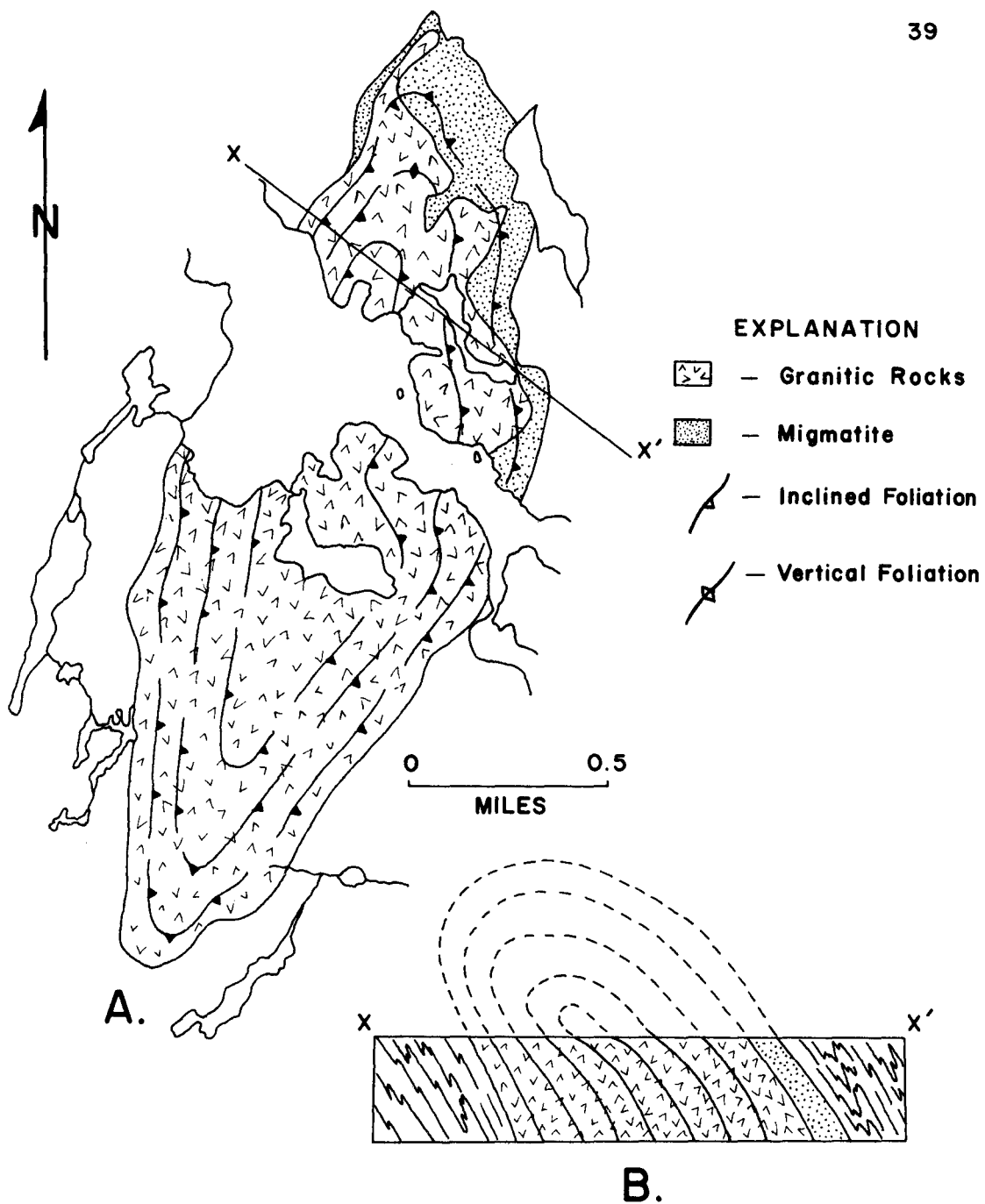
4. 2. 3. Geometries of the Structural Subdivisions

The map area has been divided into seven structural subdivisions on the basis of apparent structural homogeneity (Figure 4. 2, in pocket). Subareas A and C contain granitic rocks and migmatites intrusive into the supracrustal sequence. In these subareas structural analysis is based on penetrative foliation and lineation whereas analysis of subareas in the supracrustal rocks is based on geometries of gneissosity, lineation and folding on a mesoscopic scale.

Subarea A is characterized by tectonites having a penetrative foliation (Sp) and poorly developed mineral lineation (L). Lineation is generally absent in granitic rocks of the Anstruther-

Burleigh batholith. In general, foliation is steeply dipping in an easterly direction with lineation trending and plunging shallowly south-east. In Figure 4.3 (in pocket), the macroscopic geometries of S_p and L are shown as point maxima for poles to foliation and for axial elements such as mineral lineations and fold axes. Foliation in the granitic rocks is interpreted as primary flow foliation because of its concentric development throughout the pluton to the west and the age relations between the pluton and supracrustal rocks. This pluton, dated at 1103 ± 39 m. y. (Krogh, 1964), post-dates the main period of metamorphism in the supracrustal sequence (Lumbers, 1967a) and possesses a fabric different from that of the country rocks.

Subarea C covers the Silent Lake granite and its migmatite zone. Figure 4.3 shows a partial girdle of poles to foliation and a diffuse point maximum of axial elements. The axial elements include mineral lineations, minor fold axes and the long axis orientation of the quartz-sillimanite-plagioclase nodules common to this body. Foliation in the granite for the most part dips to the east except in the northern and southern portions of the subarea (Figure 4.4a). Here foliation is folded about an axis which appears to coincide with the point maximum of axial elements. The girdle of poles to foliation is incomplete primarily because of a lack of data along the southern margin of the stock. As detailed work continues on this body a more



complete structural interpretation will become possible. On the basis of the present data, the Silent Lake stock appears to represent a doubly plunging asymmetric dome recumbent to the west (Figure 4.4b). Foliation is thought to be an igneous flow foliation because of its concentric development within the stock and the absence of the country rock fabric on a mega and mesoscopic scale.

Subareas B and D show point maxima for poles to S_g and axial elements (Figure 4.3). The point maxima for poles to gneissic banding are a reflection of the generally tight style of folding in these areas which produces subparallel limbs and narrow, generally unexposed hinge zones. Poles to S_g in subareas E, F and G (Figure 4.3) yield complete or partial girdles showing gneissosity to be folded about an axis which in each case coincides approximately with the point maximum of axial elements.

Since the attitude of S_f in the supracrustal rocks does not vary greatly throughout the map area, data from subareas B, D, E, F and G have been combined into a single synoptic plot (Figure 4.3). The suggestion of a partial girdle of poles to foliation in this plot reflects the broad regional warp in foliation which, in a general way, conforms to the highland boundary to the northwest.

The presence of one generation of folds and one recognizable metamorphic foliation coupled with the parallelism of mineral lineations and fold axes strongly suggest the rocks in question record the results of only one period of deformation and mineral growth. In an adjacent area, extending well into the carbonate sequence south of Bancroft, rocks which certainly correlate with those of the present study show exactly the same relations (Best, 1966). In the marbles of this area, however, Best finds two distinct fold generations which may record separate metamorphic events or which:

"merely reflect pulses in space and (or) time,
of a single general orogeny" (Best, 1966, p. 452)

Since a second fold generation is not recorded in the map area, it is felt that the mineral assemblages, for the most part, are the products of a single metamorphic episode.

4.2.4. Faulting and the Highlands-Lowlands Transition

Two major shear zones have been mapped in the study area, one in the marbles to the southeast and one in the marbles and amphibolites to the northwest (Figure 2.1). They were mapped in the field on the basis of mylonite exposures and depressed, topographic linears. Neither shear zone offsets lithologic contacts, consequently their nature and amount of displacement is poorly known. Down-dip lineations in mylonite zones

found at several locations along each shear suggest dip-slip movement of undetermined sense.

The Pratt's Creek shear, named by Shaw (1962), parallels the general trend of lithologic units along the southeastern margin of the map area in Anstruther and Chandos townships. Its extension to the northeast in Cardiff and Faraday townships is not known and further mapping is required to trace its continuation. It is likely that this shear zone extends further into Anstruther township and may eventually join the Burleigh fault (Adams and Barlow, 1910) as suggested by Shaw (1962). Since the Burleigh fault cuts the Anstruther-Burleigh granite gneiss dated at 1103 ± 39 m. y. (Krogh, 1964) it is possible that the Pratt's Creek shear is a post-metamorphic break related to the 1000-800 m. y. period of regional uplift postulated by Lumbers (1967a).

The shear zone tentatively mapped along the northwestern margin of the area is likely a continuation of the Highland Boundary shear system found by Hewitt (1959) to extend from Bancroft parallel to Highway 28 to the eastern end of Lower Paudash Lake. The location of this shear system through the lake is unknown and more detailed mapping is needed to determine its regional extent and significance. In light of recent geochronologic and petrologic studies, it seems unlikely that movement along this shear system created a sharp metamorphic transition between the highlands and lowlands as suggested by Hewitt

(1959). Most probably faults which belong to this system represent post-metamorphic breaks associated with late stage uplift.

5. ORIGIN

The origin of each major rock type of the Hermon Group in the mapped area will be treated in this chapter. Both field and chemical data will be used to define protoliths for each lithologic type. These considerations will lead to the development of a model for the accumulation of the supracrustal prism in the study area.

5.1. Amphibolites

Before discussing the origin and detailed geochemistry of the Hermon Group amphibolites, it is advisable to construct a framework in which to view the so-called amphibolite problem. Accordingly, this will be the subject of a brief review.

5.1.1. Critique of the Amphibolite Problem

Perhaps the most fundamental problem related to amphibolite origins is the question of what constitutes an amphibolite. While virtually any hornblende bearing assemblage may be considered an amphibolite, the term most commonly refers to hornblende-plagioclase assemblages in which hornblende is the dominant constituent with lesser plagioclase and minor additional phases. Amphibolites

conforming to this definition show basaltic chemistries since:

"the composition field for the two-phase assemblage hornblende-plagioclase closely mimics the composition field of basic igneous rocks" (Orville, 1969, p. 64).

The name "basaltic amphibolite" may logically be applied to such rocks and it is generally accepted that they constitute the bulk of amphibolites. The coincidence of average basalt and average amphibolite compositions in Table 5.1, Columns D and B may be cited in evidence. However, some rocks mapped in the field as amphibolites on the basis of hornblende in their mode may not show basaltic chemistries because of the presence of substantial, additional mineral components. This group of amphibolites is herein termed "non-basaltic" and may be derived by a variety of means to be subsequently discussed. The crux of the amphibolite problem does not concern these rocks, however. Rather it lies in the fact that the remarkable compositional similarity between most amphibolites and basalts has alternatively been ascribed to the isochemical metamorphism of basic igneous rocks or of a variety of sedimentary rock types.

In the first study of amphibolites by modern chemical methods, Engel and Engel (1951) concluded that metamorphism of impure carbonate sediments, tuffaceous sediments or basaltic rocks could equally yield amphibolite bulk compositions. These conclusions

Table 5.1: COMPOSITIONS OF AMPHIBOLITES, BASALTS AND
POSSIBLE AMPHIBOLITE PROTOLITHS

	<u>A</u>	<u>B</u>	<u>C</u>	<u>D</u>	<u>E</u>	<u>F</u>	<u>G</u>	<u>H</u>
SiO ₂	48.12	49.73	48.6	49.3	48.8	48.4	49.34	51.6
TiO ₂	1.65	1.39	2.1	2.0	1.6	1.6	1.49	1.6
Al ₂ O ₃	14.92	14.92	16.3	16.0	15.5	16.2	17.04	16.0
Fe ₂ O ₃	4.06	2.97	3.1	3.2	2.5	2.6	1.99	3.0
FeO	7.97	8.77	8.1	7.8	8.8	7.9	6.82	7.8
MnO	0.21	0.21	0.17	0.17	0.17	0.19	0.17	0.18
MgO	7.36	6.57	6.5	6.6	8.3	7.3	7.19	5.8
CaO	8.84	9.51	9.9	9.9	10.2	10.8	11.72	9.8
Na ₂ O	3.53	2.71	3.0	2.8	2.3	2.6	2.73	2.4
K ₂ O	0.65	0.98	1.0	1.0	0.7	0.7	0.16	0.8
P ₂ O ₅	0.31	0.25	0.34	0.32	0.23	0.26	0.16	0.21
H ₂ O ⁺	1.35	-	0.9	0.9	0.9	1.0	0.69	0.8
CO ₂	0.66	0.85	-	-	-	-	-	-

A - Average Hermon Group Amphibolite (16 analyses)

B - Average of 262 Amphibolites (van de Kamp, 1964)

C - Average of 288 Olivine Alkalic Basalts + Dolerites (Manson, 1967)

D - Average of 1558 Basalts (Manson, 1967)

E - Average of 230 Olivine Tholeiitic Basalts + Dolerites (Manson, 1967)

F - Average of 127 Gabbros (Manson, 1967)

G - Average Oceanic Tholeiitic Basalts (Engel et al., 1965)

H - Average of 998 Quartz Basalts + Dolerites (Manson, 1967)

Table 5.1 (continued)

	<u>I</u>	<u>J</u>	<u>K</u>	<u>L</u>	<u>M</u>	<u>N</u>	<u>O</u>	<u>P</u>
SiO ₂	48.75	49.34	53.1	54.8	56.52	61.04	57.66	53.12
TiO ₂	2.64	2.84	0.7	0.7	0.57	0.57	0.81	0.75
Al ₂ O ₃	15.94	16.59	15.2	15.8	14.82	12.38	15.98	14.73
Fe ₂ O ₃	7.02	7.76)	5.4*)	5.6*	1.99	1.46	2.92	2.69
FeO	6.45	5.73))		2.67	3.24	3.06	2.82
MnO	0.19	0.69	-	-	0.10	0.11	-	-
MgO	8.93	4.56	7.7	6.7	6.72	6.92	7.52	10.20
CaO	6.01	6.25	12.9	11.5	11.68	9.64	6.98	11.02
Na ₂ O	2.36	3.79	3.3	3.4	3.53	2.67	1.67	1.53
K ₂ O	1.61	1.44	1.4	1.5	1.24	1.82	3.40	3.14
P ₂ O ₅	0.28	0.82	-	-	0.16	0.15	-	-
H ₂ O ⁺	-	-	-	-	-	-	-	-
CO ₂	-	-	-	-	-	-	-	-

I - Average of 4 Basaltic Tuffs (van de Kamp, 1964)

J - Analyses of Yachats Basaltic Sandstone (van de Kamp, 1964)

K - Andesite - Dolomite Mixture; 80% Average Andesite (Taylor and White, 1966): 20% Ideal Dolomite

L - Andesite - Dolomite Mixture; 85% Average Andesite (Taylor and White, 1966): 15% Ideal Dolomite

M - Dacite-Dolomite Mixture; 80% Average Dacite (Nockolds, 1954): 20% Ideal Dolomite

N - Graywacke-Dolomite Mixture; 80% Average Graywacke (Pettijohn, 1963): 20% Ideal Dolomite

O - Pelite-Dolomite Mixture; 80% Average Carbonate Free Pelite (Shaw, 1956): 20% Ideal Dolomite

P - Pelite-Dolomite Mixture; 70% Average Carbonate Free Pelite (Shaw, 1956): 30% Ideal Dolomite

* Total iron as FeO

Table 5.1 (continued)

	<u>Q</u>	<u>R</u>
SiO ₂	60.58	62.77
TiO ₂	0.18	0.34
Al ₂ O ₃	11.07	8.71
Fe ₂ O ₃	1.03	1.74
FeO	0.62	1.00
MnO	0.02	0.21
MgO	7.92	7.75
CaO	11.66	11.66
Na ₂ O	2.46	1.51
K ₂ O	4.41	4.11
P ₂ O ₅	0.06	0.17
H ₂ O ⁺	-	-
CO ₂	-	-

Q - Rhyolite-Dolomite Mixture; 70% Average Rhyolite (Nockolds, 1954):
30% Ideal Dolomite

R - Arkose-Dolomite Mixture; 70% Average Arkose (Pettijohn, 1957):
30% Ideal Dolomite

Note: Analyses K through R calculated CO₂ free. Ideal dolomite constitutes analysis of pure CaMg(CO₃)₂.

are corroborated by Flawn (1953) who suggests the following amphibolite protoliths:

- (1) Regional metamorphism of sedimentary rocks, e. g. impure carbonate rocks or marls, tuffs and uncontaminated detritus from basic igneous terrains.
- (2) Regional metamorphism of basic intrusive or extrusive rocks.
- (3) Igneous metasomatic alteration of carbonate rocks.
- (4) Granitization causing or resulting in a "basic front".

Few additional proposals of amphibolite origin have been made, rather a great deal of effort has been directed toward confirming these rock types as amphibolite protoliths. It is proposed to treat each of these possible protoliths or amphibolite producing mechanisms in terms of three general modes of amphibolite origin: (a) metamorphism of original bulk compositions, (b) addition hypotheses and (c) subtraction hypothesis. This approach is used to demonstrate that the likelihood of developing basaltic compositions in sediments is small and hence that few basaltic amphibolites are of sedimentary origin.

Metamorphism of Original Bulk Compositions:

There is little doubt that basalts and gabbroic rocks provide the most suitable and obvious protoliths for basaltic amphibolites. Their

chemical similarities in Table 5.1, Columns A-H confirm this, rendering further elaboration unnecessary.

Other unaltered bulk compositions have been suggested as amphibolite precursors. Among these are mafic tuffs and mafic graywackes as well as impure shales and graywackes (Evans and Leake, 1960; Leake, 1964; van de Kamp, 1964, 1968; Wilcox and Poldervaart, 1958; Francis, 1958; Hague et al., 1956; Walker et al., 1960; Eckelmann and Poldervaart, 1957; Engel and Engel, 1951, 1962; Schwarcz and Clayton, 1965; Shaw, 1962 etc.).

Mafic tuffs and mafic graywackes of basaltic composition may be isochemically metamorphosed to amphibolite as Columns I and J of Table 5.1 suggest. Basaltic tuffs have been proposed as the protolith of thinly banded amphibolites in presumed metasedimentary sequences (van de Kamp, 1968), but their occurrence in the geologic record is minimal according to Engel and Engel (1962, p. 76) who state:

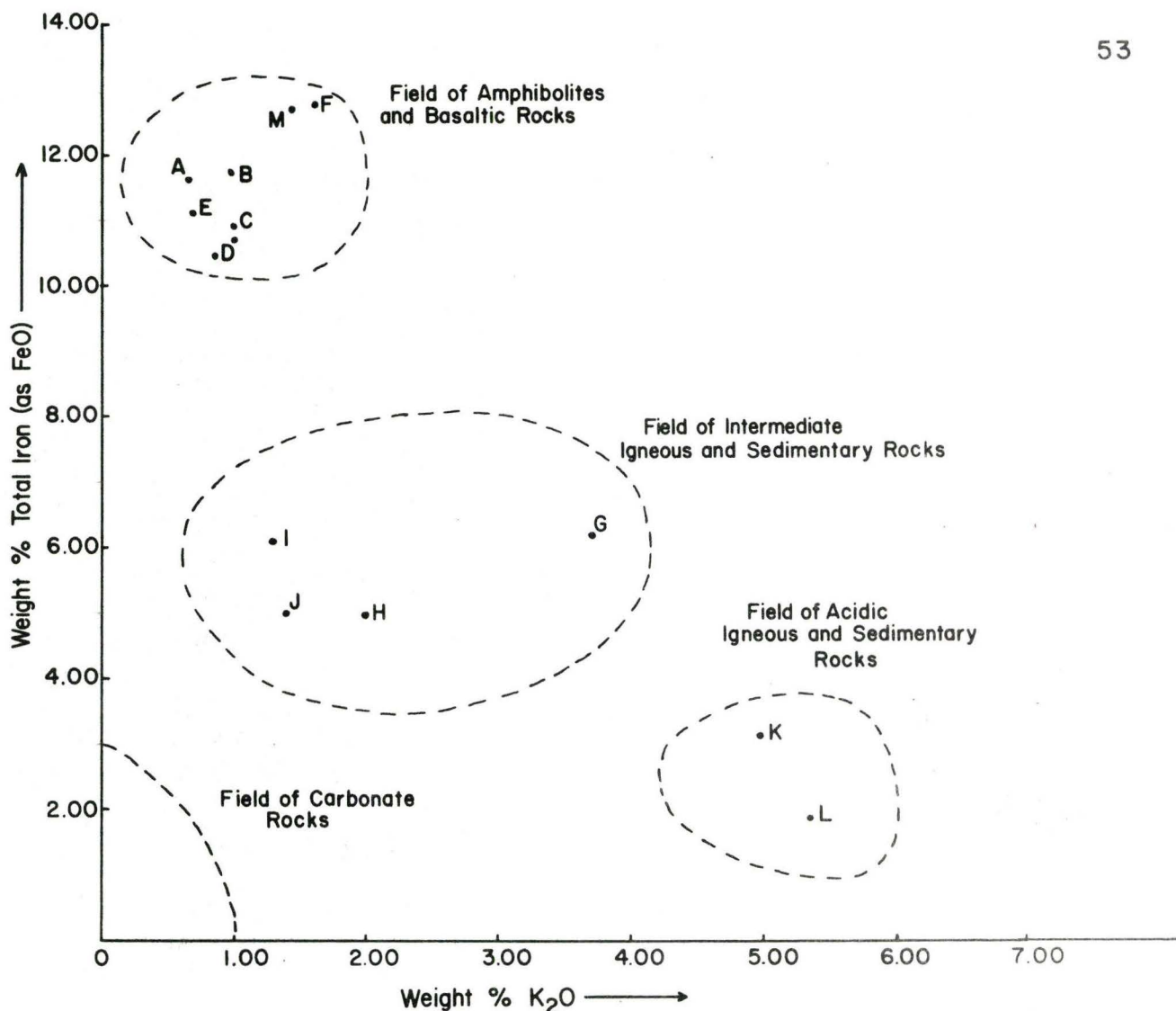
"Careful field studies and a search of the literature show that thin, persistent layers of tuff or other sediment - with the composition of basalt - are very rare in, if not absent from, least metamorphosed rock sequences of the paragneiss (meta-graywacke ?) or any other metasedimentary rock types, whether Precambrian or younger."

This view is refuted to a degree by the works of Snively and Wagner (1964), Nayudu (1964), Brew and Muffler (1965), Horn et al. (1969) and Carlisle (1963) who report the association of basaltic tuffs with basaltic

flows, pillow lavas and clastic or chemical marine sediments. The occurrence of tuffs in the Cascade and Coast Ranges of northwestern Oregon suggests that in scattered occurrences even rather thick amphibolite sequences can result from the metamorphism of tuffaceous accumulations (Hoover, 1963; Snavely and Wagner, 1964). Nonetheless, a perusal of the literature leads one to the conclusion that basaltic tuffs account quantitatively for only a small proportion of amphibolite protoliths in any given metamorphic terrain. Various studies indicate that andesitic tuffs are perhaps more common than basaltic ones (Fiske, 1963; Fiske et al., 1963 and Fiske and Matsuda, 1964), yet it is puzzling that few andesitic bulk compositions are reported in studies of amphibolites. Mafic graywackes derived from basaltic petrographic provinces and having little admixed sedimentary material constitute a plausible amphibolite protolith as indicated above. The fairly common occurrence of mafic graywackes and brecciated subaqueous basaltic flows in the Coast Range province (Snavely and Wagner, 1964; Rodgers, 1965; Peck et al., 1964; Hoover, 1963) lends support to this notion. The probability of sedimentary contamination of a primary basaltic composition is high however and it seems likely that rapid weathering of a basaltic terrain would yield a high proportion of basic sandstones and graywackes having compositions removed from that of basalt. Study of the sediments from the Lower Columbia river which drains the Columbia Flood Basalt

Province supports this contention since these sediments very closely approximate the composition of average graywacke and not basalt as might be expected (Whetten, 1966). Thus mafic graywackes are a reasonable protolith for basaltic amphibolites but are of limited quantitative importance.

Dolomitic shales and graywackes in roughly 2:1 dolomite to shale or graywacke proportions are most commonly cited as para-amphibolite progenitors. In order to evaluate models of amphibolite genesis based on the physical mixing of "end member" sedimentary and volcanic rocks in depositional environments, hypothetical mixtures of andesite, dacite, graywacke, pelite, rhyolite and arkose with pure dolomite have been calculated to approximate the composition of basaltic amphibolites as closely as possible. From the results listed in Table 5.1, Columns K-R, it can be seen that consistent compositional difficulties are encountered. Specifically, these mixtures are deficient in total iron and enriched in potash and silica. A plot of total iron versus potash for the "end member" compositions used in the calculations (Figure 5.1) shows a sharp demarcation between the field of basaltic amphibolite and basalt and the compositional fields of intermediate, acidic and carbonate rocks. Consequently, admixtures of the latter three rock types in any proportion or combination will nearly always show compositional disparities with basaltic amphibolites at least in terms of



- A- Average Hermon Group Amphibolite (16 analyses)
- B- Average of 262 Amphibolites (van de Kamp, 1964)
- C- Average of 288 Olivine Alkalic Basalts + Dolerites (Manson, 1967)
- D- Average of 1558 Basalts (Manson, 1967)
- E- Average of 230 Olivine Tholeiitic Basalts + Dolerites (Manson, 1967)
- F- Average of 4 Basaltic Tuffs (van de Kamp, 1964)
- G- Average Carbonate Free Pelite (Shaw, 1956)
- H- Average Carbonate Free Graywacke (Pettijohn, 1963)
- I- Average Andesite (Taylor and White, 1966)
- J- Average Dacite (Nockolds, 1954)
- K- Average Arkose (Pettijohn, 1957)
- L- Average Calc-Alkali Rhyolite (Nockolds, 1954)
- M- Yachats Basaltic Sandstone (van de Kamp, 1964)

Figure 5.1 Total Iron Versus K₂O for Various "End Member" Sedimentary and Volcanic Rocks, Various Basaltic Rocks and Amphibolites

total iron and potassium. A similar separation of composition fields is obtained using a projection devised by Moine and de la Roche (1968) included as Figure 5.2 for the same "end member" rock types. From these considerations it is suggested that physical mixtures of common sedimentary or volcanic rock types generally do not yield compositions similar to basaltic amphibolite. The same conclusion is reached by Moine and de la Roche (1968, p. 4) for basaltic amphibolites since:

"présentent une étroite parenté chimique avec les roches ignées basiques . . . , l'existence de para-amphibolites dans un contexte métamorphique de type isochimique paraît exclue."

While the calculated mixtures do not show a basaltic chemistry, some of these mixtures, particularly andesite-dolomite and pelite-dolomite, could, upon metamorphism, yield rocks which would be mapped in the field as amphibolite. Thus, while limited numbers of non-basaltic para-amphibolites may form in this manner basaltic para-amphibolites probably do not.

It may be fairly argued that the mixture calculations are based on average compositions and that some sediments with compositions removed from these averages may be successfully mixed to give basaltic compositions. While the argument just given does not refute this possibility entirely, it seems unrealistic to invoke uncommon protoliths for basaltic amphibolites which are one of the most common rock types in metamorphic terrains. Furthermore, the use of pure

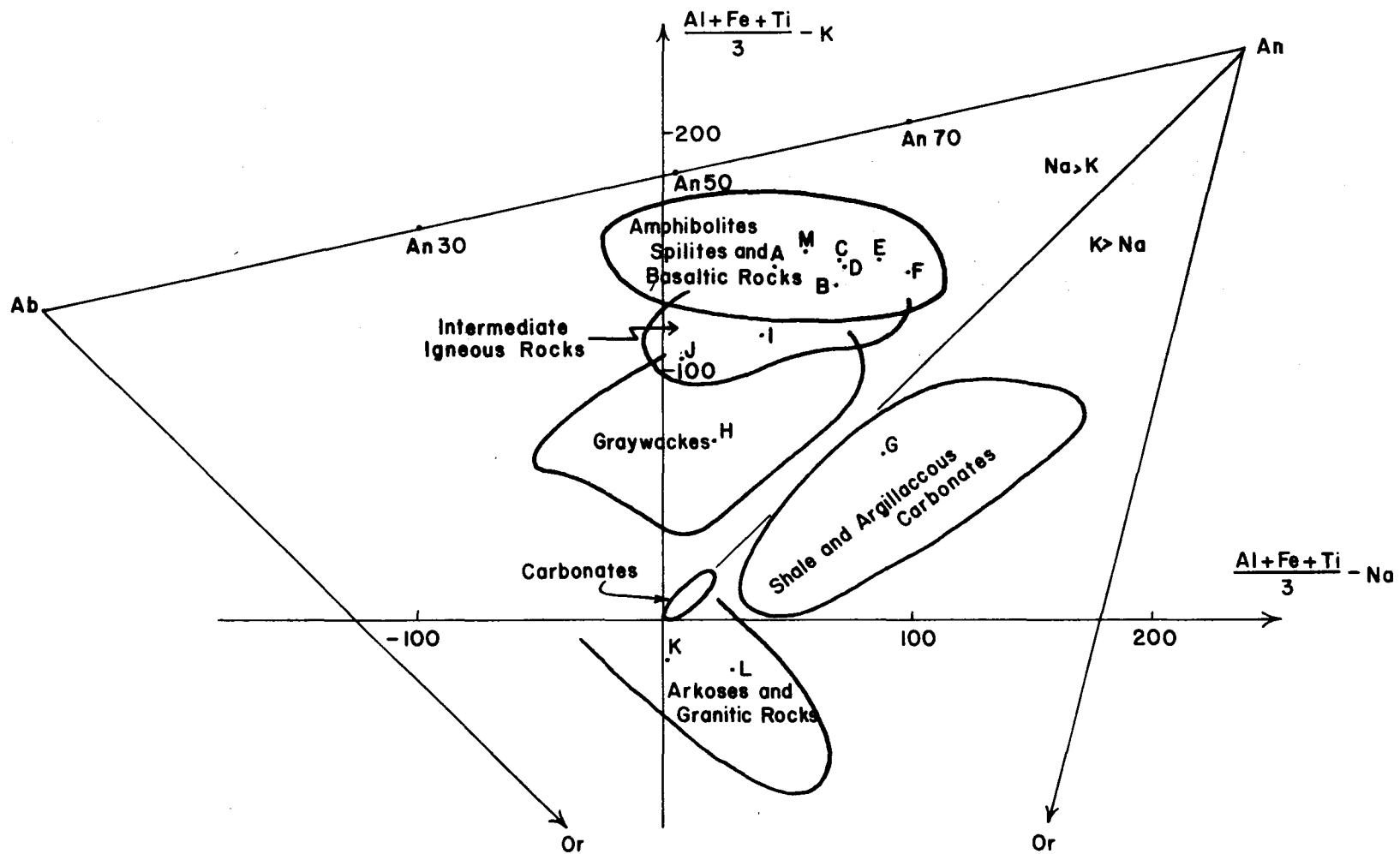


Figure 5.2 : Projection of "End Member" Sedimentary and Volcanic Rocks, Various Basaltic Rocks and Amphibolites (Modified after Moine and de la Roche, 1968) Letters same as in Figure 5.1

dolomite as a diluent imposes improbable restrictions on a sedimentary environment of protolith accumulation, yet dolomite appears to be the only component capable of increasing CaO and MgO to basaltic levels while simultaneously lowering the other oxide abundances.

In summary, the metamorphism of basic igneous rocks is the most probable mode of formation of basaltic amphibolites. Mafic tuffs and mafic graywackes are also possible basaltic amphibolite protoliths but quantitatively less important. Metamorphism of sedimentary rocks appears an infeasible way of generating basaltic amphibolites but may be responsible for the production of non-basaltic amphibolites or hornblende gneisses.

Addition Hypotheses:

Included under this heading are the metamorphic differentiation model for the origin of thin layered amphibolites postulated by Orville (1969) and the metasomatic amphibolite producing reactions between granite and marble proposed by Adams and Barlow (1910, pp. 97-110). Briefly, both of these mechanisms produce basaltic and non-basaltic amphibolite compositions in narrow bands at the interface between intermediate to acidic rocks and marble by the equilibration of chemical potential gradients across this interface.¹ Experimental and/or detailed field data lend adequate support to this general mechanism

¹ Orville (1969, pp. 78-81) gives a detailed account of the mechanism of reaction. Note the distinction between open system, selective transfer of mass and simple physical mixing.

(Orville, 1969). Particularly characteristic of these so-called "metasomatic" models is the development of mineralogic zones defined by the reactions leading to the development of an amphibolite paragenesis (e. g. Adams and Barlow, 1910, pp. 104-106). Since this mechanism is not likely to produce thick bands of amphibolite; it may successfully explain the thin bedded amphibolites of the major paragneiss in the Adirondacks studied by Engel and Engel (1962) or the feather amphibolites of the Dungannon Formation in the Bancroft-Madoc area (van de Kamp, 1968; Kudo and Shaw, 1965).

Subtraction Hypotheses:

The rather common occurrence of hornblende in migmatite melanosome raises the question of whether amphibolites of basaltic composition can be generated as the ultimate infusible residue of partial melting of rocks intermediate in composition between granite and basalt. This problem boils down to finding a common rock type which when subjected to anatectic conditions will yield the required granitic leucosome and amphibolite melanosome. The most logical choice for this parent rock is graywacke or its metamorphosed equivalent, quartzo-feldspathic gneiss. In the absence of specific examples, average graywacke and granite compositions will be used to test the plausibility of this model.

According to Pettijohn (1963, p. 56):

"there are a considerable number of chemical analyses of graywacke in the literature which show a remarkable homogeneity of composition."

It is this group of graywackes, termed eugeosynclinal graywackes by Middleton (1960), which closely resemble estimates of average continental crust in bulk composition (Condie, 1967). In fact, as inspection of Table 5.2, Columns A-H will show, average eugeosynclinal graywackes and estimates of the average continental crust composition are so close that they can be used interchangeably as parent rocks for anatectic granite. It appears logical to use either graywacke or average continental crust in our model not only because they are compositionally intermediate between granite and basalt but also because they represent bulk compositions likely to be encountered in crustal processes such as anatexis. For this reason, estimates of average total crust composition cannot be reasonably used in the model because rocks of these compositions may not occur in the geologic record since they represent weighted averages of oceanic and continental crust.

If graywacke or average continental crust is accepted as a plausible anatectite precursor it remains to find satisfactory compositions of granitic leucosome to be generated by partial fusion. Comparing the average calc-alkali granite of Nockolds (1954, Table 5.2, Column I) and the average low calcium granite of Turekian and Wedepohl

Table 5.2: COMPOSITIONS OF AVERAGE CONTINENTAL CRUST,
AVERAGE GRAYWACKE, AVERAGE GRANITE AND CALCULATED
ANATECTIC RESIDUA

	<u>A</u>	<u>B</u>	<u>C</u>	<u>D</u>	<u>E</u>	<u>F</u>	<u>G</u>	<u>H</u>
SiO ₂	64.93	64.5	66.4	65.3	60.3	64.43	66.75	65.67
TiO ₂	0.52	0.48	0.6	0.50	1.0	0.62	0.63	-
Al ₂ O ₃	14.63	16.1	15.5	16.5	15.6	15.48	13.54	12.73
Fe ₂ O ₃ *	4.42	4.1	4.9	4.3	8.0	6.54	5.53	5.09
MnO	0.068	0.08	0.1	0.04	-	0.05	0.12	-
MgO	2.24	2.3	2.0	2.6	3.9	3.12	2.15	2.40
CaO	4.12	3.3	3.8	3.5	5.8	2.22	2.54	4.20
Na ₂ O	3.46	4.0	3.5	3.6	3.2	3.74	2.93	3.04
K ₂ O	3.10	2.78	3.3	2.5	2.5	2.44	1.99	1.87
P ₂ O ₅	0.15	0.16	0.2	-	-	-	0.16	-

A - Estimate of Canadian Precambrian Shield (Shaw et al., 1967).

B - Estimate of Precambrian Shield in New Quebec (Eade, Fahrig & Maxwell, 1966).

C - Estimate of Continental Shield Crystalline Rocks (Poldervaart, 1955).

D - Estimate of Wyoming Superior Province (Condie, 1967).

E - Estimate of Continental Crust (Taylor, 1964).

F - Average of 23 Wyoming Precambrian Graywackes (Condie, 1967).

G - Average of 61 Graywackes (Pettijohn, 1963).

H - Average Eugeosynclinal Graywacke (Middleton, 1960).

* Total iron as Fe₂O₃.

Table 5.2 (continued)

	<u>I</u>	<u>J</u>	<u>K</u>	<u>L</u>	<u>M</u>	<u>N</u>	<u>O</u>
SiO ₂	72.08	74.22	67.17	69.21	58.46	59.65	64.17
TiO ₂	0.37	0.20	0.57	0.38	0.92	0.86	-
Al ₂ O ₃	13.86	13.61	15.50	14.54	16.66	16.42	9.96
Fe ₂ O ₃ *	2.71	2.03	4.23	3.86	9.89	9.22	6.83
MnO	0.06	0.04	0.05	0.05	0.05	0.05	-
MgO	0.52	0.27	1.56	0.27	6.68	5.97	3.24
CaO	1.33	0.71	3.54	2.21	2.23	2.23	4.86
Na ₂ O	3.08	3.48	3.83	3.73	3.75	3.75	2.25
K ₂ O	5.46	5.06	3.04	4.03	0.45	0.85	0.70
P ₂ O ₅	0.18	-	-	-	-	-	-

I - Average Calc-Alkali Granite (Nockolds, 1954).

J - Average Low Calcium Granite (Turekian and Wedepohl, 1961).

K - Average High Calcium Granite (Turekian and Wedepohl, 1961).

L - Average Granite (Vinogradov, 1962; Taylor, 1964).

M - Residuum, 3.6 Parts Condie's Average Graywacke (F) - 2 Parts
Vinogradov's and Taylor's Average Granite (L).

N - Residuum, 2 Parts Condie's Average Graywacke (F) - 1 Part
Vinogradov's and Taylor's Average Granite (L).

O - Residuum, 2 Parts Middleton's Average Eugeosynclinal Gray-
wacke (H) - 1 Part Turekian and Wedepohl's High Calcium
Granite (K).

* Total iron as Fe₂O₃.

(1961, Table 5.2, Column J), it is apparent from inspection that the K_2O contents of these granites are far too high to yield an amphibolite residuum when subtracted in any arbitrary proportion from average graywacke or average continental crust. The high calcium granite of Turekian and Wedepohl (1961, Table 5.2, Column K) and the average granite of Vinogradov (1962) and Taylor (1964, Table 5.2, Column 4) look more promising. Choosing proportions of graywacke (or alternatively average continental crust) and granite which when subtracted yield as close to an amphibolite residuum as possible, it is found that the residua bear some resemblance to andesites except for their extremely low CaO contents. For example, if 2 parts of Vinogradov and Taylor's average granite is subtracted from 3.6 parts of Condie's average Wyoming graywacke (Table 5.2, Column F) the residuum (Table 5.2, Column M) is similar in some respects to an andesite save the low CaO value.

Analogous difficulties are encountered in subtracting 1 part of this granite from 2 parts of Condie's graywacke (Table 5.2, Column N). Similarly, 1 part of Turekian and Wedepohl's high calcium granite subtracted from 2 parts of Middleton's average eugeosynclinal graywacke (Table 7.2, Column H) yields a residuum low in Al_2O_3 and CaO , high in SiO_2 for andesite (Table 5.2, Column O).

Obviously the residua generated by these models do not approximate the composition of basaltic amphibolite if in fact they approximate the composition of any geologic material. Because of the differentiated nature of continental crust relative to oceanic crust, it is perhaps not surprising that the calculated residua show a non-basaltic chemistry. Thus, the genesis of basaltic amphibolites as an end product of anatexis seems dubious. Nonetheless, anatectic melanosomes formed under less intense conditions where fusion is incomplete may have a more basic chemistry than their precursors (Chesworth, 1967).

To this point no mention has been made of Taylor's estimate of the composition of continental crust (Taylor, 1964). On the basis of rare earth distributions Taylor concluded that average continental crust is comprised of 1 part average granite and 1 part average basalt (Table 5.2, Column E). Clearly, partial melting of a rock of this composition could generate an amphibolite residuum. Whether rocks of this composition are geologically realistic is problematical however. Comparing Taylor's compositional estimate of the continental crust to others listed in Table 5.2, his estimate is seen to be low in SiO_2 and high in total iron magnesium and calcium. It is not certain which of these estimates is most nearly correct, but the weight of evidence does not favor Taylor's. In this light, the conclusions of the preceding paragraph remain substantially unchanged.

Conclusions:

The most probable origin for thick sequences of basaltic amphibolite is the metamorphism of intrusive and extrusive basic igneous rocks and, to a lesser degree, their derivative tuff and mafic graywackes. Thin basaltic amphibolites may be produced by the "metasomatic" models of Orville (1969) and Adams and Barlow (1910). Basaltic amphibolites are probably the most abundant type of amphibolite as the striking similarity of average amphibolite to average basalt suggests. It is this singular feature which is of most discriminatory value in deciphering the origin of a given amphibolite since it cannot be routinely developed by sedimentary processes. A basaltic chemistry with characteristic element ratio and element abundance patterns (to be discussed in the next section) are necessary and sufficient criteria to define an amphibolite as meta-igneous. Amphibolites which are non-basaltic in character may be produced by metamorphism of appropriate sediment or sediment and volcanic mixtures, certain metasomatic processes and possibly by partial melting of rocks intermediate in composition between granite and basalt. Quantitatively, these processes must be of limited importance because of the preponderance of basaltic amphibolites in metamorphic terrains.

5.1.2. Origin and Geochemistry of the Hermon Group Amphibolites

Field relations of the Hermon Group amphibolites allow certain inferences to be made regarding their origin. In general, these amphibolites occur as thick, unbanded units of massive to well foliated character, devoid of relict volcanic features and showing minor inter-banded sedimentary material. They are always concordant to gneissosity and generally show sharp contacts with adjacent lithologic units although gradational contacts have been observed. Because of their thicknesses (usually of the order of meters), the "metasomatic" models of amphibolite formation discussed above do not appear applicable. The field relations are consistent with the metamorphism of basaltic extrusives with associated mafic graywackes especially in view of their proposed correlation with the Hermon Group (especially the Tudor metavolcanics) to the east (Figure 3.1).

The basaltic nature of the Hermon Group amphibolites in the mapped area is confirmed by inspection of the analyses listed in Table 5.3¹. The accompanying norms reflect this basaltic chemistry particularly well in Figure 5.4 where the norms of various basalts, average amphibolite and the average Hermon Group amphibolite are

¹ A summary of analytical procedures and estimates of precision and accuracy are given in Appendix I and a sample location map, Figure 5.3, is provided in the map pocket.

Table 5.3: WHOLE ROCK ANALYSES OF HERMON GROUP AMPHIBOLITES

	STATEMENT OF DATA									
	1*	2*	11	17 ⁺	20	26	32*	34	41*	42
SiO ₂	47.930	49.000	52.150	48.700	47.300	50.550	48.930	44.950	46.780	47.800
TiO ₂	1.780	1.730	0.720	1.600	0.870	0.810	1.780	2.310	2.580	2.090
Al ₂ O ₃	14.320	15.060	12.440	15.600	16.950	12.620	14.120	15.740	15.100	13.920
Fe ₂ O ₃	4.940	4.640	1.970	3.300	2.550	3.990	1.850	5.160	3.210	5.580
FeO	7.480	7.720	4.880	8.740	4.920	6.700	9.660	8.160	9.410	6.640
MnO	0.210	0.210	0.140	0.200	0.120	0.140	0.270	0.230	0.220	0.180
MgO	8.460	6.050	8.620	5.400	8.560	10.150	7.530	7.940	8.210	7.930
CaO	8.460	9.340	9.100	10.300	11.420	8.680	9.260	7.470	9.320	7.840
Na ₂ O	4.710	3.580	3.120	3.760	4.100	3.140	3.030	3.880	2.460	4.220
K ₂ O	0.290	0.330	3.490	0.260	0.800	0.400	0.460	0.500	0.700	0.200
P ₂ O ₅	0.180	0.190	0.230	0.150	0.280	0.210	0.200	0.400	0.200	0.410
H ₂ O ⁺	0.000	0.000	-0.000	0.000	-0.000	-0.000	0.000	-0.000	0.000	-0.000
H ₂ O ⁻	0.000	0.000	-0.000	0.000	-0.000	-0.000	0.000	-0.000	0.000	-0.000
CO ₂	0.000	0.000	-0.000	0.000	-0.000	-0.000	0.000	-0.000	0.000	-0.000
S	-0.000	-0.000	-0.000	-0.000	-0.000	-0.000	-0.000	-0.000	-0.000	-0.000
BE	-0.000	-0.000	2.000	-0.000	1.600	1.900	-0.000	3.300	-0.000	4.200
GA	18.000	21.000	14.500	-0.000	12.500	13.300	19.000	23.000	16.000	21.000
CR	209.000	183.000	28.500	150.000	-0.000	130.000	235.000	51.000	229.000	41.000
V	470.000	460.000	325.000	433.000	116.000	118.000	600.000	180.000	482.000	215.000
LI	0.000	0.000	41.000	0.000	25.000	80.000	0.000	20.500	0.000	13.500
NI	100.000	64.000	12.000	46.000	-0.000	335.000	80.000	92.000	133.000	40.000
CU	44.000	50.000	11.500	-0.000	-0.000	11.500	234.000	11.100	57.000	7.500
Y	38.000	45.000	37.000	-0.000	-0.000	25.000	34.000	47.000	28.000	51.000
MN-SP	0.000	0.000	900.000	-0.000	720.000	820.000	0.000	1380.000	0.000	1020.000
SC	0.000	0.000	6.200	26.000	13.300	10.200	0.000	11.400	0.000	14.000
ZR	141.000	153.000	262.000	222.000	82.000	148.000	134.000	285.000	115.000	500.000
SR	251.000	332.000	240.000	240.000	-0.000	230.000	338.000	124.000	358.000	153.000
BA	163.000	215.000	470.000	46.000	140.000	155.000	210.000	120.000	260.000	59.000
RB	4.000	3.000	106.000	-0.000	6.000	15.000	4.000	27.000	-0.000	6.400
LA	9.000	8.000	-0.000	-0.000	-0.000	-0.000	8.000	-0.000	3.000	-0.000
CE	46.000	42.000	-0.000	-0.000	-0.000	-0.000	41.000	-0.000	44.000	-0.000
TH	3.000	3.000	-0.000	-0.000	-0.000	-0.000	3.000	-0.000	2.000	-0.000

* P. C. van de Kamp, Analyst.

+ J. R. Muysson, Analyst in Kudo (1962)

All other analyses by K. Ramlal.

Table 5.3 (continued)

	44	45	46	51	52	54
SI02	47.600	44.100	50.200	50.950	47.750	45.200
TI02	2.080	2.860	1.010	1.050	1.670	2.380
AL203	13.420	15.100	14.960	18.600	14.260	16.430
FE203	4.070	4.970	4.010	4.770	4.080	5.900
FE0	9.720	14.360	5.980	5.480	9.200	8.400
MN0	0.240	0.160	0.170	0.130	0.250	0.210
MG0	6.260	8.020	7.980	4.180	6.980	5.820
CA0	10.600	3.840	7.800	7.800	10.100	10.030
NA20	2.600	3.890	3.800	4.200	2.960	3.100
K20	0.600	0.040	0.970	0.700	0.320	0.300
P205	0.450	0.560	0.270	0.310	0.300	0.530
H20 +	-0.000	-0.000	-0.000	-0.000	-0.000	-0.000
H20 -	-0.000	-0.000	-0.000	-0.000	-0.000	-0.000
C02	-0.000	-0.000	-0.000	-0.000	-0.000	-0.000
S	-0.000	-0.000	-0.000	-0.000	-0.000	-0.000
BE	5.100	4.200	2.500	2.800	3.900	4.600
GA	23.000	24.000	18.000	23.000	16.500	34.000
CR	52.000	82.000	230.000	0.000	-0.000	165.000
V	310.000	243.000	220.000	250.000	285.000	340.000
LI	15.500	33.000	24.000	36.000	20.500	12.000
NI	18.200	115.000	143.000	1.500	70.000	92.000
CU	9.400	6.800	12.300	3.800	11.700	-0.000
Y	61.000	41.000	27.000	45.000	51.000	-0.000
MN-SP	1850.000	1000.000	900.000	920.000	1050.000	1080.000
SC	20.500	10.800	20.000	11.000	-0.000	19.500
ZR	355.000	378.000	110.000	212.000	210.000	335.000
SR	240.000	125.000	238.000	340.000	173.000	238.000
BA	140.000	-0.000	250.000	140.000	80.000	42.000
RB	20.000	0.000	28.600	22.500	6.400	0.000
LA	-0.000	-0.000	-0.000	-0.000	-0.000	-0.000
CE	-0.000	-0.000	-0.000	-0.000	-0.000	-0.000
TH	-0.000	-0.000	-0.000	-0.000	-0.000	-0.000

Analyses by K. Ramlal

0.000 and -0.000 signify either no information or below detection limit

Major elements in weight percent; trace elements in ppm. in this table and tables 5.5 and 5.8.

Table 5.3: NORMS AND MODES OF THE HERMON GROUP AMPHIBOLITES

	Norms																
	1	2	11	17	20	26	32	34	41	42	44	45	46	51	52	54	Mean
Quartz	0.00	0.00	0.00	0.00	0.00	0.00	0.00	0.00	0.00	0.00	0.00	0.00	0.00	1.12	0.00	0.00	0.00
Corundum	0.00	0.00	0.00	0.00	0.00	0.00	0.00	0.00	0.00	0.00	0.00	2.95	0.00	0.00	0.00	0.00	0.00
Orthoclase	1.74	2.00	21.31	1.57	4.85	2.43	2.80	3.06	4.26	1.22	3.64	0.24	5.91	4.22	1.93	1.81	3.94
Albite	32.94	30.96	21.67	32.46	17.91	27.28	26.40	31.77	21.42	36.88	22.53	33.62	33.09	36.20	25.59	26.68	30.59
Anorthite	17.34	24.58	9.94	25.43	26.04	19.67	24.28	24.87	28.91	19.06	23.74	16.10	21.51	30.39	25.22	30.55	23.51
Nepheline	4.07	0.00	3.02	0.00	9.50	0.00	0.00	1.18	0.00	0.00	0.00	0.00	0.00	0.00	0.00	0.00	0.00
Clino- wollastonite	10.10	9.03	14.73	10.78	12.60	9.72	9.12	4.60	7.29	7.78	11.45	0.00	6.92	2.99	10.10	7.06	8.16
Clino- enstatite	6.90	5.59	10.38	5.73	9.04	6.78	5.05	3.10	4.31	5.74	6.34	0.00	4.81	1.93	5.85	4.46	5.15
Clino- ferrosilite	2.41	2.92	3.10	4.71	2.42	2.13	3.71	1.15	2.62	1.30	4.67	0.00	1.53	0.86	3.78	2.16	2.51
Enstatite	0.00	8.22	0.00	0.70	0.00	15.97	8.28	0.00	7.55	5.16	9.24	9.10	7.63	8.67	7.38	4.31	3.70
Ferrosilite	0.00	4.30	0.00	0.58	0.00	5.01	6.08	0.00	4.59	1.17	6.81	8.13	2.43	3.86	4.77	2.08	1.81
Forsterite	9.67	1.12	8.26	5.11	8.93	2.24	4.19	12.15	6.43	6.66	0.28	7.92	5.61	0.00	3.18	4.19	6.96
Fayalite	3.71	0.64	2.72	4.63	2.64	0.78	3.39	4.97	4.31	1.66	0.22	7.80	1.97	0.00	2.26	2.23	3.75
Magnetite	7.27	6.88	2.95	4.88	3.78	5.94	2.76	7.73	4.79	8.36	6.04	7.36	5.98	7.05	6.04	8.70	6.03
Ilmenite	3.43	3.36	1.41	3.10	1.69	1.58	3.48	4.54	3.09	4.10	4.05	5.55	1.97	2.03	3.24	4.60	3.21
Apatite	0.40	0.42	0.52	0.33	0.63	0.47	0.45	0.90	0.45	0.93	1.01	1.25	0.65	0.69	0.67	1.18	0.69

Table 5.3 (continued)

	<u>Modes</u>																
	1†	2†	11	17	20	26	32†	34	41†	42	44	45	46	51	52	54	Mean
Hornblende	60.0	59.6	66.0	44.8	53.2	37.2	55.0	47.0	60.0	45.0	68.8	21.0	41.2	31.0	66.6	67.8	51.5
Clino- pyroxene	-	-	-	4.8	-	-	-	-	-	-	-	-	-	-	-	-	0.3
Cummingto- nite	-	-	-	-	-	15.2	-	6.4	-	-	-	36.6	-	-	-	-	3.6
Plagioclase	35.0	34.5	30.4	41.0	41.2	39.6	35.0	35.8	32.0	37.0	21.4	27.4	43.0	58.2	26.0	29.4	35.4
Scapolite	-	-	-	-	3.4	-	-	-	-	-	-	-	-	-	-	-	0.2
Biotite	0.1	0.1	0.4	-	-	2.8	2.0	-	2.0	1.0	3.4	-	6.4	5.0	0.2	0.4	1.5
Chlorite	-	-	-	-	-	-	4.0	2.0	-	5.8	-	-	3.2	-	-	-	0.9
Oxides	4.0	3.3	2.8	0.4	-	1.2	2.0	5.6	1.0	6.4	2.6	15.0	3.8	3.8	2.2	2.4	3.5
Epidote	-	-	-	1.6	-	-	-	-	-	-	-	-	-	-	-	-	0.1
Tourmaline	-	-	-	-	-	2.4	-	0.4	-	0.2	-	-	-	-	-	-	0.2
Quartz	1.0	1.6	-	-	-	1.0	-	0.8	3.0	1.6	1.4	-	0.4	0.8	4.6	-	1.0
Sphene	-	0.2	0.4	3.2	0.4	-	-	-	-	-	2.2	-	-	-	-	-	0.4
Carbonate	-	0.7	-	4.2	1.8	0.6	0.5	2.0	-	3.0	0.2	-	2.2	-	0.4	-	1.0
Plag. Comp.	-	An ₄₂	An ₄₇	An ₄₆	An ₅₄	An ₃₈	-	An ₄₀	-	An ₃₃	An ₄₀	An ₄₀	An ₄₂	An ₅₄	An ₃₆	An ₅₈	An ₄₄

† Taken from van de Kamp (1968)

Table 5.3: CALCULATED DATA

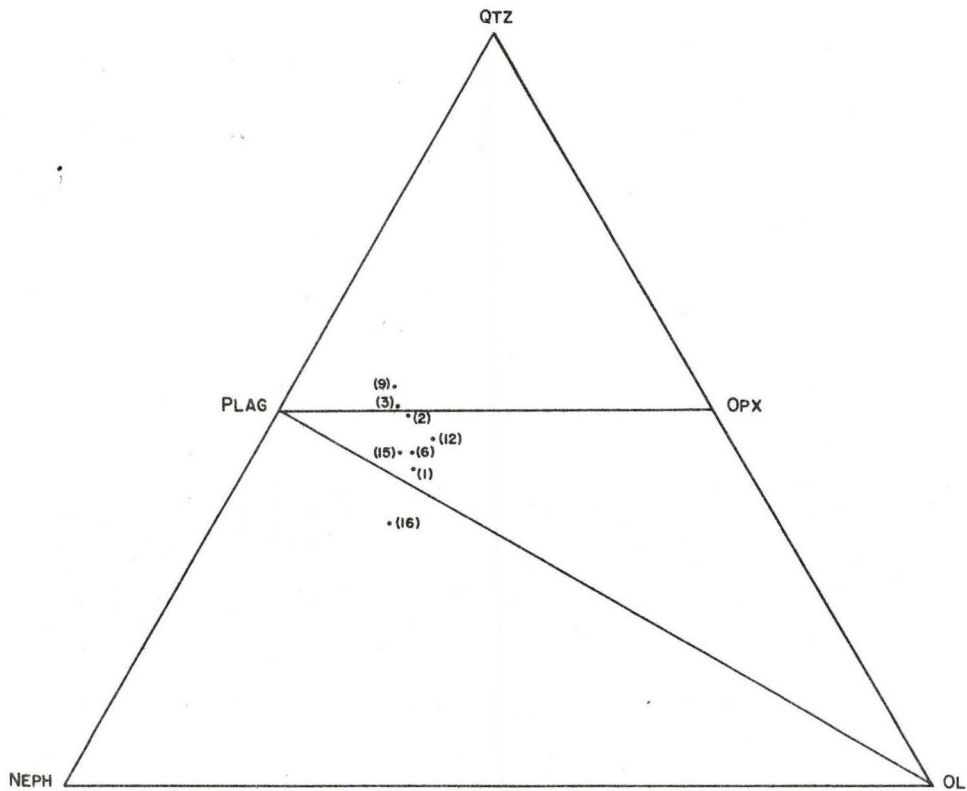
	<u>1</u>	<u>2</u>	<u>11</u>	<u>17</u>	<u>20</u>	<u>26</u>	<u>32</u>	<u>34</u>	<u>41</u>
Oxidation Ratio	37.2	35.1	26.7	25.4	31.8	34.9	14.6	36.2	23.4
K	2400	2700	29,000	2200	6600	3300	3800	4200	5800
Ca	60,100	66,300	64,600	73,100	81,100	61,600	65,700	53,000	66,200
K/Rb	600	900	274	-	1100	220	950	156	290
Ca/Sr	239	200	269	305	-	268	194	427	185
Rb/Sr	0.016	0.009	0.442	-	-	0.065	0.012	0.218	0.056
Ba/Sr	0.65	0.65	1.96	0.19	-	0.67	0.62	0.97	0.73
Ba/Rb	40.75	71.67	4.43	-	23.33	10.33	52.50	4.44	13.00
La/Ce	0.20	0.19	-	-	-	-	0.20	-	0.07
Fe Total	92,800	92,500	51,800	91,100	56,200	80,000	88,100	99,600	95,700
Fe Total/ Σ Cr+V+Ni	119	131	142	145	-	137	96	308	113

Table 5.3: (continued)

	<u>42</u>	<u>44</u>	<u>45</u>	<u>46</u>	<u>51</u>	<u>52</u>	<u>54</u>	<u>Mean</u>
Oxidation Ratio	43.0	27.3	23.7	37.6	43.9	28.5	38.7	
K	1700	5000	300	8100	5800	2600	2500	5400
Ca	55,700	75,300	27,300	55,400	55,400	70,700	70,200	62,800
K/Rb	283	250	-	300	252	433	-	257
Ca/Sr	364	314	218	233	163	409	295	272
Rb/Sr	0.039	0.083	-	0.122	0.068	0.035	-	0.097
Ba/Sr	0.39	0.58	-	1.05	0.41	0.46	0.18	0.68
Ba/Rb	9.83	7.00	-	8.62	6.09	13.33	-	20.41
La/Ce	-	-	-	-	-	-	-	0.17
Fe Total	90,700	104,100	146,500	74,600	76,000	100,100	106,600	90,400
Fe Total/ Σ Cr+V+Ni	306	273	333	126	-	-	179	167

All values in parts per million

Oxidation Ratio = molecular % $\frac{2\text{Fe}_2\text{O}_3 \times 100}{2\text{Fe}_2\text{O}_3 + \text{FeO}}$ (after Chinner, 1960)



- (1) Average Hermon Amphibolite
- (2) Average of 262 Amphibolites (van de Kamp, 1964)
- (3) Average of Oceanic Tholeiitic Basalt (Engel et al, 1965)
- (6) Average Gabbro (Manson, 1969)
- (9) Average Qtz. Basalts + Qtz. Dolerites (Manson, 1967)
- (12) Average Ol. Tholeiitic Basalts + Ol. Dolerites (Manson, 1967)
- (15) Average Ol. Alkali Basalts + Ol. Alkali Dolerites (Manson, 1967)
- (16) Average Neph. Basalts + Neph. Dolerites (Manson, 1967)

Figure 5.4: Norms of Basalts and Amphibolites Projected onto Base of Haplobasalt Tetrahedron of Yoder and Tilley (1962)

projected onto the base of the simplified haplobasalt tetrahedron (Yoder and Tilley, 1962). From this diagram and comparison of columns A and C, Table 5.1, the similarity of the average Hermon Group amphibolite and average alkali-olivine basalt is apparent. This similarity is not without exception as analysis 11, Table 5.3 shows. The high values of K_2O and SiO_2 coupled with low total iron and alumina suggest either the addition of pelitic material to an original basaltic composition or a pelite-dolomite mixture similar to Column P, Table 5.1. This occurrence will be discussed further under quartzofeldspathic gneiss origins.

Further hints of an igneous lineage for the Hermon Group amphibolites are provided by the projections of Moine and de la Roche (1968) and Shaw (in preparation). The former study shows the clear basaltic affinities of the amphibolites (Figure 5.2). The latter projection, a modification of that devised by Köhler and Raaz (1951), classifies the amphibolites as either basalts of alkalic character (Figure 5.5) or as carbonate sediments (Figure 5.6). This overlap is a function of the projection since the Hermon amphibolites are certainly not carbonate metasediments.

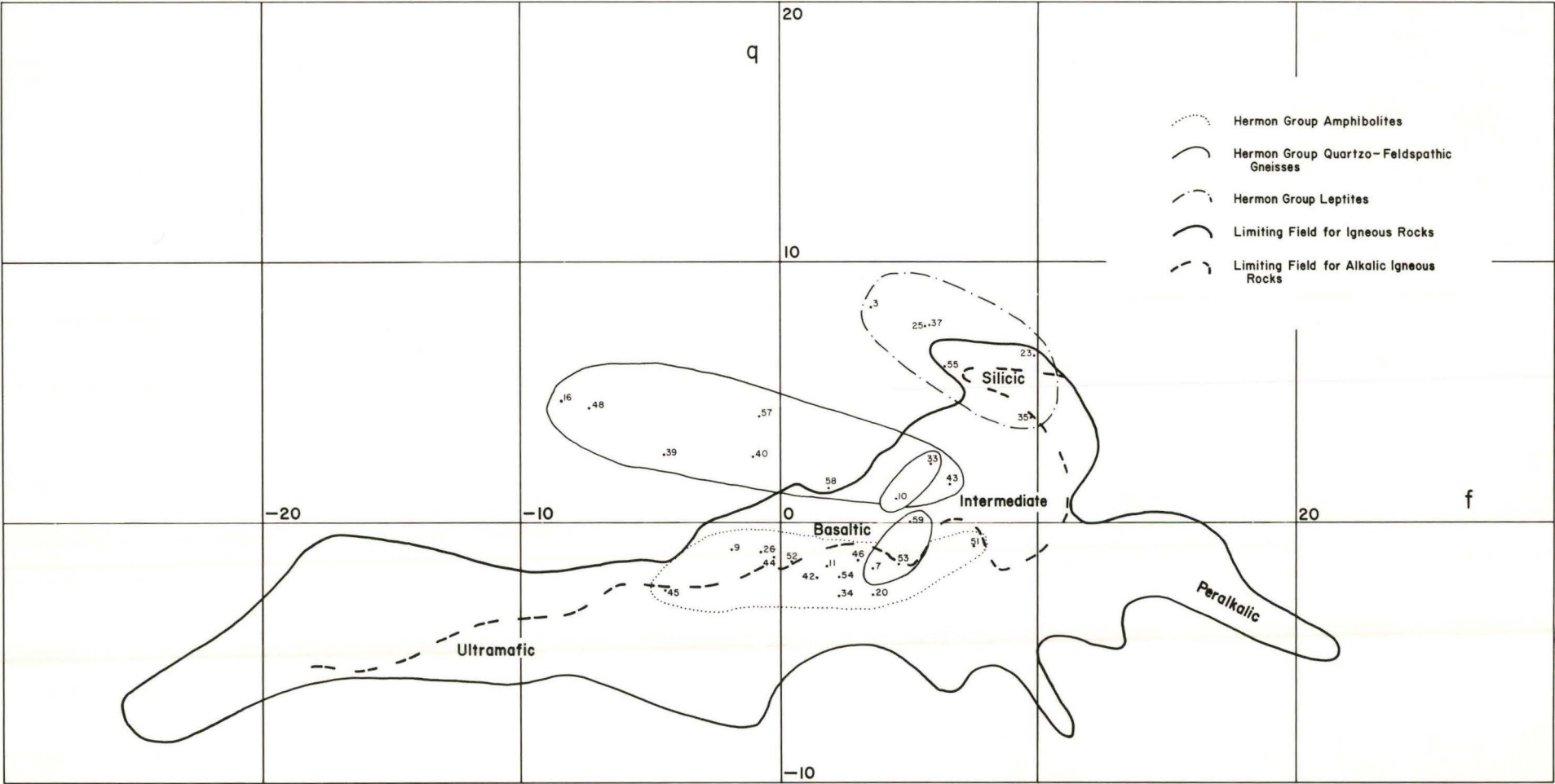


Figure 5.5: Modified Köhler-Raaz Diagram Showing Compositional Fields for 560 Igneous Rocks and the Analysed Hermon Group Rocks (after Shaw, in preparation)

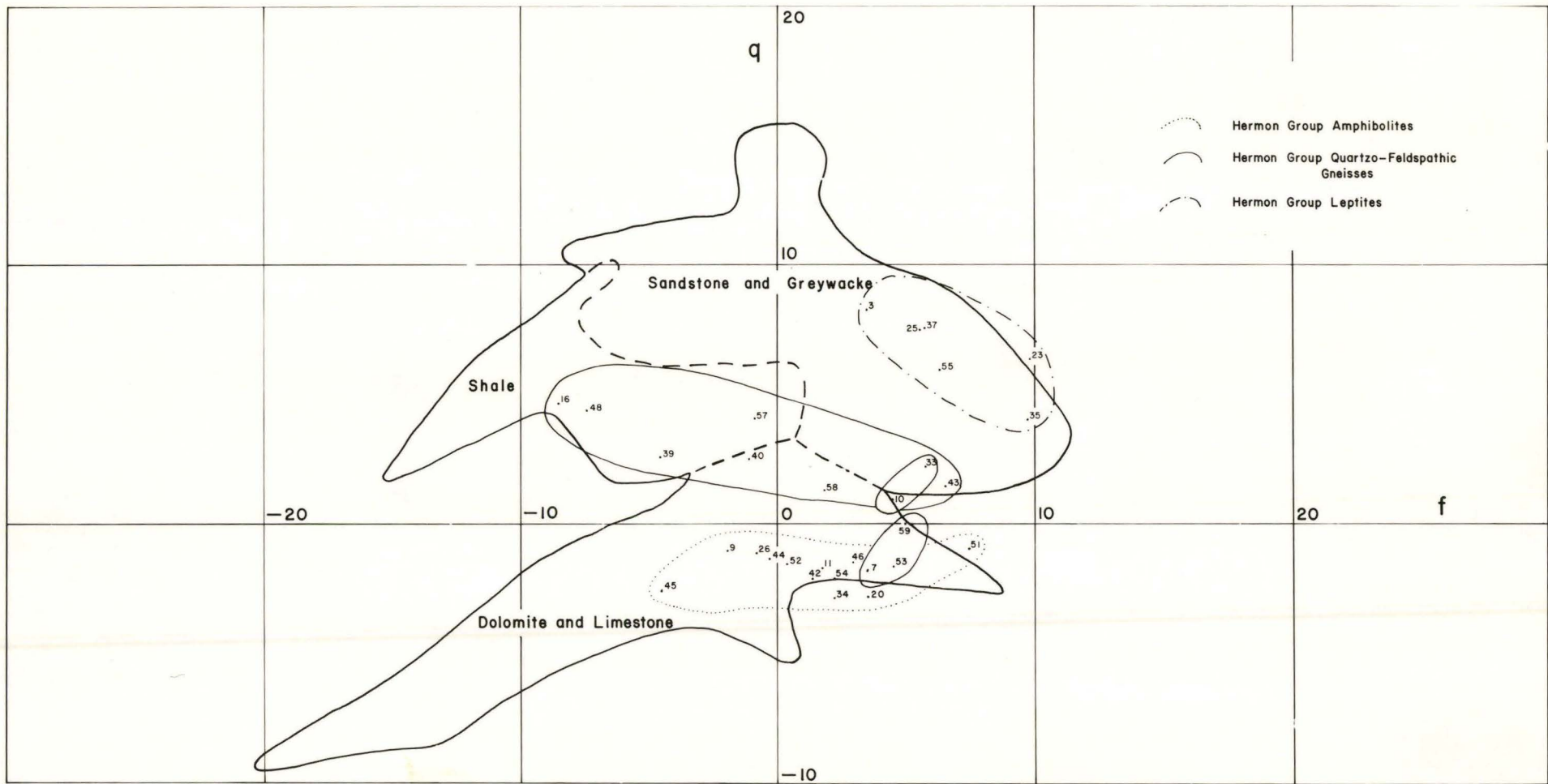


Figure 5.6: Modified Köhler-Raaz Diagram Showing Compositional Fields for 678 Sedimentary Rocks and the Analysed Hermon Group Rocks (after Shaw, in preparation)

In order to demonstrate the trace element similarity of the amphibolites to basalt, three approaches have been used. The ratio of two elements in a rock (either two trace or a trace and major element pair) showing strong geochemical coherence but which fractionate differently in geological processes is a potentially strong indicator of the genetic history of the rock. A number of these ratios might then be used to support a mode of origin for a given rock sequence. These ratios coupled with ratio data for element pairs concentrating in different stages of a differentiation sequence and general trace element abundance data should reveal a convincing protolith for the Hermon Group amphibolites.

The element ratios used in this study include Rb/Sr, Ba/Sr, Ba/Rb, Ca/Sr, K/Rb, La/Ce and $\frac{\text{Fe total}}{\sum \text{Cr+V+Ni}}$. As in parts of the preceding discussion, various estimates of average rock type compositions have been used to establish approximate ranges for a given rock type and trends of variation between rock types for a given ratio. The data thus accumulated are presented in Table 5.4 along with abundance data for thorium, chromium, vanadium and nickel. The very approximate nature of this appraisal is appreciated, but the general trends of variation of the ratio and abundance data with varying rock type are considered significant.

Table 5.4: ELEMENT RATIOS AND TRACE ELEMENT ABUNDANCE DATA FOR VARIOUS ROCK TYPES INCLUDING THE

Rock Type	HERMON GROUP AMPHIBOLITES									
	Rb/Sr	Ba/Sr	Ba/Rb	Ca/Sr	La/Ce	Th	Cr	V	Ni	$\frac{Fe_T}{\sum Cr+V+Ni}$
Gabbro, basalt	0.06 ^a -0.10 ^g	0.54 ^d -0.71 ⁱ	6.00 ^g -11.00 ⁱ	129 ^f -166 ^d	0.14 -0.42 ^c	0.18 -5.4 ^e	168 ^a -300 ^g	200 ^g -250 ^{d,i}	90 ^a -160 ^g	119 ^d -165 ^f
Diorite, andesite	0.09 ^g -0.18 ^b	0.70 -0.81 ^g	9.29 ^g -11.4 ^d	58 ^g -177 ^d	0.39 -0.71 ^d	0.5 -4.7 ^d	56 ^g -153 ^d	100 ^g -173 ^d	49 ^d -55 ^g	277 ^g -375 ^d
Grano- diorite	0.25 ^{di} -0.28 ^b	0.95 ⁱ -1.14 ^d	3.82 ⁱ - 4.50 ^d	58 ^{d,i}	0.38 -0.74 ^c	8.5 ⁱ -14 ^d	22 ⁱ - 30 ^d	75 ^d -88 ⁱ	15 ^{d,i}	237 ⁱ -245 ^d
Granite, rhyolite	0.51 ^d -1.70 ⁱ	2.10 ^d -8.40 ⁱ	2.08 ^g - 4.94 ⁱ	43 -60 ^h	0.28 -0.76 ^e	8.0 -56.0 ^e	4 ⁱ -25 ^g	40 ^{d,g} -44 ⁱ	4 ^d -15 ⁱ	268 ⁱ -467 ^d
Carbon- ates	0.005 ⁱ -0.008 ^b	0.02 ⁱ	3.33 ⁱ	495 ⁱ -656 ^h	0.50 ^c	0.05 -2.5 ^e	11 ⁱ	20 ⁱ	20 ⁱ	75 ⁱ
Pelites	0.47 ⁱ -0.89 ^g	1.78 -1.93 ⁱ	200 ^g -4.14 ⁱ	56 ^g -167 ^h	0.39 -0.72 ^c	10 -13 ^e	90 ⁱ -160 ^g	130 ^{g,i}	68 ⁱ -95 ^g	86 ^g -164 ⁱ
Gray- wackes	-	1.5 ^j	-	1950 ⁱ	0.73 ^c	6.7 ^e	35 ⁱ -140 ^j	20 ⁱ -67 ^j	2 ⁱ -43 ^j	172 ⁱ
Arkoses	-	2.0 ^j	-	-	-	5 ^e	88 ^j	43 ^j	27 ^j	-
Hermon Group* Amphibolites	0.10	0.68	20.41	272	0.17	3	137	315	89	167

a Prinz (1967); b Faure and Hurley (1963); c Haskin et al. (1966); d Taylor and White (1966); e Herrmann (in press);
f Manson (1967) and Prinz (1967); g Vinogradov (1956); h Turekian and Kulp (1956); i Turekian and Wedepohl (1961); j Weber and Middleton (1961)

* Calculated from arithmetic means of data in Table 5.3.

Inspection of Table 5.4 shows a strong similarity between the Hermon Group amphibolites and basic igneous rocks in terms of the various element ratios and thorium abundance levels. Cr and Ni are seen to be depleted in the amphibolites while they are enriched in V with respect to basic igneous rocks. It is important to note that particularly the ratio values cannot be generated by simple physical mixing of "end member" sediments or volcanics, thus militating strongly against a sedimentary origin for at least the bulk of the Hermon Group amphibolites. In fact, the "metasomatic" processes of amphibolite formation previously discussed may not fractionate trace elements in a manner similar to basaltic distributions providing a means of discriminating magmatic from "metasomatic" amphibolites in the absence of other criteria.

The Ba/Sr and Ca/Sr ratios in Table 5.4 and some of the K/Rb ratios in Figure 5.7 for the Hermon Group amphibolites imply a fairly primitive chemistry, not far removed from that of oceanic tholeiites. While it is not suggested that the amphibolites resemble oceanic tholeiites in overall aspect and history, their primitive character makes origins other than igneous ones, unlikely.

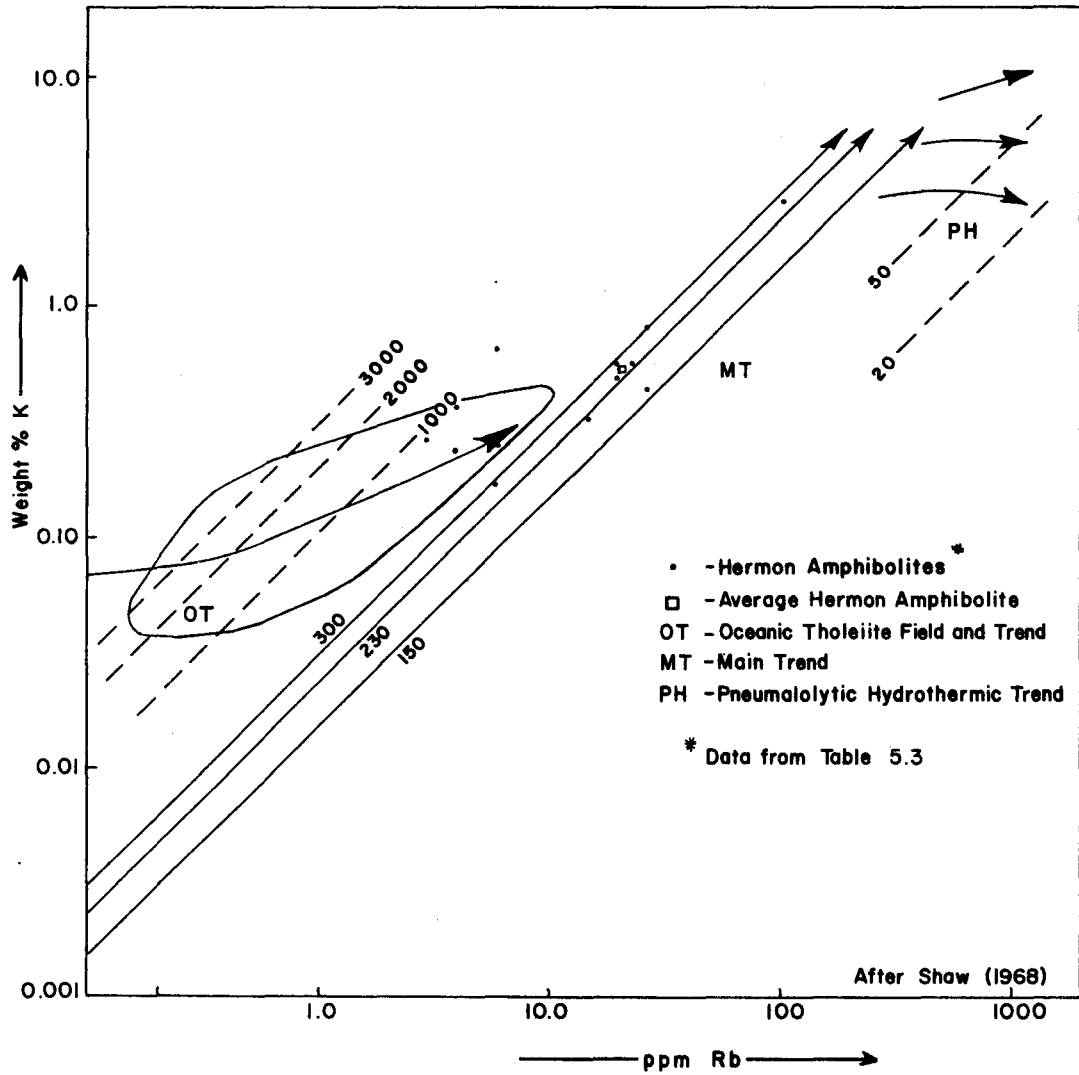


Figure 5.7 Potassium-Rubidium Covariance in the Hermon Group Amphibolites

Viewing the field and chemical data together in light of the discussion of amphibolite origins, the Hermon Group amphibolites most probably represent an isochemically metamorphosed series of basaltic flows and minor derivative mafic sediments similar to alkali-olivine basalts. Their position and role in the development of the Hermon Group supracrustal sequence will be considered more fully in terms of a depositional model in the concluding chapter.

5.2. Quartzo-Feldspathic Gneisses

Field relations have a considerable bearing on the origin of this lithologic unit. Simple cross bedding in the thick gneiss unit northeast of Silent Lake (Figure 2.1) and graded bedding in this same unit northeast of Port Hope Lake are suggestive of a sedimentary history as are scattered occurrences of ortho-quartzite in the gneisses of central northwestern Chandos township. In general, these gneisses show a conspicuous lateral gradation into leptite throughout the entire map area. Compositional banding is also characteristic of this unit. Contacts between quartzo-feldspathic gneiss and other lithologies show fairly consistent relations with sharp gneiss-amphibolite contacts and gradational contacts between gneiss and leptite. In light of this evidence, a sedimentary history for at least some of the quartzo-feldspathic gneisses must be admitted.

Since sedimentary structures are not found in all or even most gneissic units, whole rock analyses will be used in an attempt to establish an origin for this rock type as a whole. Specimens for analysis were selected to proportionally represent the most common gneiss varieties defined in the field. Analyses, norms, modes, and calculated data of thirteen such specimens are given in Table 5.5. Inspection of this table shows the extreme compositional variability in this general map unit. In order to determine whether discreet compositional subgroups occur within the broad category "quartzo-feldspathic gneiss", the CIPW norms in Table 5.5 as well as norms of common volcanic and sedimentary rocks have been plotted in a normative tetrahedron with the components QTZ, PLAG, OR and FEM as apices (Figures 5.8 and 5.9). From these diagrams two broad compositional groupings are found, one silica-rich, the other silica-poor. This latter group is tentatively divided into three subgroups, sodic, mafic and potassic gneisses as shown in Figure 5.9 and arranged in Table 5.5. In view of the extreme compositional variability of the gneisses in general, it is possible that compositions intermediate to all these groups could be found upon detailed sampling. Thus, the normatively defined groups are designated for convenience of treatment and may not prove valid subdivisions upon additional analytical study. For the

Table 5.5: ANALYSES OF QUARTZO-FELDSPATHIC GNEISSES

	STATEMENT OF DATA									
	Silica Rich							Sodic		
	16	39	40	43	48	57	58	7	53	59
SI02	62.200	57.600	58.950	59.050	62.500	63.300	58.500	51.050	48.600	53.900
TI02	1.100	1.260	0.900	0.790	1.070	0.920	1.040	2.430	1.710	2.380
AL203	18.070	16.760	16.320	13.160	16.100	15.150	16.900	22.430	20.050	14.200
FE203	5.300	1.350	7.560	4.920	6.880	3.660	2.590	1.980	11.410	3.260
FE0	2.640	9.120	1.780	6.440	1.700	3.400	7.100	5.840	2.140	9.180
MN0	0.110	0.190	0.170	0.510	0.100	0.130	0.050	0.100	0.120	0.260
MG0	2.120	3.840	3.760	1.520	3.500	3.700	2.640	2.220	1.890	3.240
CA0	1.240	2.780	2.570	3.800	1.090	2.720	1.800	2.600	4.080	5.330
NA20	1.300	2.080	1.840	3.220	1.470	1.730	3.490	4.420	4.300	3.940
K20	3.840	2.540	3.920	3.450	3.520	3.180	3.810	5.300	2.880	1.510
P205	0.270	0.340	0.220	0.220	0.230	0.220	0.220	0.560	0.380	0.590
H20 +	-0.000	-0.000	-0.000	-0.000	-0.000	-0.000	-0.000	-0.000	-0.000	-0.000
H20 -	-0.000	-0.000	-0.000	-0.000	-0.000	-0.000	-0.000	-0.000	-0.000	-0.000
C02	-0.000	-0.000	-0.000	-0.000	-0.000	-0.000	-0.000	-0.000	-0.000	-0.000
S	-0.000	-0.000	-0.000	-0.000	-0.000	-0.000	-0.000	-0.000	-0.000	-0.000
BE	3.800	2.700	3.300	7.100	3.000	3.000	3.600	4.700	2.500	2.800
GA	24.500	21.000	24.000	30.500	22.000	32.000	31.000	27.000	-0.000	23.000
CR	60.000	68.000	41.000	0.000	-0.000	96.000	95.000	61.000	-0.000	0.000
V	130.000	-0.000	142.000	21.000	118.000	154.000	165.000	400.000	188.000	182.000
LI	20.000	34.000	48.000	12.500	33.000	37.000	40.000	25.000	23.000	16.700
NI	16.200	30.000	26.000	21.000	22.000	24.000	23.000	15.500	19.400	0.000
CU	-0.000	-0.000	2.900	13.300	4.700	6.000	0.000	75.000	-0.000	4.200
Y	-0.000	72.000	45.000	108.000	62.000	46.000	54.000	41.000	45.000	83.000
MN-SP	960.000	1150.000	1100.000	3600.000	460.000	840.000	220.000	630.000	580.000	1450.000
SC	11.700	17.500	11.000	10.200	-0.000	0.000	13.000	36.000	21.600	13.700
ZR	349.000	500.000	295.000	6800.000	315.000	270.000	345.000	315.000	-0.000	475.000
SR	157.000	-0.000	124.000	-0.000	-0.000	133.000	99.000	173.000	-0.000	182.000
BA	360.000	252.000	490.000	880.000	390.000	330.000	190.000	9999.990	160.000	320.000
RB	125.000	82.000	155.000	141.000	142.000	175.000	200.000	121.000	84.000	50.000

Analyses by K. Ramlal

Table 5.5 (continued)

	Mafic	Potassic	
	9	10	33
SI02	51.650	56.850	63.150
TI02	0.700	1.620	1.010
AL203	11.060	16.400	16.980
FE203	2.710	0.900	3.810
FE0	5.320	8.440	1.120
MN0	0.170	0.080	0.030
MG0	8.980	1.800	0.440
CA0	12.800	2.100	0.220
NA20	1.160	0.780	1.600
K20	3.720	8.280	9.340
P205	0.240	0.250	0.200
H20 +	-0.000	-0.000	-0.000
H20 -	-0.000	-0.000	-0.000
C02 -	-0.000	-0.000	-0.000
S	-0.000	-0.000	-0.000
BE	2.000	2.400	3.200
GA	16.000	23.000	18.000
CR	23.000	68.000	42.000
V	103.000	200.000	165.000
LI	20.500	28.000	21.500
NI	12.400	26.000	5.300
CU	5.000	6.500	13.700
Y	28.000	32.000	47.000
MN-SP	1140.000	560.000	145.000
SC	9.800	19.000	13.300
ZR	247.000	262.000	365.000
SR	162.000	182.000	92.000
BA	745.000	850.000	270.000
RB	100.000	198.000	176.000

Analyses by K. Ramlal

0.000 and -0.000 signify either no information or below detection limit

Table 5.5: NORMS AND MODES OF THE HERMON GROUP QUARTZO-FELDSPATHIC GNEISSES

	Norms												Grand Mean	Mean Silica Rich	Mean Silica Poor	Mean Sodic	Mean Mafic	Mean Potassic	
	16	39	40	43	48	57	58	7	53	59	9	10							33
Quartz	35.44	19.08	23.14	15.70	34.12	29.95	12.38	0.00	2.01	7.10	0.00	8.69	17.81	14.94	24.68	3.93	2.14	0.00	13.90
Corundum	10.29	6.40	4.95	0.00	8.54	4.47	4.31	5.96	3.34	0.00	0.00	2.94	4.35	2.52	5.24	0.00	2.46	0.00	3.66
Orthoclase	23.13	15.35	23.66	21.02	21.21	19.17	22.96	31.69	17.46	9.13	22.34	50.23	56.43	25.66	20.96	31.20	19.46	21.86	53.33
Albite	11.20	17.98	15.89	28.06	12.67	14.92	30.09	33.47	37.29	34.09	9.96	6.77	13.83	20.81	18.66	23.30	36.36	16.65	10.30
Anorthite	4.65	12.05	11.69	11.60	4.13	12.44	7.78	9.71	18.46	16.98	14.19	9.18	0.00	15.01	10.10	18.95	17.16	12.06	4.51
Nepheline	0.00	0.00	0.00	0.00	0.00	0.00	0.00	2.35	0.00	0.00	0.00	0.00	0.00	0.00	0.00	0.00	0.00	1.02	0.00
Clino- wollastonite	0.00	0.00	0.00	2.71	0.00	0.00	0.00	0.00	0.00	2.72	20.40	0.00	0.00	0.00	0.00	0.71	0.00	17.58	0.00
Clino- enstatite	0.00	0.00	0.00	0.94	0.00	0.00	0.00	0.00	0.00	1.17	14.36	0.00	0.00	0.00	0.00	0.44	0.00	12.38	0.00
Clino- ferrosilite	0.00	0.00	0.00	1.84	0.00	0.00	0.00	0.00	0.00	1.55	4.30	0.00	0.00	0.00	0.00	0.23	0.00	3.70	0.00
Enstatite	5.38	9.77	9.56	2.96	8.88	9.39	6.70	0.00	4.82	7.08	2.24	4.60	1.12	7.75	7.65	7.43	6.21	0.00	2.85
Ferrosilite	0.00	14.21	0.00	5.79	0.00	1.98	9.45	0.00	0.00	9.41	0.67	12.54	0.00	3.70	3.38	3.88	2.68	0.00	4.87
Forsterite	0.00	0.00	0.00	0.00	0.00	0.00	0.00	3.92	0.00	0.00	4.28	0.00	0.00	0.00	0.00	0.00	0.00	7.05	0.00
Fayalite	0.00	0.00	0.00	0.00	0.00	0.00	0.00	4.11	0.00	0.00	1.41	0.00	0.00	0.00	0.00	0.00	0.00	2.32	0.00
Magnetite	5.78	2.00	3.76	7.35	2.76	5.41	3.83	2.90	2.39	4.83	3.99	1.34	0.80	6.41	6.82	5.93	8.20	3.47	3.50
Hematite	1.41	0.00	5.12	0.00	5.11	0.00	0.00	0.00	10.05	0.00	0.00	0.00	3.34	0.00	0.00	0.00	0.00	0.00	0.00
Ilmenite	2.13	2.45	1.74	1.55	2.07	1.78	2.01	4.67	3.33	4.62	1.35	3.16	1.96	2.52	1.96	3.18	4.20	1.36	2.57
Apatite	0.60	0.76	0.49	0.50	0.51	0.49	0.49	1.24	0.85	1.31	0.53	0.56	0.45	0.67	0.56	0.83	1.14	0.54	0.51

Table 5.5 (continued)

	<u>Modes</u>													Mean Silica Rich	Mean Silica Poor	Mean Sodic	Mean Mafic	Mean Potassic
	16	39	40	43	48	57	58	7	53	59	9	10	33					
Plagioclase	33.6	57.0	56.4	58.8	44.8	61.0	56.6	36.6	51.8	47.4	11.2	26.6	10.6	52.6	30.7	45.3	20.8	18.6
K-feldspar	2.0	-	0.6	8.6	-	-	-	24.0	5.6	-	5.6	35.2	49.6	1.6	20.0	9.9	2.8	42.4
Quartz	10.4	5.6	5.6	2.8	4.2	4.2	8.8	4.0	3.2	1.4	-	1.2	18.0	5.9	4.6	2.9	-	9.6
Biotite	7.2	28.0	31.8	14.8	22.6	31.6	34.2	23.8	9.0	21.2	0.2	24.6	8.0	24.3	14.5	18.0	0.3	16.3
Muscovite	35.8	1.8	2.6	-	22.6	1.8	0.4	8.8	14.6	-	-	1.2	12.4	9.3	6.2	7.8	-	6.8
Sillimanite	6.0	0.4	-	-	3.2	-	-	-	-	-	-	-	-	1.4	-	-	-	-
Garnet	-	6.8	-	2.2	-	-	-	-	-	-	-	9.4	-	1.3	1.6	-	-	4.7
Hornblende	-	-	-	1.6	-	-	-	-	-	24.6	42.2	-	-	0.2	11.1	8.2	54.1	-
Clinopyroxene	-	-	-	-	-	-	-	-	-	-	31.8	-	-	-	5.3	-	15.9	-
Oxides	4.8	0.2	2.8	4.8	2.6	1.2	-	2.8	15.2	2.6	-	1.6	1.4	2.3	3.9	6.9	1.4	1.5
Scapolite	-	-	-	-	-	-	-	-	-	-	4.8	-	-	-	0.8	-	2.4	-
Chlorite	-	-	-	-	-	-	-	-	-	-	-	-	-	-	-	-	-	-
Tourmaline	0.2	0.2	-	-	-	0.2	-	-	0.2	-	1.0	0.2	-	0.1	0.2	0.1	0.5	0.1
Carbonate	-	-	-	5.2	-	-	-	-	0.4	2.8	3.2	-	-	0.7	1.1	1.1	1.6	-
Sphene	-	-	-	-	-	-	-	-	-	-	-	-	-	-	-	-	0.2	-
Epidote	-	-	0.2	1.2	-	-	-	-	-	-	-	-	-	0.2	-	-	-	-
Plag. Comp.	An ₃₆	An ₄₆	An ₃₃	An ₂₈	An ₃₅	An ₄₃	An ₃₂	An ₃₅	An ₃₆	An ₃₅	An ₄₀	An ₃₀	An ₃₀	An ₃₆	An ₃₄	An ₃₅	An ₄₄	An ₃₀

Table 5.5: CALCULATED DATA

	<u>16</u>	<u>39</u>	<u>40</u>	<u>43</u>	<u>48</u>	<u>57</u>	<u>58</u>	<u>7</u>	<u>53</u>	<u>59</u>
Oxidation Ratio	64.4	11.7	79.3	40.7	78.5	49.1	24.6	23.3	82.8	24.2
K	31,872	21,082	35,536	28,635	29,216	26,394	31,623	44,000	23,904	12,533
K/Rb	255	257	210	203	206	151	158	364	285	251
Rb/Sr	0.80	-	1.25	-	-	1.32	2.02	0.70	-	0.27
Ba/Rb	2.88	3.07	3.16	6.24	2.75	1.89	0.95	-	1.90	6.40
Ba/Sr	2.29	-	3.95	-	-	2.48	1.92	-	-	1.76
Sc/Y	-	0.24	0.24	0.09	-	-	0.24	0.87	0.48	0.17
Fe _{Total}	82,500	50,500	72,300	58,400	91,800	59,300	71,500	55,400	92,900	33,800
Fe _{Total} / ΣCr+V+Ni	400	-	346	-	-	216	253	116	-	-
Al+Fe ⁺³ / Scx10 ³	11.34	6.51	12.66	10.20	-	-	8.28	3.68	8.61	7.15

Table 5.5 (continued)

	9	10	33	Grand Mean	Mean Silica Rich	Mean Silica Poor	Mean Sodic	Mean Mafic	Mean Potassic
Oxidation Ratio	31.4	8.7	75.4						
K	30,876	68,724	77,522	35,532	29,194	42,927	26,812	29,922	73,123
K/Rb	309	347	440	264	206	332	300	291	394
Rb/Sr	0.62	1.09	1.91	1.11	1.35	0.92	0.48	0.53	1.50
Ba/Rb	7.45	4.29	1.53	3.54	2.99	4.31	4.15	5.94	2.91
Ba/Sr	4.60	4.67	2.93	3.08	2.66	3.49	-	3.28	3.80
Sc/Y	0.35	0.59	0.28	0.36	0.20	0.46	0.51	0.26	0.44
Fe _{Total}	79,800	63,600	58,500	66,946	69,471	64,000	60,700	65,800	61,050
Fe _{Total} / Σ Cr+V+Ni	578	216	276	300	304	297	-	360	246
Al+Fe ⁺³ / Sc x 10 ³	7.91	4.90	8.76	8.10	9.62	6.84	6.48	10.38	6.83

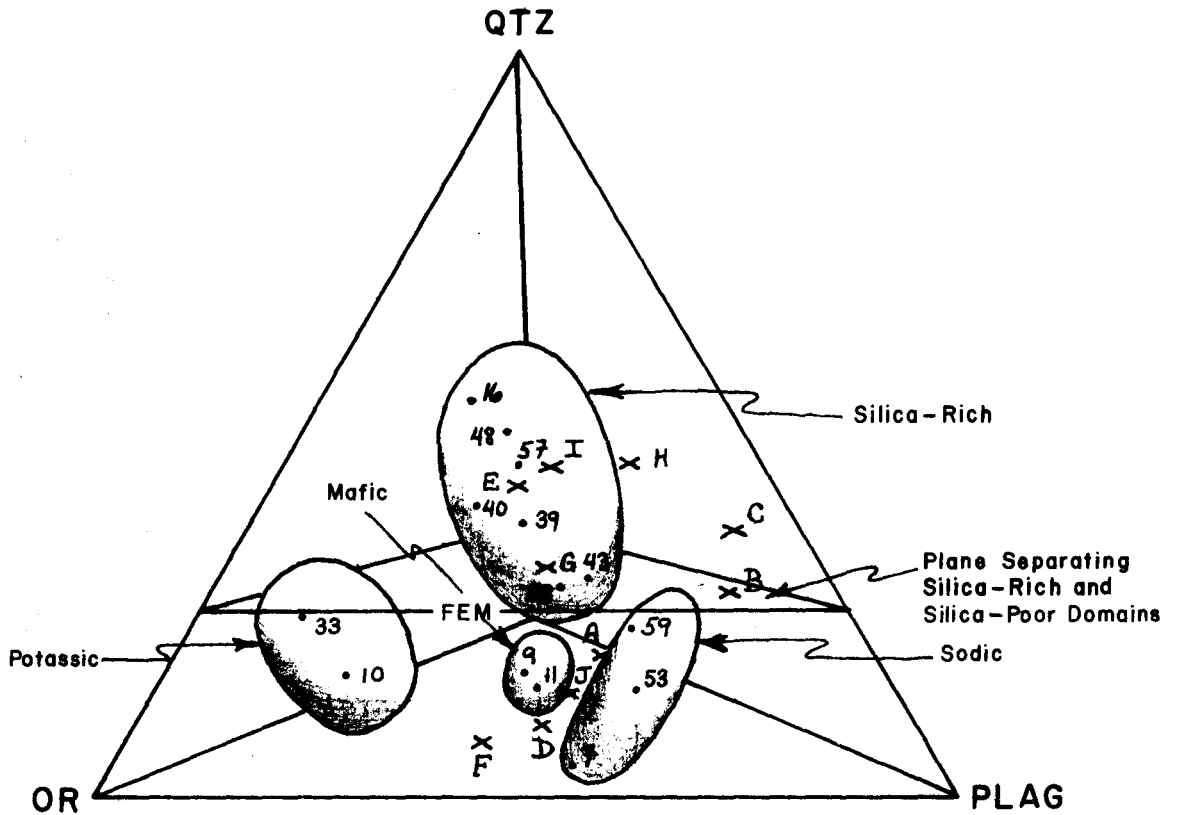


Figure 5.9: Normative Tetrahedron of Figure 5.8 Showing Compositional Fields of Quartzo-Feldspathic Gneisses. Letters Same as Figure 5.8

present purpose of protolith discrimination, these compositional groups are considered meaningful. The major and trace element compositions of these groups will be used in the following paragraphs as clues to their respective origins.

The average major element compositions of each group are given in Table 5.6 along with the grand average for all the samples analysed. From this table, the average silica-rich gneiss (Column B) is seen to be closely comparable to average pelite (Column G) in all aspects. This similarity is shown particularly well in Figure 5.9 where average pelite compositions plot well within the silica-rich gneiss volume. The modified Köhler-Raaz plot of Shaw (in preparation) also suggests a pelitic precursor for this gneiss type (Figure 5.6) as does the Moine and de la Roche diagram of Figure 5.10. These relations plus the restriction of sedimentary structures to this group make parent rocks other than pelites improbable.

The origin(s) of the silica poor gneisses is, unfortunately, not as clear. Their general similarity to intermediate igneous rocks is indicated by comparison of Columns C and H of Table 5.6 and by their location in Figure 55. The sodic gneisses show the strongest resemblance to intermediate igneous rocks in the modified Köhler-Raaz diagram and in Figure 5.10. They are close in composition to latites or alkalic doreites as shown in Columns D, H and I of Table 5.6.

Table 5.6: AVERAGE COMPOSITIONS OF THE VARIOUS QUARTZO-FELDSPATHIC GNEISS TYPES AND COMPOSITIONALLY SIMILAR ROCKS

	A	B	C	D	E	F	G	H	I
SiO ₂	57.49	60.30	54.20	51.15	51.90	60.00	61.54	54.02	51.32
TiO ₂	1.30	1.01	1.64	2.17	0.71	1.32	0.82	1.18	2.29
Al ₂ O ₃	16.43	16.07	16.85	19.03	11.75	16.69	16.95	17.22	16.64
Fe ₂ O ₃	4.33	4.61	4.01	5.55	2.34	2.36	2.36	3.83	3.24
FeO	4.93	4.60	5.34	5.72	5.10	4.78	3.90	3.98	6.48
MnO	0.16	0.18	0.13	0.16	0.15	0.06	-	0.12	0.16
MgO	3.05	3.01	3.10	2.45	8.80	1.12	2.52	3.87	4.30
CaO	3.32	2.29	4.52	4.00	10.95	1.16	1.76	6.76	7.17
Na ₂ O	2.41	2.16	2.70	4.22	2.14	1.19	1.84	3.82	4.78
K ₂ O	4.25	3.47	5.17	3.23	3.61	8.81	3.45	4.43	2.33
H ₂ O ⁺	0.00	1.42	1.24	1.05	1.17	1.58	3.47	0.78	0.63
CO ₂	0.00	0.31	0.40	0.45	0.68	0.37	1.67	-	-
P ₂ O ₅	0.30	0.25	0.37	0.51	0.24	0.23	-	0.49	0.66

- A - Average Hermon Group Quartzo-Feldspathic Gneiss (13 samples)
 B - Average Silica Rich Hermon Group Quartzo-Feldspathic Gneiss (7 samples)
 C - Average Silica Poor Hermon Group Quartzo-Feldspathic Gneiss (6 samples)
 D - Average Sodic Hermon Group Quartzo-Feldspathic Gneiss (3 samples)
 E - Average Mafic Hermon Group Quartzo-Feldspathic Gneiss (2 samples)
 F - Average Potassic Hermon Group Quartzo-Feldspathic Gneiss (2 samples)
 G - Average Pelite (Shaw, 1956)
 H - Average Latite (Nockolds, 1954)
 I - Average Alkali Doreite (Nockolds, 1954)

Table 5.6 (continued)

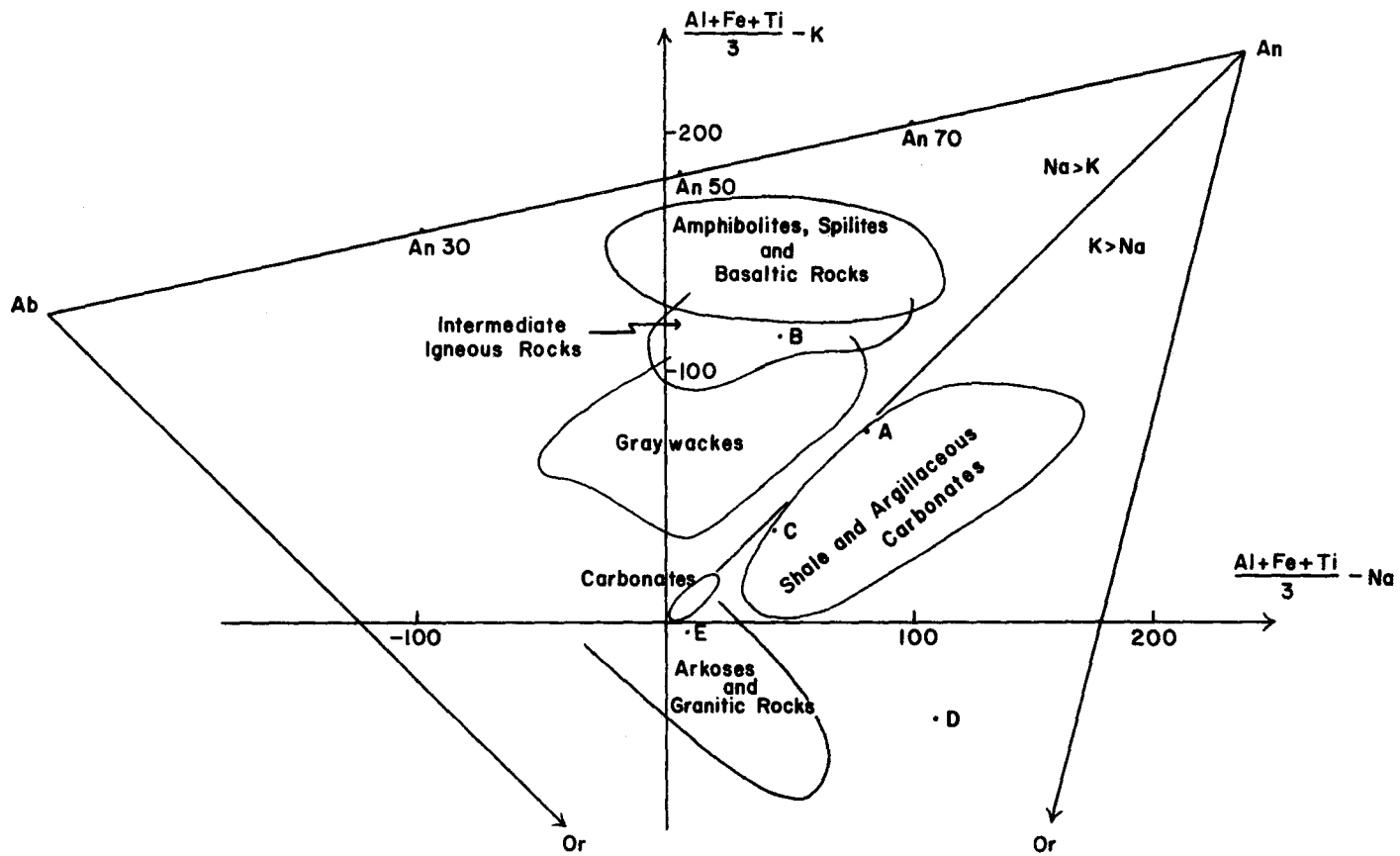
	<u>J</u>	<u>K</u>	<u>L</u>	<u>M</u>
SiO ₂	47.42	55.44	51.75	52.93
TiO ₂	1.66	1.41	0.86	0.63
Al ₂ O ₃	16.03	16.48	13.78	19.89
Fe ₂ O ₃	5.68	2.78	3.95	4.15
FeO	5.16	6.13	3.94	2.29
MnO	0.25	0.09	0.16	-
MgO	3.35	4.56	8.81	1.62
CaO	6.99	5.83	10.67	0.00
Na ₂ O	7.67	2.32	1.85	0.60
K ₂ O	3.50	2.23	2.97	8.33
H ₂ O ⁺	1.36	2.24	1.00	3.73
CO ₂	0.22	-	-	-
P ₂ O ₅	0.71	0.16	0.20	3.95

J - Average Malignite (Nockolds, 1954)

K - One Part Average of 1558 Basalts (Manson, 1967) to One Part Average Pelite (Shaw, 1956)

L - Pelite-Dolomite Mixture; 75% Average Pelite (Shaw, 1960): 25% Ideal Dolomite Normalized CO₂ Free

M - Potassic Shale (Schmitt, 1924) Recalculated Carbonate Free



- A- Average Silica-Rich Gneiss
- B- Average Sodic Gneiss
- C- Average Mafic Gneiss
- D- Average Potassic Gneiss
- E- Average Leptite

Figure 5.10: Projections of Average Compositions of Quartzo-Feldspathic Gneiss Varieties and Leptites Showing Similarities to Common Igneous and Sedimentary Rock Types (Modified after Moine and de la Roche, 1968).

The norms of these rocks agree with those of the sodic gneisses in that latites are slightly oversaturated similar to analyses 53 and 59 of Table 5.5 while alkalic doreites are slightly undersaturated like analysis 7 of the same table. Malignites (Column J, Table 5.6) bear a resemblance to the sodic gneisses but are too strongly nepheline normative to be a convincing protolith. In general, the sodic gneisses are enriched in Al_2O_3 and K_2O and are depleted in CaO and MgO relative to these possible progenitors and intermediate igneous rocks in general. Thus, the presumed similarities of the sodic gneisses to intermediate igneous rocks may be more apparent than real. Alternatively, the major element chemistry of these gneisses does not resemble that of any common sedimentary rock type. Superficially, they might be interpreted as admixtures of basaltic fragmentals and pelitic debris (common bulk compositions in the map area), but simple mixture calculations attempting to duplicate the mean composition of the sodic gneisses prove a mixing model improbable (Column K, Table 5.6). Such mixtures are enriched in SiO_2 , CaO and MgO and are depleted in Al_2O_3 and alkalis relative to sodic gneiss. In short, the major element chemistry of the sodic gneisses suggests an igneous origin more strongly than a sedimentary one. The field relations, particularly their wide lateral extent and lateral gradation into other lithologies, are most compatible with a tuffaceous origin.

Only one example of mafic gneiss interbanded with quartzofeldspathic gneiss was analysed in this study. The mode of this specimen (sample 9, Table 5.5) shows a close resemblance to amphibolite in mineralogic composition. Its analysis is nearly identical to that of amphibolite 11 of Table 5.3 which is non-basaltic in character and probably represents either a mixture of basaltic and pelitic debris or a pelite-dolomite mixture. Since these two mafic gneisses or amphibolites are mineralogically and chemically similar, they will be treated together as a distinct compositional group. The mean of their analyses appears in Column E of Table 5.6 and they are seen to occupy a discreet compositional volume in the normative tetrahedron of Figure 5.9. Inspection of the two analyses and Figure 5.9 reveals their lack of compositional similarity to common "end member" igneous and sedimentary rocks although they are classified as either basaltic igneous rocks or carbonate rich sediments in the modified Köhler-Raaz plots in Figures 5.5 and 5.6 and as argillaceous carbonates in Figure 5.10. Their low values of SiO_2 , Al_2O_3 and total iron and high values of CaO , MgO and K_2O coupled with their positions in the Moine and de la Roche plot strongly suggest a pelite-dolomite mixture as a parent rock. Comparison of Columns E and L of Table 5.6 demonstrates this mixture to be a reasonable protolith for these gneisses. It also demonstrates that pelite-

dolomite mixtures are realistic precursors for non-basaltic amphibolites as discussed in the preceding section. Basalt-pelite mixtures are not likely progenitors for the mafic gneisses because it is difficult to balance the silica and potash abundance levels near those of the mafic gneisses. It thus seems probable that the mafic gneisses or para-amphibolites represent original dolomitic shales interbanded either with quartzo-feldspathic gneiss as in the case of sample 9 or with basaltic amphibolites as in the case of sample 11.

The potassic gneisses (Table 5.5 and Figure 5.9) represent the most unusual bulk compositions encountered in this study by virtue of their extremely high K_2O contents. The two specimens of this type of gneiss define a distinct compositional volume in Figure 5.9 and are classified alternatively as intermediate igneous rocks or unusual sandstones in the Köhler-Raaz plots of Figures 5.5 and 5.6. Their field occurrence sheds no light on their mode of origin. A careful comparison of major element data shows a rather surprising similarity between these gneisses and average pelite except for the high potash and low MgO , CaO and Na_2O values (Columns F and G of Table 5.6). High potash shales are known to occur in the geologic record (Schmitt, 1924 and Gruner and Thiel, 1937) and could represent the unmetamorphosed equivalents of the potassic gneisses (Column M, Table 5.6). Intermediate igneous rocks are generally enriched in CaO , MgO and Na_2O and are strongly de-

pleted in K_2O relative to the potassic gneisses. On the basis of the limited major element data, the origin of these gneisses is unclear since their analyses do not resemble any common sedimentary or igneous rock in a compelling way. Potassic shales, however, remain a possibility.

The trace element data for each gneissic variety should reflect their modes of origin to a limited degree. Trace element ratios will be used to emphasize the geological process by which each variety came into being and to augment the interpretations of origin based on the major element chemistry. The element ratios used toward this end are listed in Table 5.7 for the means of the quartzo-feldspathic gneiss varieties and other common rock types. By comparing the values of a particular ratio in the gneisses to these common rock types, similarities in origin may be deduced.

In terms of the Rb/Sr , Ba/Sr , Ba/Rb , Sc/Y and $Al+Fe^{+3}/Sc$ ratios the silica-rich gneisses closely resemble granitic rocks or shales while their origin is equivocal according to the $Fe_T/\Sigma Cr+V+Ni$ ratio (Table 5.7). The lack of a granitic major element chemistry, the presence of sedimentary structures and high Zr and V concentrations (Table 5.5) in this variety favors these ratios as reflecting a sedimentary history. In general, the weight of evidence supports a pelitic protolith for the silica-rich gneisses.

Table 5.7: ELEMENT RATIOS FOR VARIOUS ROCK TYPES INCLUDING THE HERMON GROUP QUARTZO-FELDSPATHIC GNEISSES

Rock Type	Rb/Sr	Ba/Sr	Ba/Rb	$\text{Fe}_T / \sum \text{Cr} + \text{V} + \text{Ni}$	$\text{Al} + \text{Fe}^{+3} / \text{Sc} \times 10^3$	Sc/Y	
Gabbro, basalt	0.06 ^a - 0.10 ^g	0.54 ^d - 0.71 ⁱ	6.00 ^g - 11.00 ⁱ	119 ^d - 165 ^f	2.71 ^d - 3.24 ^f	1.06 ^f - 1.52 ^d	
Diorite, andesite	0.09 ^g - 0.18 ^b	0.70 ^d - 0.81 ^g	9.29 ^g - 11.40 ^d	277 ^g - 375 ^d	3.30 ^d	0.50 ^g - 1.55 ^d	
Granodiorite	0.25 ^{d,i} - 0.28 ^b	0.95 ⁱ - 1.14 ^d	3.82 ⁱ - 4.50 ^d	237 ⁱ - 245 ^d	6.60 ^d	0.40 ^{d,i}	
Granite, rhyolite	0.51 ^d - 1.70 ⁱ	2.10 ^d - 8.40 ⁱ	2.08 ^g - 4.94 ⁱ	268 ⁱ - 467 ^d	14.83 ^d	0.15 ^d - 0.35 ^g	
Carbonates	0.005 ⁱ - 0.008 ^b	0.02 ⁱ	3.33 ⁱ	75 ⁱ	-	0.03 ⁱ	
Pelites	0.47 ⁱ - 0.89 ^g	1.78 ^g - 1.93 ⁱ	2.00 ^g - 4.14 ⁱ	86 ^g - 164 ⁱ	8.17 ^k	0.33 ^g - 0.50 ⁱ	
Graywackes	-	1.5 ^j	-	172 ⁱ	-	-	
Arkoses	-	2.0 ^j	-	-	-	-	
Hermon Group Quartzo-Felds- pathic Gneiss- es*	Silica Rich	1.35	2.66	2.99	3.04	9.62	0.20
	Silica Poor	0.92	3.49	4.31	297	6.84	0.46
	Sodic	0.48	-	4.15	-	6.48	0.51
	Mafic	0.53	3.28	5.94	360	10.38	0.26
	Potassic	1.50	3.80	2.91	246	6.83	0.44
	Mean	1.11	3.08	3.54	300	8.10	0.36

- a Prinz (1967)
- b Fauer and Hurley (1963)
- d Taylor and White (1966)
- f Manson (1967) and Prinz (1967)
- g Vinogradov (1956)
- i Turekian and Wedepohl (1961)
- j Weber and Middleton (1961)
- k Shaw (1956)

* Calculated from arithmetic means of data in Table 5.5.

The trace element data suggests that the broad grouping of silica-poor gneisses is of uncertain origin (Table 5.7). Some of the uncertainty is removed by considering the sodic, mafic and potassic subgroups individually. The Sc/Y and $\text{Al+Fe}^{+3}/\text{Sc}$ ratios are compatible with an intermediate igneous parent for the sodic gneisses while Rb/Sr values are within the range of those shown by pelitic rocks (Table 5.7). The Ba/Rb ratio yields equivocal results for this variety and is of no use in deciphering its history. While the argument is not overly convincing the available data supports an intermediate volcanic precursor for the sodic gneisses.

Formation of the mafic gneisses by metamorphism of pelite-dolomite mixtures is not refuted by the available trace element data. The Rb/Sr, Ba/Sr, Sc/Y and $\text{Al+Fe}^{+3}/\text{Sc}$ ratios are not similar to intermediate igneous rocks yet they bear a resemblance to pelitic or granitic compositions (Table 5.7). Ba/Rb is, however, similar to basic igneous rocks.

The ratio data for the two potassic gneisses serves only to confuse an already complex picture. The Rb/Sr, Ba/Sr and Ba/Rb ratios resemble either pelites or granites while the $\text{Sc/Y, Fe}_T/\sum\text{Cr+V+Ni}$ and $\text{Al+Fe}^{+3}/\text{Sc}$ values compare favorably with intermediate igneous rocks. On the basis of their whole rock chemistry, the potassic gneisses could be of either metaigneous or metasedimentary origin.

Integration of field and chemical data on the four types of quartzo-feldspathic gneiss allows the following conclusions to be drawn:

- (1) The silica-rich gneisses are metamorphosed pelitic sediments
- (2) Intermediate tuffs are the most probable protolith for the sodic gneisses
- (3) Dolomitic shales metamorphosed to non-basaltic para-amphibolites are the most probable mode of origin for the mafic gneisses
- (4) The origin of the potassic gneisses is uncertain but potassic shales remain a possible protolith.

These conclusions are incorporated in a model of accumulation for the Hermon Group in the final chapter and will be reappraised there.

5.3. Leptites

In the field, the leptites are seen to be rather poorly foliated, compositionally banded rocks of granitic appearance which grade laterally into quartzo-feldspathic gneiss. This is perhaps their most singularly interesting feature for this lateral transition to gneissic lithologies imparts a distinct wedgelike character to many of the leptite horizons. Several such examples are found in the vicinity of Port Hope Lake in southeastern Cardiff township (Figure 2.1) where leptites perceptibly

grade into quartzo-feldspathic gneiss parallel to gneissosity over an interval of several hundred feet. This gradation is marked principally by the increased abundance of phyllosilicates in leptite as quartzo-feldspathic gneiss is approached. Interdigitation of leptite and gneiss occurs on a larger scale as well. For instance, the thick leptite unit east of Silent Lake (Figure 2.1) stretches for over six miles before intertonguing in complex fashion with gneiss in both its northern and southern extremities.

Compositional banding has been observed on many scales in the leptites. In outcrop, compositional banding is emphasized by variable amounts of biotite and feldspar proportions in adjacent bands. Variability in the $\text{Na}_2\text{O}/\text{K}_2\text{O}$ ratio between bands is a function of variable plagioclase and K feldspar proportions often on a thin section scale. The heterogeneous mineralogical character of the leptites can be appreciated by inspection of typical modes listed in Table 5.8.

One occurrence of orthoquartzite pods in leptite has been found in northwestern Chandos township. These pods, while poorly exposed in general, have dimensions on the order of less than ten feet. It is also interesting to note a conglomeratic horizon in leptite from northwestern Chandos reported by Shaw (1962). Both of these features indicate a sedimentary history for at least some of the leptite units.

In general, the field relations cited above seem to favor a sedimentary, probably arkosic, origin for the leptites. However, the broad compositional similarity of leptite and rhyolite, the wide stratigraphic extent of many leptite units and the interdigitation with quartzofeldspathic gneiss are also compatible with a volcanic origin. If a volcanic origin is entertained, certain genetic restrictions can be inferred. The relatively large volume of leptite relative to basic and intermediate compositions in the map area virtually precludes a comagmatic differentiation origin from any or all of these rock types. If the leptites are metamorphosed acidic volcanics, they are probably derived from a magma unrelated to the parent of the amphibolites. The practically universal occurrence of gradational contacts between leptite and gneiss militates against an effusive flow mode of origin. Thus, if the leptites are considered volcanic in origin, they probably represent acidic explosives derived from a magma whose intermediate and basic differentiation products are not recorded in the map area. Such a model would probably generate leptites of homogeneous chemical and mineralogical composition, devoid of included quartzitic or conglomeratic material (if deposited as an ash flow or water laid tuff) with little restriction of lithologic association.

On the basis of their mineralogical heterogeneity wedge-like character, intertonguing relations with quartzo-feldspathic gneiss, relatively restricted stratigraphic association with these gneisses and interbanding with minor quartzitic and conglomeratic material, the leptites are best interpreted as arkosic wedges or fans in thick pelitic horizons in turn interbedded with basaltic extrusives. The whole rock chemistry of the leptites will be used to substantiate an arkosic origin in the following paragraphs.

Analyses, norms, modes and calculated data for six leptites are given in Table 5.8. The major element compositions for these rocks are surprisingly uniform with most variation occurring in Na_2O and K_2O abundances in accordance with field and petrographic observations. The mean of these analyses is closely comparable to calc-alkali rhyolites, arkoses and taphrogeosynclinal sandstones as shown in Table 5.9. Thus, any or all of these rock types could be protoliths for the Hermon Group leptites. While average subgraywacke resembles the leptites in most respects (Table 5.9) it is too calcic to be considered a reasonable protolith. Unfortunately, the major element data as arranged in Table 5.9 do not permit us to choose between these alternatives. An igneous origin for the leptites might be suspected if their norms plotted in or near the ternary minimum of the haplogranite system. Accordingly, the norms of Table 5.8 have been plotted in this system

Table 5.8. ANALYSES

OF

LEPTITES

STATEMENT OF DATA

	3	23	25	35	37	55
SI02	75.100	77.350	77.050	71.550	77.800	75.100
TI02	0.160	0.110	0.160	0.420	0.090	0.210
AL203	12.260	10.720	11.100	12.690	10.500	11.900
FE203	3.900	1.450	2.940	3.980	2.230	2.880
FE0	0.400	0.680	1.060	0.520	1.040	1.660
MN0	0.050	0.020	0.050	0.030	0.020	0.020
MG0	0.370	0.140	0.240	0.260	0.250	0.250
CA0	1.260	0.100	1.360	0.080	0.650	0.190
NA20	1.680	3.120	3.980	2.300	1.500	2.820
K20	4.010	5.010	0.740	7.820	5.080	4.780
P205	0.010	0.040	0.060	0.170	0.030	0.020
H20 +	-0.000	-0.000	-0.000	-0.000	-0.000	-0.000
H20 -	-0.000	-0.000	-0.000	-0.000	-0.000	-0.000
C02	-0.000	-0.000	-0.000	-0.000	-0.000	-0.000
S	-0.000	-0.000	-0.000	-0.000	-0.000	-0.000
BE	25.000	3.300	2.900	1.400	3.300	4.900
GA	270.000	24.500	33.000	19.400	24.500	24.500
CR	0.000	0.000	0.000	0.000	0.000	0.000
V	5100.000	0.000	0.000	13.000	0.000	0.000
LI	92.000	10.000	17.000	14.300	15.400	4.700
NI	195.000	1.550	2.750	1.800	3.600	3.100
CU	-0.000	8.800	5.100	4.300	0.000	-0.000
Y	4.600	23.000	86.000	55.000	88.000	144.000
MN-SP	25.000	46.000	220.000	720.000	390.000	60.000
SC	0.000	0.000	0.000	0.000	0.000	0.000
ZR	0.000	800.000	1150.000	570.000	2080.000	995.000
SR	25.000	98.000	88.000	0.000	25.000	117.000
BA	3.300	290.000	80.000	490.000	330.000	420.000
RB	96.000	112.000	26.000	107.000	162.000	61.000

Analyses by K. Ramlal

0.000 and -0.000 signify either no information or below detection limit

Table 5.8. NORMS AND MODES OF HERMON GROUP LEPTITES

	<u>Norms</u>						<u>Mean</u>
	<u>3</u>	<u>23</u>	<u>25</u>	<u>35</u>	<u>37</u>	<u>55</u>	
Quartz	47.12	40.21	48.58	28.18	48.32	39.57	40.88
Corundum	2.91	0.08	1.44	0.70	1.43	1.79	1.10
Orthoclase	23.91	30.01	4.43	46.34	30.29	28.32	27.18
Albite	14.33	26.73	34.10	19.50	12.80	23.90	23.40
Anorthite	6.24	0.24	6.44	-	3.05	0.81	2.65
Enstatite	0.93	0.35	0.61	0.65	0.63	0.62	0.63
Ferrosilite	-	-	-	-	-	0.36	-
Magnetite	1.00	1.96	3.16	0.56	3.18	4.18	2.43
Ilmenite	0.31	0.21	0.31	0.80	0.17	0.40	0.36
Hematite	3.24	0.12	0.80	3.60	0.05	-	1.24
Apatite	0.02	0.09	0.14	0.40	0.07	0.05	0.14

	<u>Modes</u>						<u>Mean</u>
	<u>3</u>	<u>23</u>	<u>25</u>	<u>35</u>	<u>37</u>	<u>55</u>	
Quartz	39.0	34.6	38.0	28.2	42.6	32.8	36.8
K-Feldspar	22.0	36.4	4.6	56.2	29.8	12.4	27.6
Plagioclase	31.6	23.8	51.4	9.8	16.0	39.2	26.8
Biotite	1.2	2.0	1.6	1.2	0.4	4.0	1.7
Muscovite	2.6	2.0	0.2	1.8	8.8	9.0	4.2
Oxides	2.8	1.0	4.0	2.8	2.4	2.0	2.6
Epidote	0.8	0.2	0.2	-	-	-	0.2
Carbonate	-	-	-	-	-	0.6	0.1

Table 5.8. CALCULATED DATA

	<u>3</u>	<u>23</u>	<u>25</u>	<u>35</u>	<u>37</u>	<u>55</u>	<u>Mean</u>
Oxidation Ratio	89.9	65.7	71.3	87.3	65.9	61.0	
K	33,290	41,590	7,140	64,920	42,180	39,680	37,970
Ca	9,010	710	9,720	570	4,650	1,360	4,340
K/Rb	347	371	307	607	260	650	424
Ca/Sr	360	7	110	-	49	12	108
Rb/Sr	3.84	1.14	0.23	-	1.71	0.52	1.49
Ba/Sr	0.13	2.96	0.91	-	3.47	3.59	2.21
Ba/Rb	0.03	2.59	4.00	4.58	2.04	6.89	3.36
Ca/Y	1,959	9	113	10	52	9	359

All values in parts per million

Oxidation ratio = molecular % $\frac{2\text{Fe}_2\text{O}_3 \times 100}{2\text{Fe}_2\text{O}_3 + \text{FeO}}$ (after Chinner, 1960)

Table 5.9. COMPOSITION OF LEPTITES AND POSSIBLE LEPTITE
PROTOLITHS

	<u>A</u>	<u>B</u>	<u>C</u>	<u>D</u>	<u>E</u>
SiO ₂	75.66	73.66	76.50	77.10	72.94
TiO ₂	0.19	0.22	-	-	0.44
Al ₂ O ₃	11.53	13.45	9.74	9.85	9.56
Fe ₂ O ₃	2.90	1.25	1.34	2.40*	1.99
FeO	0.89	0.75	0.78	-	2.37
MnO	0.03	0.03	-	-	0.10
MgO	0.25	0.32	0.43	0.51	1.34
CaO	0.61	1.13	2.42	2.68	7.04
Na ₂ O	2.57	2.99	1.74	1.24	1.80
K ₂ O	4.57	5.35	4.27	3.05	1.63
H ₂ O ⁺	-	0.78	0.71	-	0.64
CO ₂	-	-	-	-	0.00
P ₂ O ₅	0.06	0.07	-	-	0.15

A - Average Hermon Group Leptite (6 analyses)

B - Average Calc-Alkali Rhyolite+Rhyolite Obsidian (Nockolds, 1954)

C - Average of 12 Arkoses compiled from Pettijohn (1963) and
Elliot and Morton (1965)

D - Average Taphrogeosynclinal Sandstone (Middleton, 1960)

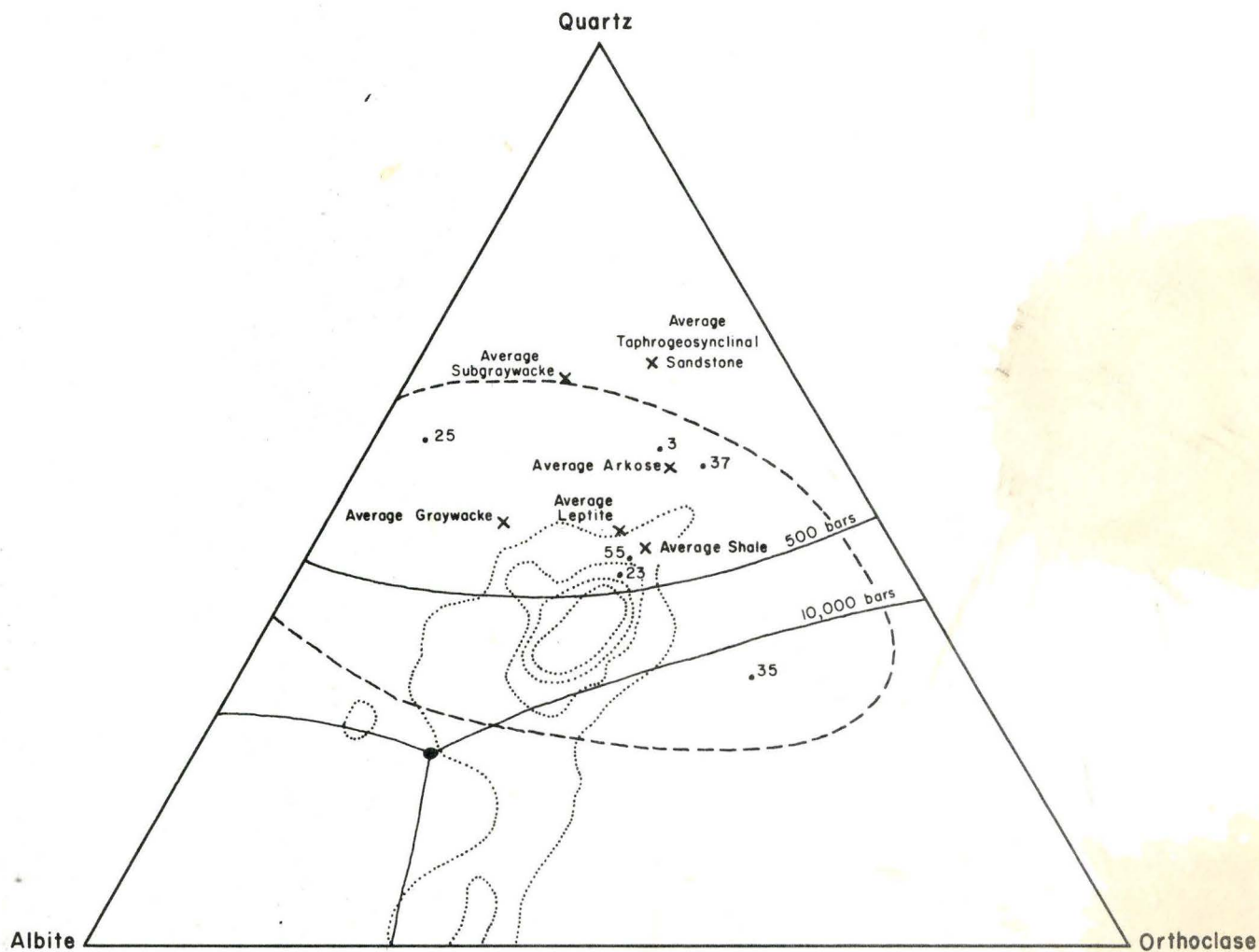
E - Average of 7 Subgraywackes (Pettijohn, 1957, 1963) Normalized CO₂
Free

* Total iron as Fe₂O₃

reproduced as Figure 5.11. In addition to the norms of the Hermon Group leptites, the norms of 362 extrusive rocks from Washington's tables carrying 80% or more normative quartz, albite and orthoclase have also been plotted in this system (Tuttle and Bowen, 1958). The lack of similarity of the leptites to these extrusives is apparent, implying a non-rhyolitic origin. The large field of modal variability for the leptites superimposed on Figure 5.11 further serves to demonstrate their non-igneous character.

The projection devised by Moine and de la Roche in Figure 5.10 is of little use in discriminating the origin of the leptites since the arkosic and granitic compositional fields overlap. This overlap is less pronounced in the modified Köhler-Raaz plots of Figures 5.5 and 5.6. In the former, the field of leptites extends considerably beyond that of silicic igneous rocks but falls predominantly within the range of sandstone compositions in the latter. On these grounds, an arkosic origin seems probable.

The element ratio data of Table 5.10 is inconclusive in distinguishing an igneous or sedimentary origin for the leptites principally because of the lack of data for arkosic sediments. From this table all ratios of the mean data except Ca/Sr show granitic affinities. The extreme variability of these ratios between the individual analyses, how-



- 
 Field of 362 Extrusive Rocks Carrying 80% or More Normative Qtz+Ab+Or. Contours More than 1, 2, 3 and 4% per 1% Area. (After Tuttle and Bowen, 1958, p. 78)
- 
 Field of Observed Modal Variability in Hermon Group Leptites. Field Based on 20 Modal Analyses
- 
 Cotectics and Ternary Eutectics at Various P_{H_2O} s (After Luth et al, 1964, p. 766)

Figure 5.11: Haplogranite System Showing Normative Plots of Hermon Group Leptites and 362 Extrusive Igneous Rocks

Table 5.10. TRACE ELEMENT RATIOS FOR VARIOUS ROCK TYPES
INCLUDING THE HERMON GROUP LEPTITES

<u>Rock Type</u>	<u>Rb/Sr</u>	<u>Ba/Sr</u>	<u>Ba/Rb</u>	<u>Cu/Sr</u>	<u>Ca/Y</u>
Gabbro, basalt	0.06 ^a - 0.10 ^g	0.54 ^d - 0.71 ⁱ	6.00 ^g - 11.00 ⁱ	129 ^f - 166 ^d	2281 ^f - 3733 ^g
Diorite, andesite	0.09 ^g - 0.18 ^b	0.70 ^d - 0.81 ^g	9.29 ^g - 11.40 ^d	58 ^g - 177 ^d	1550 ^g - 2960 ^d
Granodiorite	0.25 ^{d,i} - 0.28 ^b	0.95 ⁱ - 1.14 ^d	3.82 ⁱ - 4.50 ^d	58 ^{d,i}	723 ⁱ - 726 ^d
Granite, rhyolite	0.51 ^d - 1.70 ⁱ	2.10 ^d - 8.40 ⁱ	2.08 ^g - 4.94 ⁱ	43 - 60 ^h	128 ⁱ - 790 ^g
Carbonates	0.005 ⁱ - 0.008 ^b	0.02 ⁱ	3.33 ⁱ	495 ⁱ - 656 ^h	10,077 ⁱ
Pelites	0.47 ⁱ - 0.89 ^g	1.78 ^g - 1.93 ⁱ	2.00 ^g - 4.14 ⁱ	56 ^g - 167 ^h	767 ^g - 850 ⁱ
Graywackes	-	1.5 ^j	-	1.50 ⁱ	-
Arkoses	-	2.0 ^j	-	-	-
Hermon Group* Leptites	1.49	2.21	3.36	108	359

* Calculated from arithmetic means of data in Table 5.8.

a Prinz (1967)

b Faure and Hurley (1963)

d Taylor and White (1966)

f Manson (1967) and Prinz (1967)

g Vinogradov (1956)

h Turekian and Kulp (1956)

i Turekian and Wedepohl (1961)

j Weber and Middleton (1961)

ever, might be construed as evidence of sedimentary fractionation processes (Table 5.8).

In short, the weight of evidence favors an arkosic origin for the Hermon Group leptites. A rhyolitic origin is rejected on the basis of the field characteristics and associations of the leptites, their lack of similarity to eruptive volcanic rocks in the haplogranite system and their similarity to sandstones in the Köhler-Raaz plots. The minor element chemistry may support a sedimentary origin as well.

5.4. Conclusions

It is difficult to conceive of geologic processes capable of producing basaltic bulk compositions other than magmatic ones. A basaltic chemistry is therefore the most useful parameter in discriminating the origin of amphibolites. The Hermon Group amphibolites possess such a chemistry in terms of both their major and minor element compositions. Their compositional relations and projections in the modified Köhler-Raaz and Moine and de la Roche diagrams imply an alkali-olivine basaltic protolith. Minor, non-basaltic amphibolites or mafic gneisses interbanded with either quartzo-feldspathic gneisses or basaltic amphibolites probably represent metamorphosed dolomitic shales.

The silica-rich quartzo-feldspathic gneisses are demonstrably similar to pelites in terms of their whole rock chemistry, field relations and projection in the Köhler-Raaz and Moine and de la Roche plots. By the same criteria, the sodic gneisses are concluded to be the metamorphosed equivalents of intermediate tuffaceous rocks. Potassic shales are the most reasonable protolith for the potassic gneisses.

Complex stratigraphic interfingering with quartzo-feldspathic gneiss, the general wedgelike character and occurrence of minor clastic relicts make an arkosic origin probable for the Hermon Group leptites. The lack of similarity between the leptites and rhyolite in the haplogranite system reinforces this argument as does the Köhler-Raaz diagram by classifying the leptites as sandstones.

The postulated origins for the various rock types may seemingly create difficulties in depositional associations. An integrated and geologically reasonable model for the accumulation of the Hermon Group protoliths is given in the concluding chapter which will hopefully dispel any such difficulties.

6. METAMORPHISM

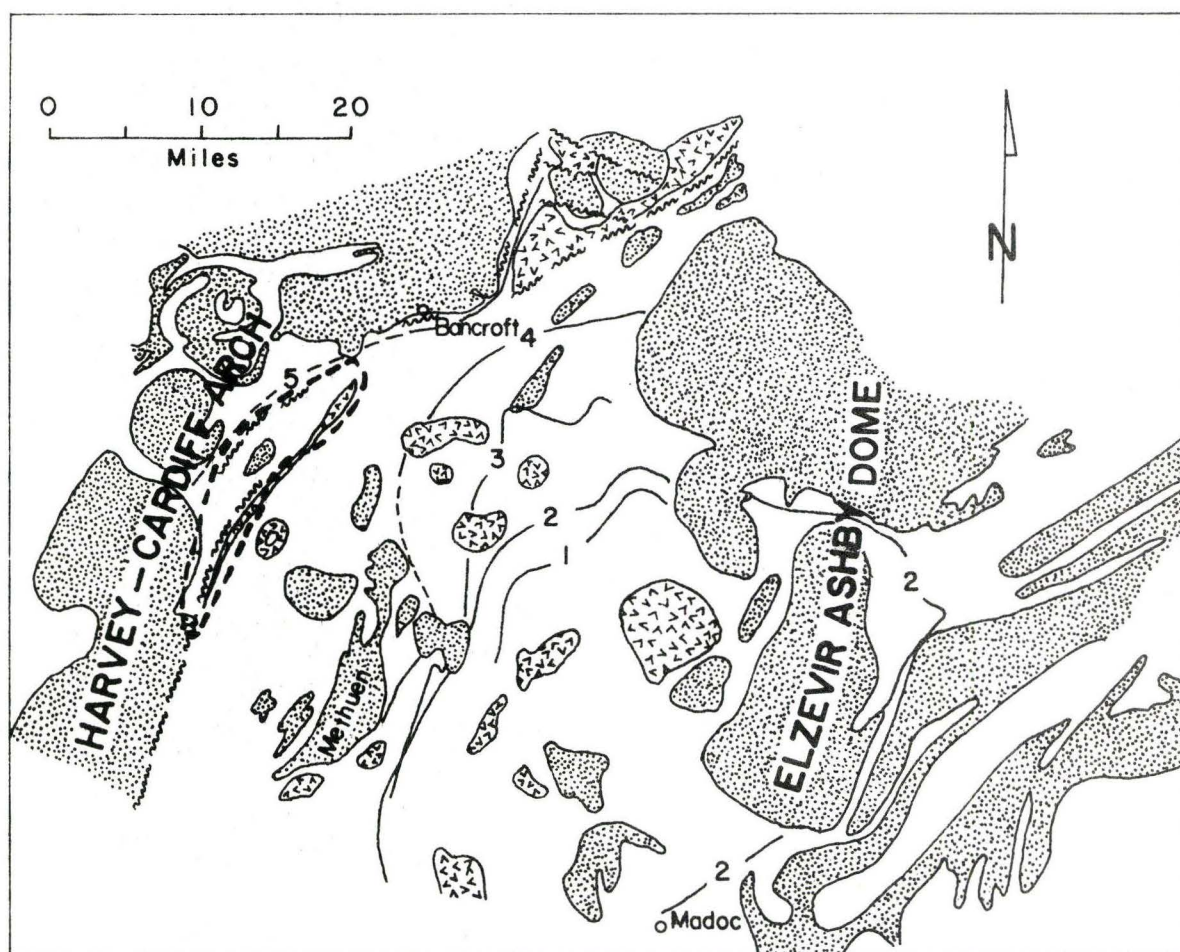
To better interpret the metamorphic history of the map area, a brief review of regional metamorphism in the Bancroft-Madoc area will first be undertaken. Using this review as a framework, the prograde and retrograde metamorphisms in the map area will be considered using petrographic evidence and the data of experimental petrology to place limits on the physical and chemical history of the area.

6.1. Regional Metamorphism in the Bancroft-Madoc Area

The general pattern and chronological succession of metamorphic events in this broad area have been documented by Lumbers (1967a) and Silver and Lumbers (1966). They have defined two major metamorphic culminations. The first, dated at 1250 ± 25 m. y., accompanied the intrusion of Lumbers' biotite-diorite intrusive series and was responsible for the development of the three plagioclase isograds and the greenschist and lower almandine-amphibolite terrains of this region (Lumbers, 1967a). The second and most intense metamorphic event, dated at 1125 ± 25 m. y., accompanied the intrusion of Lumbers' quartz-monzonite group, producing the sillimanite isograd and upper amphibolite facies terrain flanking but not affecting the previously

developed lower grade area (Lumbers, 1967a). It is this event which is recorded as the prograde event in the study area.

The approximate disposition of regional metamorphic isograds in the Bancroft-Madoc area is given in Figure 6.1. From this diagram, metamorphic grade is seen to increase radially outward from the Elzevir-Ashby Dome beginning with the zoned albite isograd, or garnet isograd in rocks of appropriate bulk composition. Toward the northwest, the oligoclase/staurolite, andesine/andalusite/diopside and sillimanite/cordierite isograds are progressively encountered. These isograds mark the first appearance of the above index minerals in basic volcanics, quartzo-feldspathic gneisses and carbonate meta-sediments. It is emphasized that the reactions accounting for the formation of these minerals are unknown and that more than one reaction may define the first appearance of a given mineral. Southwest of the Copeway and Burnt Lake granites in Lake Township, Carmichael (1968) has mapped a kyanite isograd marking the first appearance of kyanite-biotite at the expense of chlorite-muscovite-staurolite-quartz. It is curious that the location of this isograd coincides with that of Lumbers' andesine/andalusite/diopside isograd. This coupled with the narrow width of Carmichael's kyanite zone could be taken to indicate metamorphic conditions close to the triple point in the aluminosilicate system in this region. In the northwestern portion of the Bancroft-Madoc



(Modified after Lumbers, 1967a & Carmichael, 1968)

EXPLANATION

Isograds

- (1) Zoned albite / garnet
- (2) Oligoclase / staurolite
- (3) Andesine / andalusite / diopside
- (4) Sillimanite / cordierite
- (5) Orthopyroxene / forsterite-chondrodite /
and disappearance of muscovite

Lithologies

-  Granitic intrusive rocks
-  Basic intrusive rocks
-  Supracrustal rocks

 = isograd  = map area  = shear zone

FIGURE 6.1 Approximate disposition of regional metamorphic isograds in the Bancroft-Madoc area.

supracrustal sequence, Lumbers (1967a,b) has very approximately located another metamorphic boundary corresponding to the appearance of (1) orthopyroxene in basic metavolcanics and quartzo-feldspathic gneisses (2) forsterite and chondrodite in carbonate metasediments and (3) the disappearance of muscovite in sillimanite bearing quartzo-feldspathic gneisses. It is interesting to note at this point that staurolite persists above the sillimanite/cordierite isograd throughout much of the northwestern part of the Bancroft-Madoc area (Carmichael, 1968; Evans, 1964; Lal and Moorhouse, 1969; Shaw, 1962). This point will be considered in detail later.

From the foregoing discussion of phase changes with increasing metamorphic grade and the detailed petrographic studies of Lumbers (1967a), Chesworth (1967), Shaw (1962), Carmichael (1968) and the writer, it is possible to draw some general conclusions concerning the metamorphic facies series in the Bancroft-Madoc area. In this context, the following observations are relevant:

- (1) Biotite, chlorite and quartz appear to coexist in stable equilibrium in the greenschist terrain (Lumbers, 1967a; Carmichael, 1968).
- (2) Chloritoid and quartz coexist in parts of the greenschist facies terrain (Lumbers, 1967a).

- (3) The three alumino-silicate polymorphs occur in close association in central Lake township. While andalusite and sillimanite occur in separate, widespread zones in the northwestern portion of the Bancroft-Madoc area, occurrences of kyanite are scarce (Lumbers, 1967a; Carmichael, 1968).
- (4) Andalusite and cordierite coexist in part of the amphibolite facies terrain (Lumbers, 1967a).
- (5) The assemblage hornblende-almandine-quartz is not commonly developed in the amphibolite facies terrain (Chesworth, 1967; present study).
- (6) Sillimanite, muscovite and quartz coexist throughout most of the sillimanite zone (Lumbers, 1967a; Carmichael, 1968; Shaw, 1962; present study).

The presence of kyanite in the higher grade terrain and of chloritoid plus quartz in the greenschist terrain bears a resemblance to assemblages of the respective Barrovian zones (Winkler, 1967, pp. 94-115). However, the assemblages sillimanite, andalusite, andalusite-cordierite, sillimanite-muscovite-quartz and the general absence of the assemblage hornblende-almandine-quartz in the amphibolite terrain resemble assemblages found in the high grade terrains of the Central Abukuma Plateau (Miyashiro, 1958). The stable coexistence of chlorite-biotite-

quartz is characteristic of lower grades at Abukuma as well (Miyashiro, 1968). Thus it seems reasonable to suggest that the facies series in the Bancroft-Madoc area

"is intermediate between the Barrovian-type facies series of the Scottish Highlands which was formed under relatively high pressures and the Abukuma-type facies series of Japan which was formed under relatively low pressures" (Lumbers, 1967a, p. 203.)

This interpretation is in accord with that of Chesworth (1967) for the metamorphic sequence between Chandos and Glamorgan townships and finds support in the compilation of worldwide facies series of Hietanen (1967).

In addition to two prograde metamorphic events:

"evidence of retrograde metamorphism is found locally throughout the region in shear zones and along fractures in the superficial rocks" (Lumbers, 1967a, p. 201.)

This retrogression may be related to the tectonic activity responsible for the development of many of the large, late stage shear systems characteristic of the Bancroft-Madoc area. There is some evidence that this retrograde event is more extensive than previously thought. This evidence will be considered at some length in a later section.

6.2. Metamorphism in the Mapped Area

Two metamorphic events have been recognized in the study area. The prograde event probably correlates with the 1125 ± 25 m. y. culmination recognized by Lumbers (1967a) and the retrograde event may be related to a late stage regional uplift as previously mentioned. Each of these events and their effects on the diverse lithologies of the study area will be considered separately in the following sections.

6.2.1. Prograde Metamorphism

Prograde metamorphism is of amphibolite facies rank throughout the area considered. The effects of this event on each of the lithologic types are documented below.

Amphibolites

Following the recommendations of Shaw (1957), the name amphibolite is applied to rocks containing predominantly amphibole and essential plagioclase with other characterizing minerals such as clinopyroxene, biotite, cummingtonite, quartz and oxides. The amphibolites under discussion are medium grained, nematoblastic tectonites with the afore-mentioned prograde major constituents associated with minor carbonate, sphene, epidote minerals, apatite and tourmaline. Hornblende (X = yellowish green, Y = dark green to olive green, Z = blue-green),

and biotite (X = light tan, YZ = reddish brown to brown), generally show a preferred orientation in thin section defining foliation. Hornblende may be intimately intergrown with the Fe-Mg amphibole, cummingtonite. Plagioclase compositions are quite variable in the range An_{24} to An_{58} . Generally, the more calcic plagioclases are associated with a relatively large amount of free carbonate. Two Fe-Ti oxide phases are commonly present. Magnetite often occurs as sub to euhedral grains associated with rhombohedral oxides on the hematite-ilmenite join. These rhombohedral oxides usually show complex exsolution textures. Minor pyrite, chalcopyrite or pyrrhotite may also be seen in polished sections.

Four amphibolite varieties have been recognized petrographically in the present investigation (1) amphibolite (2) biotite amphibolite, (3) cummingtonite amphibolite and (4) clinopyroxene amphibolite. The geographic distribution of these four varieties throughout the area shows no mappable bulk compositional or metamorphic control. Amphibolites and biotite amphibolites constitute the bulk of the mapped amphibolite units while clinopyroxene amphibolites have the lowest frequency of occurrence. It is probable that the biotite, cummingtonite and clinopyroxene amphibolites developed in response to slight deviations from an average basaltic composition, the biotite variety being more potassic, the cummingtonite variety being sub-calcic and the clinopyroxene amphibolites slightly more calcic.¹ A summary of prograde amphibolite

¹ These predicted compositional relations are rudely supported by the data of Table 5.3.

phase assemblages is given in Table 6.1. ACKF phase compatibilities are shown in Figure 6.2 and representative modes are found in Table 5.3.

From the ACKF plots it is evident that the phase assemblages occur in the amphibolite facies of regional metamorphism and pose no particular problems of interpretation. The co-existence of the two clinoamphiboles hornblende and cummingtonite in approximately 15% of the amphibolites studied, however, warrants further comment.

The association of cummingtonite with hornblende in metamorphic rocks has been well documented by Eskola (1950), Jaffe et al. (1968), Klein (1968), Miyashiro (1958), Ross et al. (1968), Shido (1958), Vernon (1962) and Watters (1959). In these studies the clinoamphibole pair is seen to occur in one or more of the following ways:

- (a) As independent grains of each phase (Vernon, 1962; Watters, 1959).
- (b) As one phase rimming the other (Watters, 1959).
- (c) As homoaxial, patchy intergrowths with optically and chemically sharp phase boundaries (Eskola, 1950; Vernon, 1962; Klein, 1968).
- (d) As lamellae of one phase in the other along preferred crystallographic directions (Vernon, 1962; Jaffe et al. 1968; Ross et al., 1968; Klein, 1968).

Table 6.1

AMPHIBOLITE PHASE ASSEMBLAGES

<u>Amphibolite Type</u>	<u>Characteristic Assemblages</u>
Amphibolite	Hornblende-Plagioclase-Oxides±Carbonate
	Hornblende-Plagioclase-Quartz-Oxides
Biotite Amphibolite	Hornblende-Biotite-Plagioclase-Oxides±Carbonate
	Hornblende-Biotite-Plagioclase-Quartz-Oxides
Cummingtonite Amphibolite	Hornblende-Cummingtonite-Plagioclase-Oxides - Carbonate±Clinzoisite
	Hornblende-Cummingtonite-Plagioclase-Quartz-Oxide
	Hornblende-Cummingtonite-Biotite-Plagioclase-Oxide
Clinopyroxene Amphibolite	Hornblende-Clinopyroxene-Plagioclase
	Hornblende-Clinopyroxene-Plagioclase-Quartz - Carbonate-Oxides
	Hornblende-Clinopyroxene-Biotite-Plagioclase
	Hornblende-Clinopyroxene-Scapolite-Quartz - Carbonate-Oxides
	Hornblende-Clinopyroxene-Scapolite-K feldspar - Quartz-Carbonate-Oxides

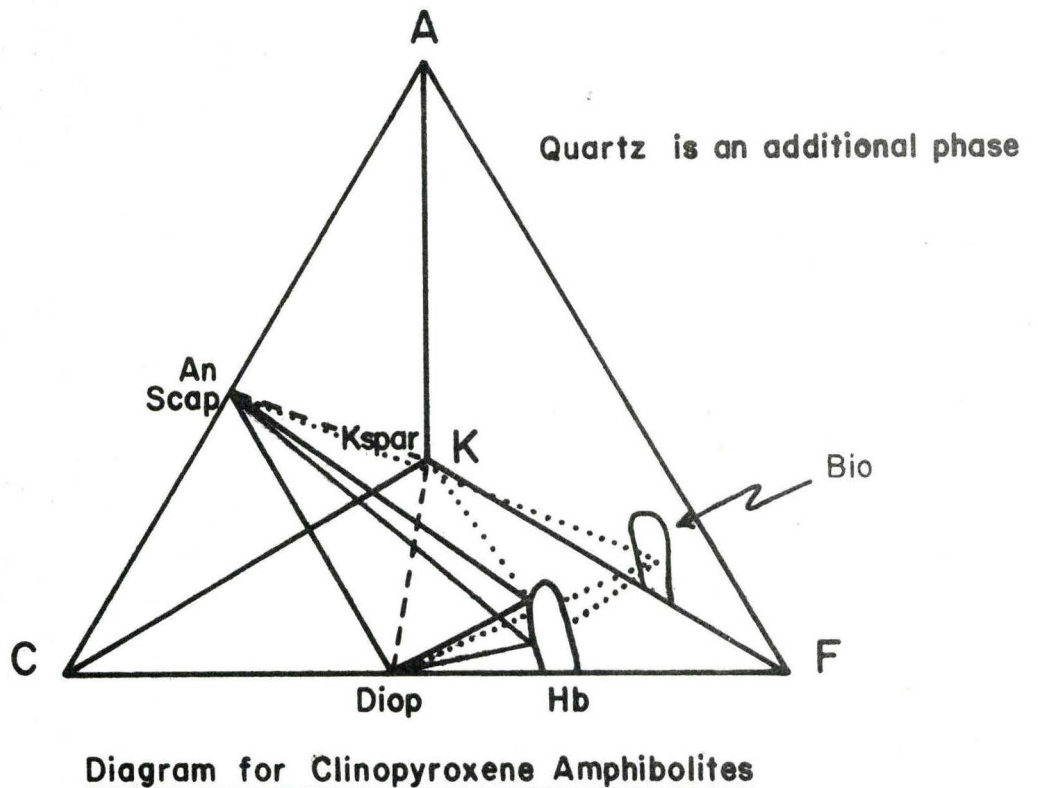
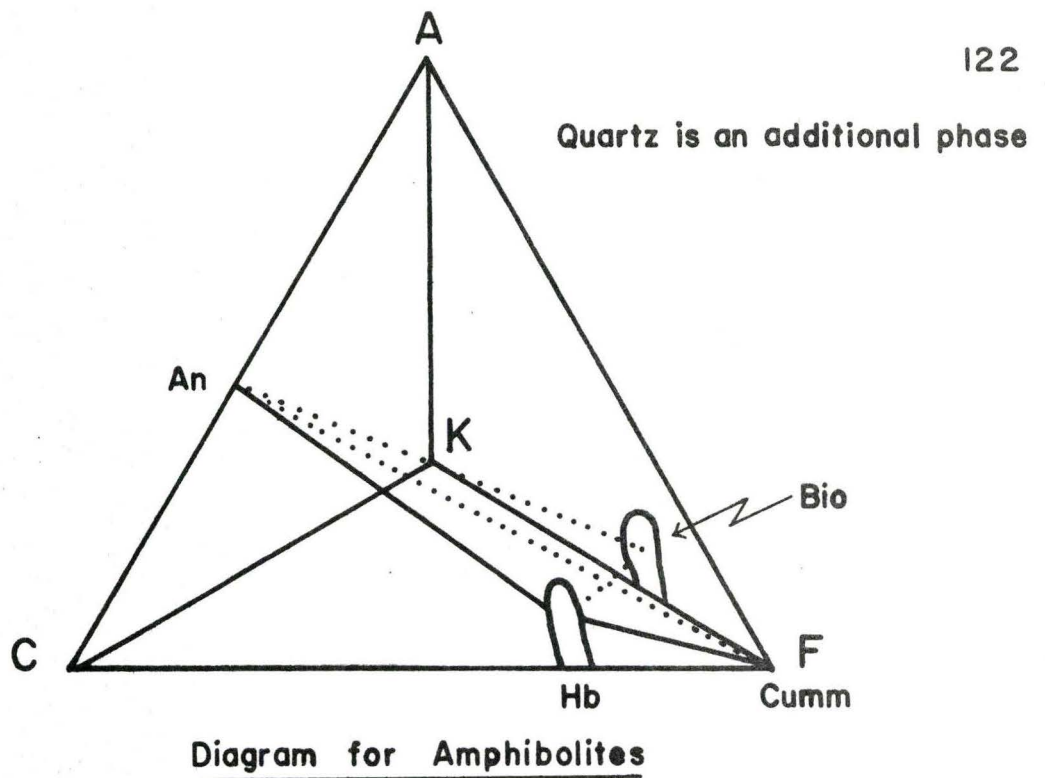
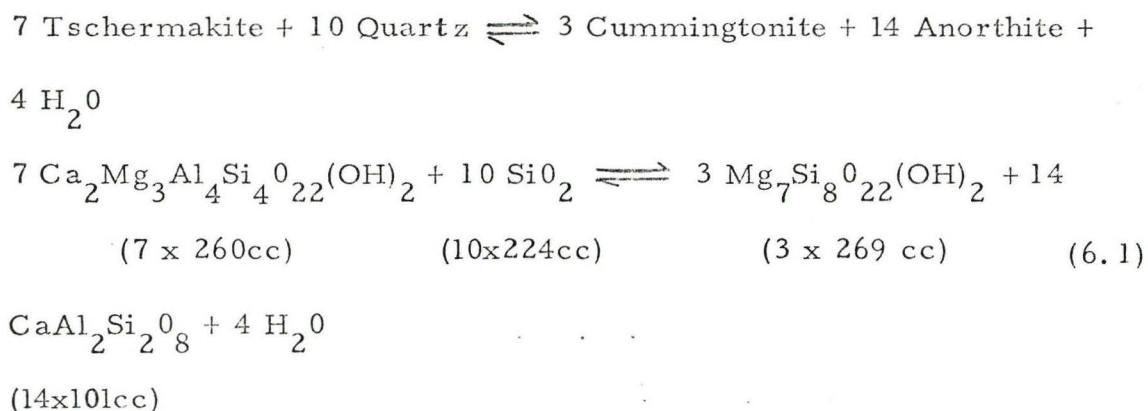


Figure 6.2: ACKF Diagrams for Amphibolites. Note that tie lines on the front face of the tetrahedron are shown by solid lines, those on the three back faces by dashed lines, and those within the volume by dotted lines.

The origin of this two-amphibole assemblage has long been a subject of discussion with compositional miscibility gaps being the mechanism originally (Asklund, 1923, p. 30) and most frequently appealed to. Shido (1958) has proposed an alternative mechanism of expulsion of the cummingtonite "molecule" from the hornblende structure under low pressure metamorphism. Her mechanism is based on the reaction (Shido, 1958, p. 212):



$$\Delta V_{\text{Solid}} = V_{\text{Products}} - V_{\text{Reactants}} = 2221 - 2044 \text{ cc} = +177\text{cc}.$$

From this, she argues that cummingtonite-bearing assemblages are favored at low pressures relative to cummingtonite free amphibole assemblages for a given bulk composition. This reaction appears improbable for basic rocks from the point of view of the amount of quartz required and the amount of anorthite produced. It is also interesting to note that coexisting cummingtonite and hornblende have been found in certain Norwegian eclogites (Ross et al., 1968), which may represent a high pressure environment. For these reasons, Shido's mechanism is discredited.

In the amphibolites of the study area more than 15% show coexisting cummingtonite and hornblende. The textural relations between these two phases are in all respects similar to those previously cited. In some cases, all the above textural relations are found in a single thin section (Figure 6.3), but most commonly cummingtonite is found as homoaxial, patchy intergrowths or thin lamellae in hornblende (Figure 6.4). The converse applies for hornblende in cummingtonite. These two textures are most often ascribed to exsolution of one phase from another parallel to $(\bar{1}01)$ and (100) . Detailed electron microprobe and X-ray studies in the literature have confirmed the existence of the two amphiboles on a microscopic level (Jaffe et al. 1968; Klein, 1968; Ross et al., 1968). Klein (1968) has shown the approximate limits of the miscibility gap between the calcic and Mg-Fe clinoamphiboles in a compositional quadrilateral similar to that used for the pyroxenes (Figure 6.5). Compositional data on these coexisting amphibole pairs from a wide variety of geologic environments imply very steep slopes for each solvus limb. It is thought that the hornblende-cummingtonite pairs encountered in this investigation have exsolved along or have equilibrated across this miscibility gap in response to a particular set of P-T conditions imposed upon a subcalcic amphibolite bulk composition. Since Klein's work (1968, p. 320) indicates exsolution does occur in high temperature volcanic rocks, it is likely that the amphibole pairs encountered in this study represent prograde exsolution phenomena.



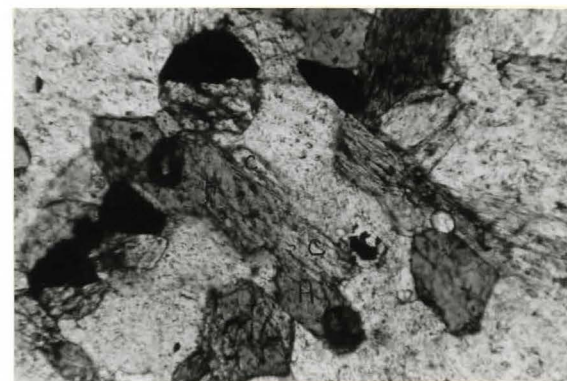
A



B



C



D

Figure 6.3. Hornblende(H)-cummingtonite(C) textures in specimen 2a-24, 120X:

- A - Cummingtonite as partial rim on hornblende
- B - Cummingtonite as a discrete grain
- C - Lamellae of hornblende in cummingtonite
- D - Homoaxial hornblende-cummingtonite intergrowth.



Figure 6.4: Hornblende (H)-cummingtonite (c) exsolution relations. Exsolution lamellae of one phase in the other occur parallel to $(\bar{1}00)$ and (100) . Specimen An-200, 120 X.

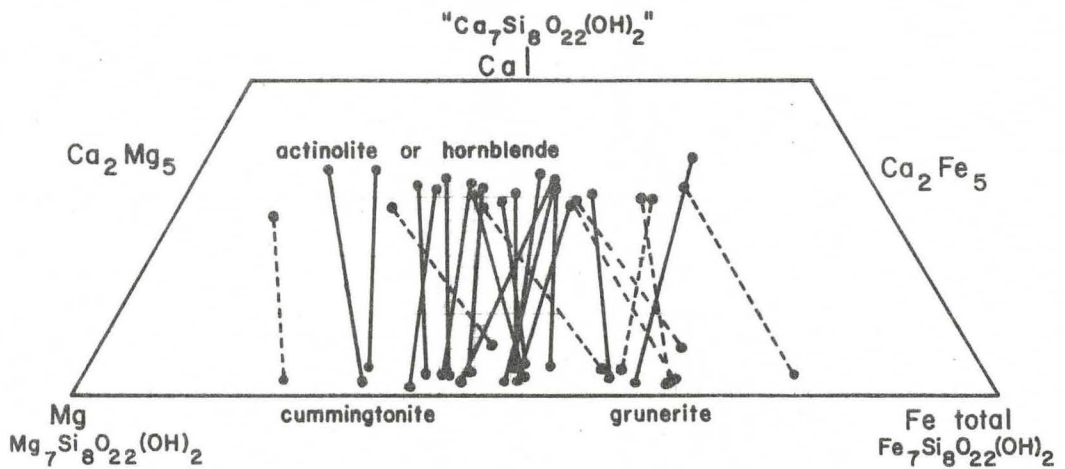


Figure 6.5: Compositional quadrilateral showing extent of miscibility gap between calcic and Mg-Fe clinoamphiboles. (After Klein, 1968, p. 308)

Quartzo-Feldspathic Gneisses

This name is applied to pelitic and psammite bulk compositions of gneissic character. Commonly referred to as "Grenville paragneisses" these rocks are comprised predominantly of feldspars, micas, quartz, hornblende, clinopyroxene, garnet, sillimanite and oxides. Characteristic accessory phases include epidote minerals, sphene, tourmaline, carbonate, apatite and sulfides. Inequant minerals such as hornblende (X=yellowish green, Y = dark green to olive green, Z = blue green), biotite (X = light tan to medium brown, YZ = medium brown to reddish brown to very dark brown) muscovite and sillimanite are preferentially aligned parallel to foliation imparting a lepidoblastic texture to the rock. Compositional banding is commonly preserved on a thin section scale often resulting in the recognition of several phase assemblages in the same slide. Occasionally, banding is lamellar in nature and is preserved through individual porphyroblasts of garnet similar to occurrences in the nearby Whetstone Lake area (Carmichael, 1968). Staurolite occurs infrequently as rounded, optically continuous reaction relicts in plagioclase. It is associated with cordierite in the two occurrences of this mineral in the study area. Plagioclase compositions fall in the range An_{20} to An_{50} with the bulk falling between An_{30} and An_{45} . Magnetite and exsolved hematite-ilmenite solid solutions are nearly ubiquitous in this rock type although occurrences of one oxide phase are not unknown. Minor pyrite, chalcopyrite or

pyrrhotite may accompany these oxide phases.

As in the case of the preceding amphibolites, four varieties of quartzo-feldspathic gneisses have been recognized in thin section: (1) sub-aluminous, (2) aluminous, (3) hornblende and (4) clinopyroxene gneisses. Like the amphibolite varieties, these four gneissic types cannot be mapped in the field at the scale of the current investigation.¹ They occur rather intimately interbanded on an outcrop scale exemplifying the effect of highly variable bulk compositions on equilibrium phase assemblages. A summary of prograde quartzo-feldspathic gneiss phase assemblages is given in Table 6.2. Sub-aluminous gneisses occur 2-3 times more frequently than the other varieties listed. ACFK and AFM compatibility diagrams for equilibrium assemblages in the four gneiss varieties are shown in Figure 6.6. Representative modes are listed in Table 5.5.

From the compilation of aluminous quartzo-feldspathic gneiss phase assemblages, the following are incompatible in ACKF space and are indicative of disequilibrium:

¹ The agreement between the compositional groupings of Chapter 5 and the petrographic varieties is poor, hence the petrographic grouping is used throughout this chapter.

Table 6.2

PHASE ASSEMBLAGES IN QUARTZO-FELDSPATHIC GNEISSES

<u>Gneissic Type</u>	<u>Characteristic Assemblages</u>
Sub-Aluminous Gneisses	Biotite-Plagioclase-Quartz-Oxides
	Biotite-Muscovite-Plagioclase-Quartz-Oxide
	Biotite-Plagioclase-K-feldspar-Quartz-Oxides
	Biotite-Muscovite-Plagioclase-K-feldspar-Quartz-Oxides
	Biotite-Plagioclase-K-feldspar
	Garnet-Biotite-Plagioclase-Quartz-Oxides
	Garnet-Biotite-Muscovite-Plagioclase-Quartz-Oxides
	Garnet-Biotite-Plagioclase-K-feldspar-Quartz-Oxides
Aluminous Gneisses	Sillimanite-Biotite-Plagioclase-Quartz-Oxides
	Sillimanite-Biotite-Muscovite-Plagioclase-Quartz-Oxides
	Sillimanite-Biotite-Muscovite-Plagioclase-K-feldspar-Quartz-Oxides
	Sillimanite-Garnet-Biotite-Plagioclase-Quartz-Oxides

Staurolite-Sillimanite-Garnet-
Cordierite-Biotite-Plagioclase-Quartz

Staurolite-Cordierite-Garnet-Biotite-
Plagioclase-Quartz

Staurolite-Sillimanite-Garnet-Biotite-
Plagioclase-Quartz

Staurolite-Sillimanite-Biotite-
Muscovite-Plagioclase-Quartz

Hornblende Gneisses

Hornblende-Plagioclase-Quartz-Oxides

Hornblende-Biotite-Plagioclase-
Carbonate-Oxides

Hornblende-Biotite-Plagioclase-Quartz-
Oxides

Hornblende-Biotite-Plagioclase-K-
feldspar-Quartz±Oxides

Hornblende-Plagioclase-K-feldspar-
Quartz

Hornblende-Plagioclase-Scapolite-K-
feldspar-Oxides

Hornblende-Garnet-Plagioclase-K-
feldspar-Quartz-Oxides

Clinopyroxene Gneisses

Clinopyroxene-Plagioclase-Carbonate

Clinopyroxene-Plagioclase-Quartz-
Carbonate-Oxides

Clinopyroxene-Biotite-Plagioclase-Quartz

Clinopyroxene-Biotite-Plagioclase-
Carbonate-Oxides

Clinopyroxene-Plagioclase-K-feldspar

Clinopyroxene-Plagioclase-K-feldspar-
Quartz

Clinopyroxene-Biotite-Plagioclase-
K-feldspar-Oxides

Clinopyroxene-Biotite-Plagioclase-
K-feldspar-Quartz-Oxides

Clinopyroxene-Scapolite-K-feldspar-
Sphene-Carbonate-Oxides

Clinopyroxene-Hornblende-Plagioclase-
Quartz-Oxides

Clinopyroxene-Hornblende-Plagioclase-
K-feldspar-Quartz-Carbonate

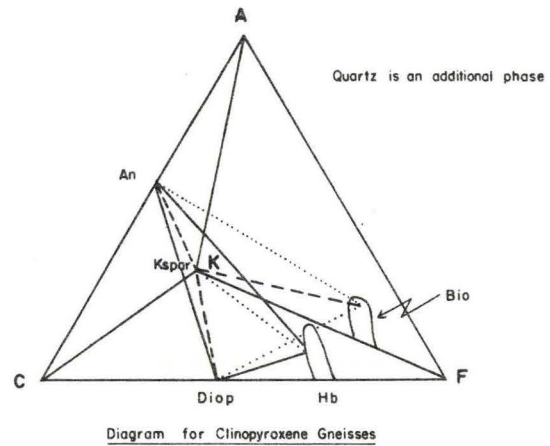
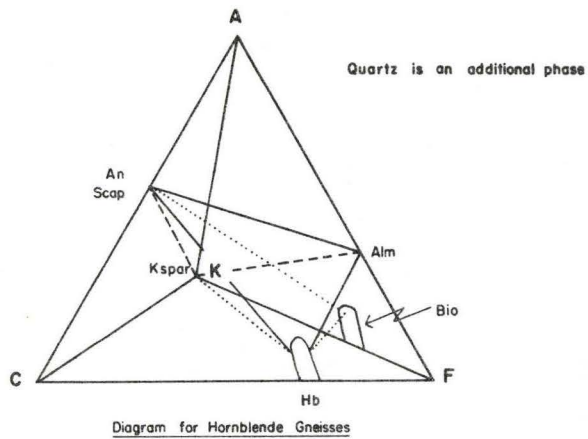
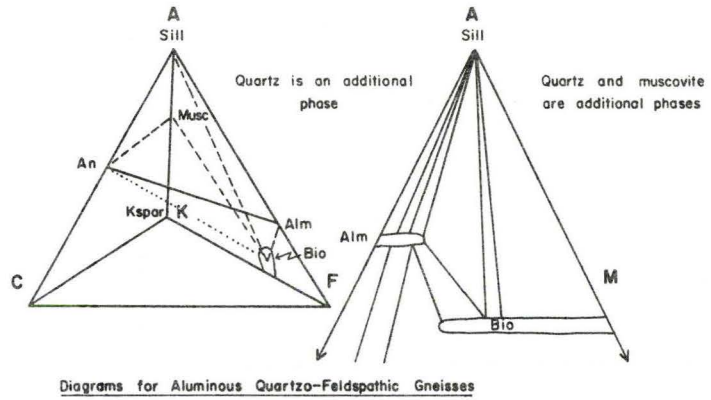
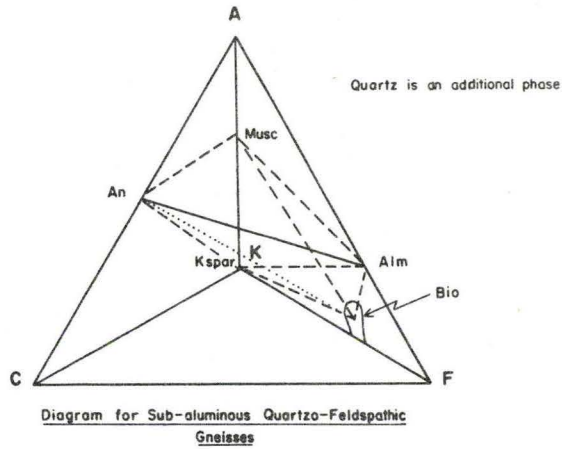
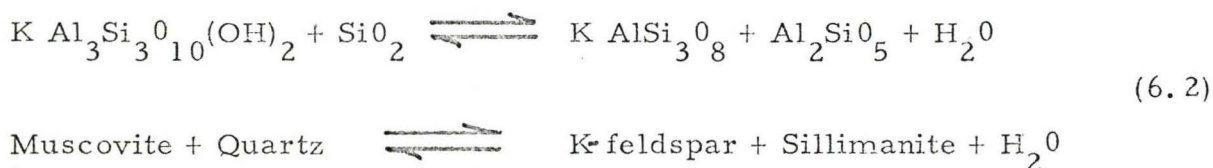


FIGURE 6.6 : ACKF and AFM Diagrams for Quartzo-Feldspathic Gneisses. Note that tie lines on the front face of the tetrahedron are shown by solid lines, those on the back three faces by dashed lines, and those within the volume by dotted lines.

- (1) Sillimanite-Biotite-Muscovite-Plagioclase-K-feldspar-
Quartz-Oxides
- (2) Staurolite-Sillimanite-Garnet-Cordierite-Biotite-
Plagioclase-Quartz
- (3) Staurolite-Garnet-Cordierite-Biotite-Plagioclase-Quartz
- (4) Staurolite-Sillimanite-Garnet-Biotite-Plagioclase-Quartz
- (5) Staurolite-Sillimanite-Biotite-Muscovite-Plagioclase-Quartz

The occurrence and significance of muscovite-quartz-K-feldspar-sillimanite as well as staurolite bearing assemblages will be treated forthwith.

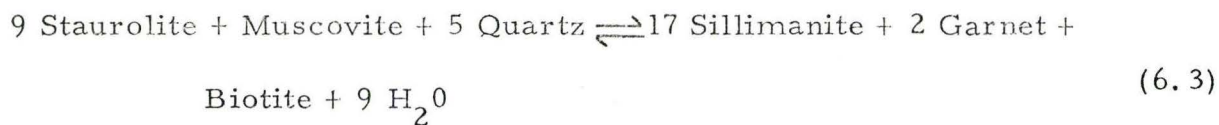
The reaction:



is generally considered to account for the disappearance of the stable assemblage muscovite+quartz in pelitic rocks of the almandine amphibolite facies (Turner and Verhoogan, 1960, p. 552). This reaction occurs in the four component system $\text{K}_2\text{O}-\text{Al}_2\text{O}_3-\text{SiO}_2-\text{H}_2\text{O}$. A phase rule analysis of this system shows that the assemblage Muscovite+Quartz+K-feldspar+Sillimanite represents univariant conditions if H_2O is assumed to be present as a discrete phase in the assemblage. That this is probable is born out by the not uncommon occurrence of minute fluid inclusions in metamorphic minerals. With this assumption in mind the distribution of

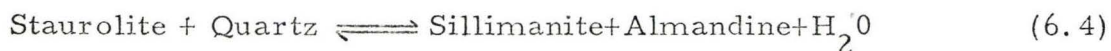
the assemblage muscovite+quartz may be used to define the locus of the above reaction in the field. Upon inspection, muscovite+quartz is seen to co-exist in apparent stable equilibrium throughout the study area except in four instances where this assemblage is seen in contact with K-feldspar and sillimanite. The random occurrence of these four examples suggests perhaps that f_{H_2O} for these specimens was sufficiently low for the total pressure and temperature of metamorphism to allow initiation of the reaction. Further investigation to the northwest of the study area is needed to define the systematic, large scale breakdown of muscovite in the presence of quartz.

Considering the staurolite bearing assemblages, it was noted earlier that staurolite persists above the line of first sillimanite appearance throughout much of the Bancroft-Madoc area. In the map area, staurolite occurs as rounded grains with textural relations suggestive of frozen staurolite breakdown reactions in the prograde phase assemblages of pelitic and semi-pelitic gneisses. Carmichael (1969) has written two reactions to account for the formation of sillimanite in pelitic rocks of the nearby Whetstone Lake area in Lake Township. In the first and lowest grade reaction, sillimanite forms from kyanite by a net polymorphic inversion but in the second reaction at a very slightly higher grade, sillimanite forms at the expense of staurolite according to (Carmichael, 1969, p. 259):



Consequently, at least part of the sillimanite encountered in the amphibolite facies terrain of the Bancroft-Madoc area appears to form from the breakdown of staurolite.

The rather widespread occurrence of staurolite between 5 and 10 miles above Lumbers (1967a) sillimanite isograd (Figure 6.1) suggests that the breakdown of staurolite is not instantaneous with the complete loss of all staurolite across a reaction surface or isograd. Thus the reaction commonly used to express the disappearance of staurolite+quartz (Turner and Verhoogan, 1960, p. 548):



does not appear to be directly applicable to the Bancroft-Madoc area in this simple form. In addition, Carmichael's staurolite breakdown reaction does not apply to rocks of the study area because staurolite in muscovite and quartz bearing assemblages is not associated with garnet as shown in Table 6.2. Thus, alternative explanations for the apparent breakdown of staurolite in rocks of the Hermon Group must be found.

In the present investigation, textural relations, AKFM plots and phase rule considerations of the staurolite bearing assemblages have been used to formulate general reactions explaining the progressive or continuous disappearance of staurolite with changing metamorphic

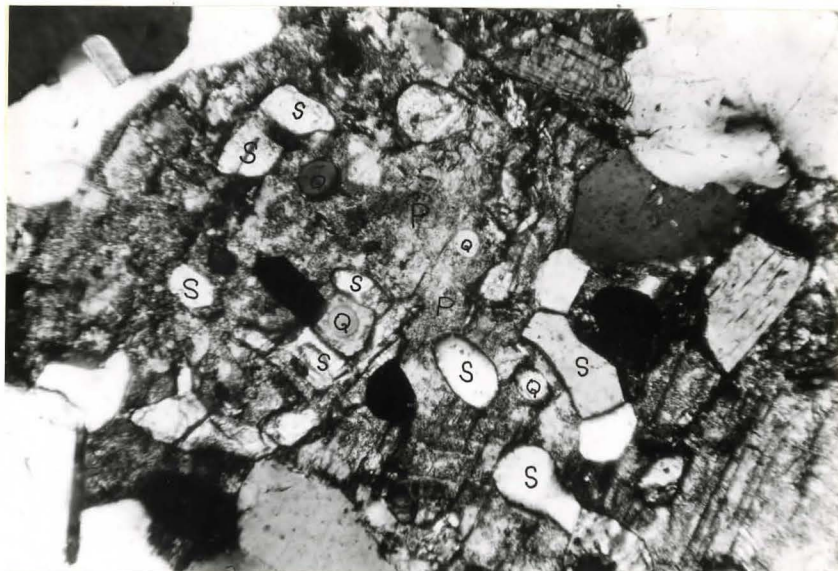
conditions. These general reactions are then evaluated in terms of experimental investigations of the upper stability of staurolite.

In thin section, many textures are seen suggesting the instability of staurolite at the time of prograde metamorphism. These textures are documented below for each staurolite bearing assemblage. Reactions relating the respective phases are deduced from AKFM phase compatibilities in light of the textural relations.

Assemblage (2): Staurolite-Sillimanite-Garnet-Cordierite-Biotite-

Plagioclase-Quartz

- (1) Staurolite and quartz occur as rounded grains in large plagioclase and/or cordierite grains (Figure 6.7). The rounded grains of staurolite have the same crystallographic orientation as deduced from the optical continuity of the individual grains. It is appealing to think of these staurolites as remnants of single porphyroblasts which have reacted with quartz and/or contiguous micas to form plagioclase or cordierite (c.f. Carmichael, 1969).
- (2) Garnet, while highly sieved with plagioclase and quartz, is not rimmed by a second generation of homogeneous garnet as seen in other assemblages in the present study. This implies the garnet is either newly formed as a reaction product or is in the process of decomposition.



A



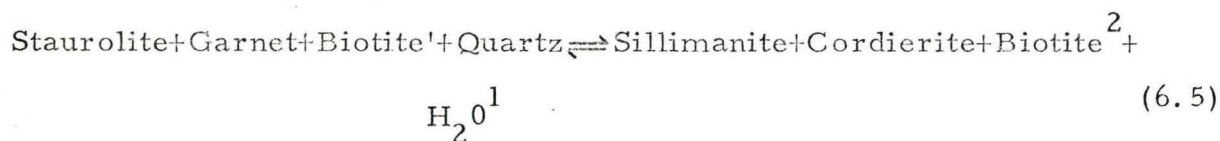
B

Figure 6.7. A. Staurolite (S) and quartz (Q) relicts in plagioclase (P). Specimen Ch-10, crossed nicols, 120X.

B. Staurolite (S) relicts in cordierite (C). Specimen 68-74-17, 120X.

- (3) Fibrolitic sillimanite is intergrown with biotite suggesting contemporaneous crystallization as reaction products (Figure 6.8).

From these textures staurolite appears to be breaking down to cordierite, plagioclase, sillimanite and biotite. In the AKFM tetrahedron of Thompson (1957), phase compatibilities suggest a reaction of the form (Figure 6.9):



Plagioclase should be added to each side of this equilibrium to express the correct form of the reaction for the natural assemblage. This reaction, as well as the following ones involving staurolite, is degenerate (i. e. it may be written for arbitrary amounts of reactants and product phases) and therefore is not shown as a balanced reaction.

Assemblage (3): Staurolite-Garnet-Cordierite-Biotite-Plagioclase-Quartz

- (1) Staurolite relicts occur in plagioclase and cordierite similar to the examples in Figure 6.7 implying the growth of these phases at the expense of staurolite.

1) This reaction on the basis of the textural evidence could be written:
 $\text{Staurolite} + \text{Biotite}^1 + \text{Quartz} \rightleftharpoons \text{Sillimanite} + \text{Cordierite} + \text{Garnet} + \text{Biotite}^2 + \text{H}_2\text{O}$
 However, this introduces a four phase product assemblage which is incompatible in AKFM space.

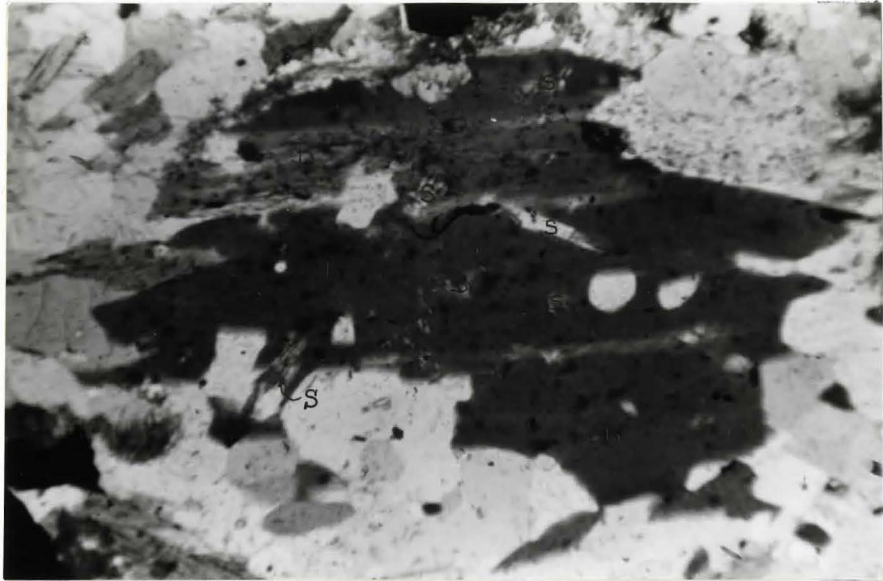


Figure 6.8 Fibrolitic sillimanite (S) intergrown with biotite (B). Specimen 67-171-9, 42X

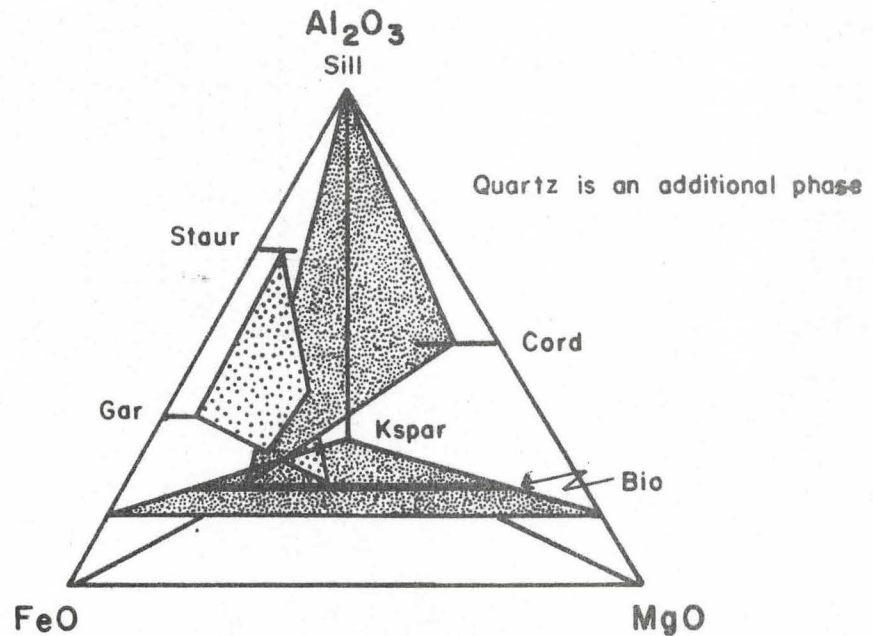
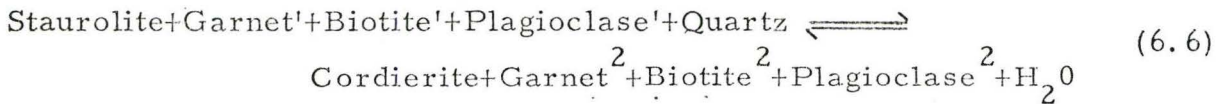


Figure 6.9: AKFM Diagram for Assemblage (2)

- (2) Garnet has a sieved core with homogeneous rims of garnet (Figure 6.10) suggesting the growth of prograde garnet on pre-existing sieved porphyroblasts.
- (3) Two generations of biotite are seen as a result of the recrystallization of this mineral synchronous with the breakdown of staurolite (Figure 6.11).

As in the preceding assemblage, staurolite appears to be reacting to cordierite and plagioclase. Garnet and biotite are recrystallizing as staurolite disappears as shown in the AKFM diagram of Figure 6.12. The reaction applicable to this assemblage is:



It should be pointed out that assemblages (2) and (3) are singular occurrences in the map area. Further detailed study of staurolite parageneses to the northwest and southeast of the map area may show that the reactions proposed for these assemblages are incorrect. Thus, they should be regarded merely as potential explanations of the disappearance of staurolite in cordierite-bearing rocks.

Assemblage (4): Staurolite-Sillimanite-Garnet-Biotite-Plagioclase-Quartz

- (1) Staurolite relicts and rounded blebs of quartz are found in large plagioclase grains as in the previous examples.



Figure 6.10. Texturally zoned garnet showing sieved core and homogeneous rim. Specimen 2Pb-9, 42X.

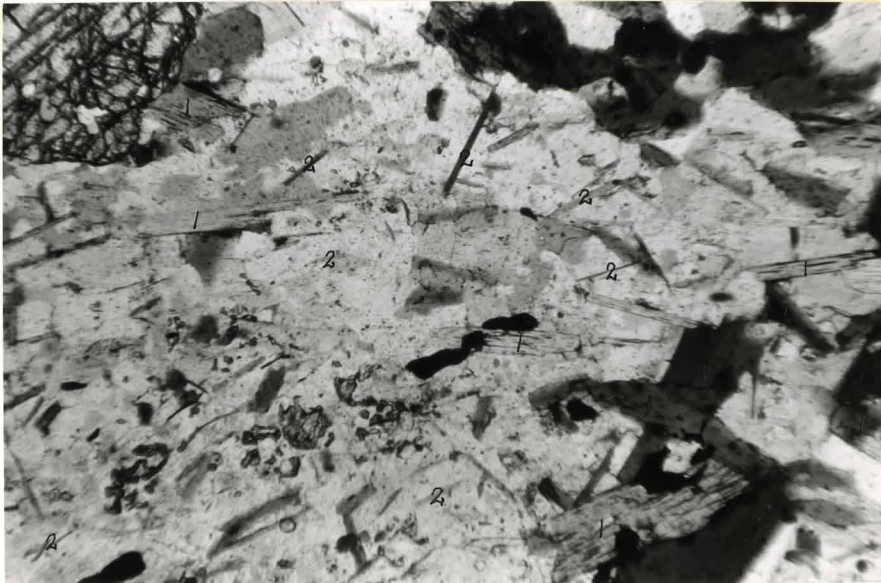


Figure 6.11. Two generations of biotite (1 and 2) in staurolite-bearing gneiss. Specimen 68-74-17, 42X.

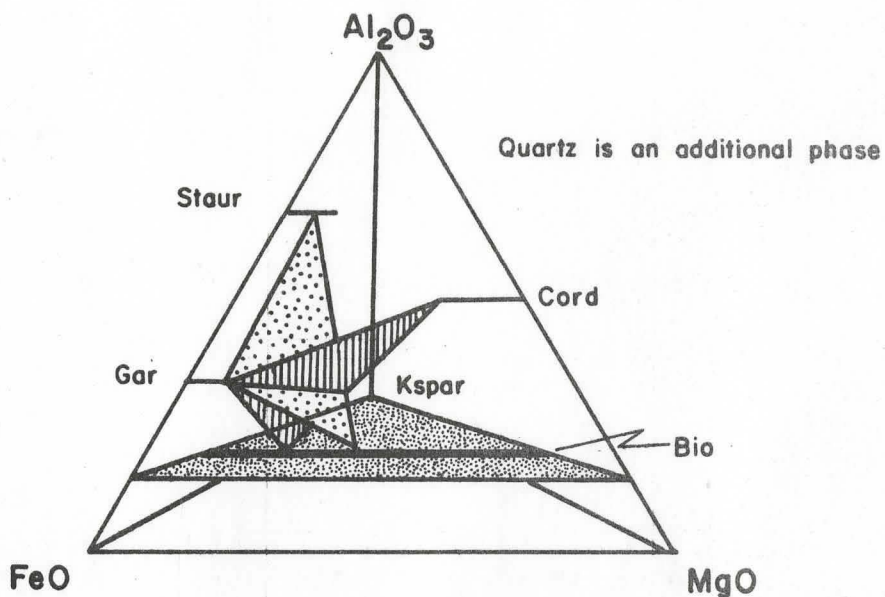


Figure 6.12: AKFM Diagram for Assemblage (3)

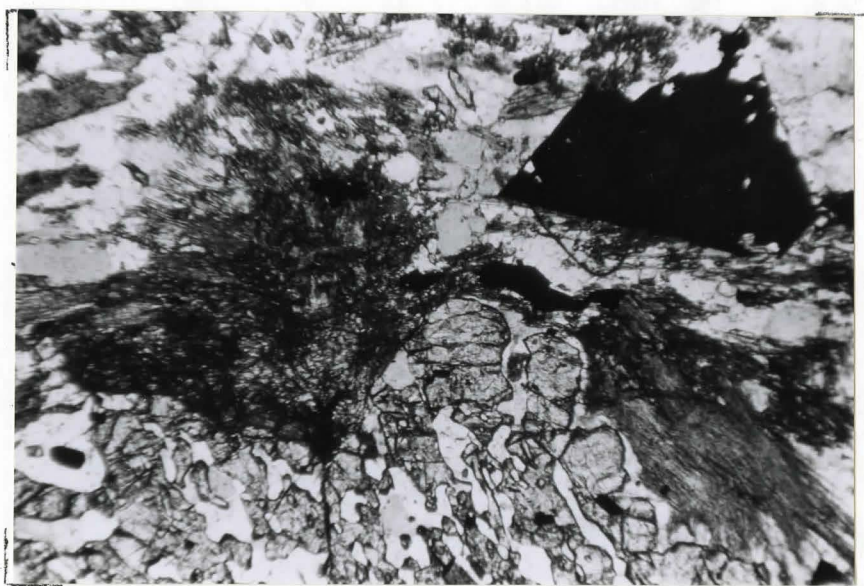
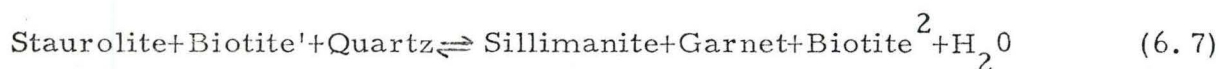


Figure 6.13 Garnet (G) rimmed by and intergrown with fibrolitic sillimanite (S). Specimen 2Pb-8, 42X.

- (2) Garnets are texturally unzoned and are always rimmed by tuffs of fibrolite which is commonly intergrown with the garnet (Figure 6.13). This implies contemporaneous crystallization of sillimanite and garnet in place of the chemically equivalent assemblage, staurolite+quartz.
- (3) Intergrown fibrolite and biotite are common as in assemblage (2).
- (4) Two generations of biotite are present confirming the recrystallization of biotite with the breakdown of staurolite.

The AKFM diagram of Figure 6.14 indicates the reaction relating these phases to be:



In this diagram, the tie line staurolite-biotite is seen to give way to the tie figure sillimanite-garnet-biotite. This reaction agrees well with the textural relations.

Assemblage (5): Staurolite-Sillimanite-Biotite-Muscovite-Plagioclase-Quartz

- (1) Staurolite and quartz occur as rounded reaction relicts in plagioclase.
- (2) Muscovite occurs as corroded laths of low abundance implying instability.
- (3) Biotite and fibrolite show intergrowth relations similar to those of Figure 6.8. This intergrowth presumably represents contem-

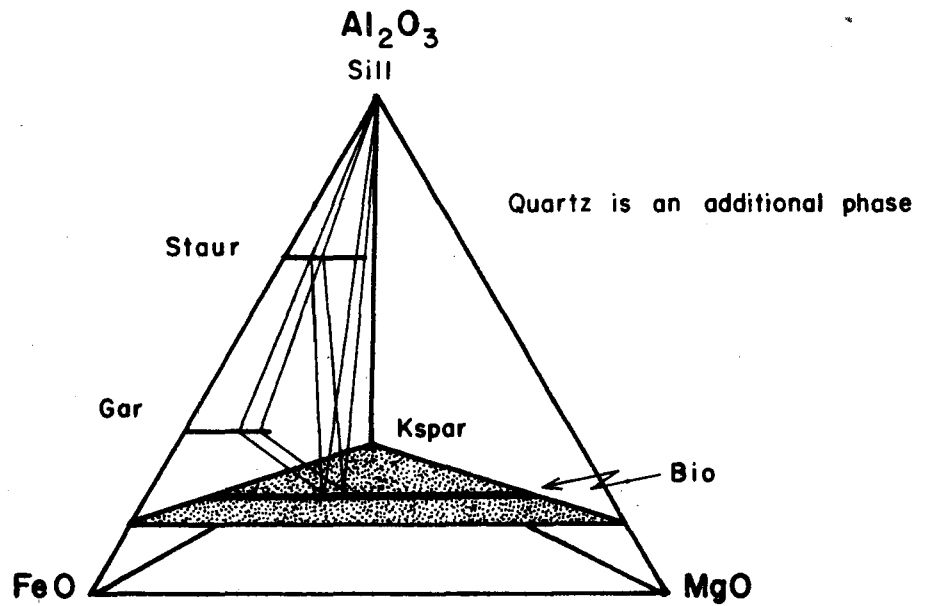


Figure 6.14 AKFM Diagram for Assemblage (4)

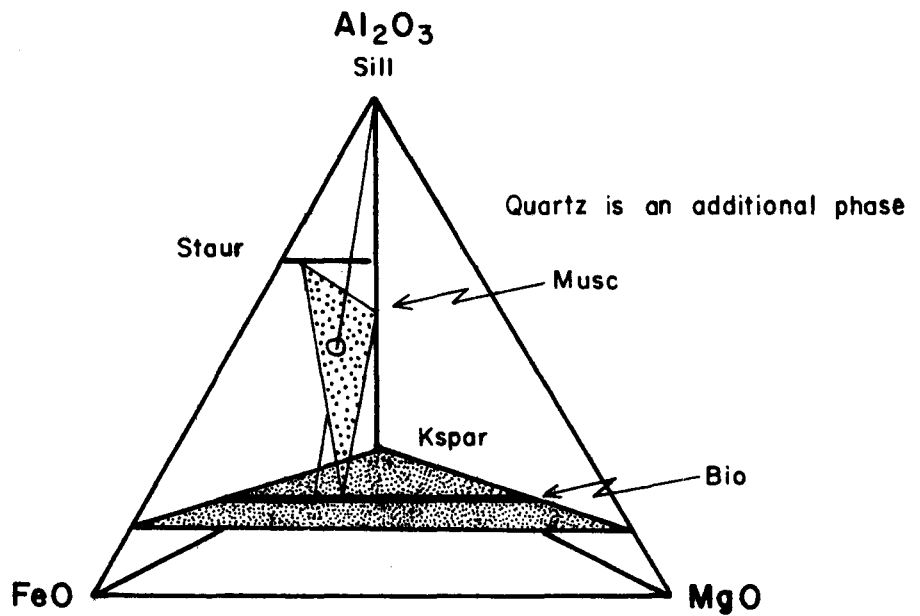
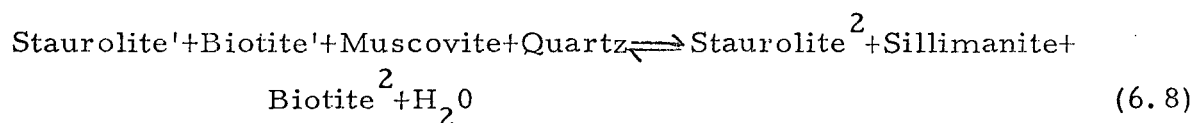


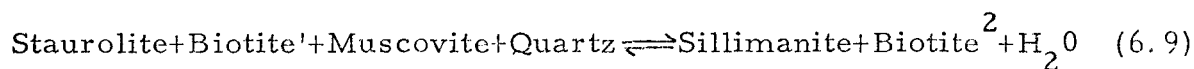
Figure 6.15 AKFM Diagram for Assemblage (5)

poraneous crystallization of the two phases as products of a staurolite decomposition reaction.

Plotting this assemblage in the AKFM tetrahedron (Figure 6.15), the staurolite-muscovite-biotite tie figure is seen to be pierced by the tie line sillimanite-biotite. Movement of this three phase area in response to changing metamorphic conditions occurs through successive reactions of the type (c.f. Chinner, 1965, p. 139):



The final disappearance of staurolite of a particular composition defined by a particular rock bulk composition would be of the form:



Plagioclase should be added to both sides of the reaction in order to effect agreement between the reaction and the textures of assemblage (5). It would be useful to have sufficient data on coexisting mineral compositions to be able to assess the direction of movement of the three phase area staurolite-biotite-muscovite in order to work out the stoichiometry of this reaction. It is worth noting that local ionic exchange equilibria considerations similar to those of Carmichael (1969) were made for all four staurolite assemblages in an attempt to reconcile textures with a reaction on a thin section scale. These considerations

met with little success because of the apparent recrystallization of solid solution minerals of unknown composition in each reaction.

The phase equilibria involving staurolite can best be represented in the system $\text{Na}_2\text{O}-\text{K}_2\text{O}-\text{FeO}-\text{MgO}-\text{Al}_2\text{O}_3-\text{SiO}_2-\text{H}_2\text{O}$. In order to treat phase equilibria in this system in terms of the Gibbs Phase Rule it is necessary to define the number of independently variable intensive parameters capable of affecting equilibrium relations. The two most obvious such parameters are total pressure and temperature, however, oxygen fugacity is also of paramount importance in iron-bearing systems. Because of the variability of rock oxidation ratios between hand specimens (see Tables 5.3, 5.5 and 5.8) and the constancy of the optical properties of iron-bearing minerals within individual compositional bands in thin sections, it is proposed that there is little or no exchange of oxygen between layers in compositionally banded rocks. Thus, the oxygen fugacity of a reacting system may, to a first approximation, be considered to be controlled by the mineral assemblage.

From the phase rule where:

$$f = c - p + 2$$

reactions involving seven solid phases plus a fluid phase (e.g. assemblage (2)) in the seven component system are univariant in $P_T - T - f_{\text{O}_2}$ space. By similar argument, the reactions in assemblages (3), (4) and (5) must occur across divariant surfaces in $P_T - T - f_{\text{O}_2}$ space.

From these considerations it is apparent that at least three of the postulated staurolite decomposition reactions can occur over a range of metamorphic conditions as observed in the Bancroft-Madoc area.

It is predominantly the partitioning of iron and magnesium between the reactant and product phases with changing metamorphic grade that permits staurolite to persist stably above the sillimanite isograd. Each of the four staurolite reactions written above defines the upper stability limit of staurolite solid solutions in different bulk compositions subjected to specific but not necessarily identical metamorphic conditions. Reactions of this type cannot be conveniently used to define isograds in regionally metamorphosed terrains because of the seeming overlap of product and reactant assemblages (c. f. Carmichael, 1969, p. 257), even though complete recrystallization of mineral solid solutions has taken place. This type of reaction has been used by Chinner (1965) in a study of the kyanite isograd in Glen Clova.

The experimental work of Richardson (1968) and Hoschek (1969) defines the maximum stability fields of Fe-staurolite+quartz and of staurolite, muscovite plus quartz and is useful in the interpretation of the reactions involving staurolite. That the stability field of Fe-staurolite+quartz in Figure 6.16 is a maximum can be seen from consideration of factors which would affect the topology of this stability field. Since staurolite usually coexists with quartz in metamorphic

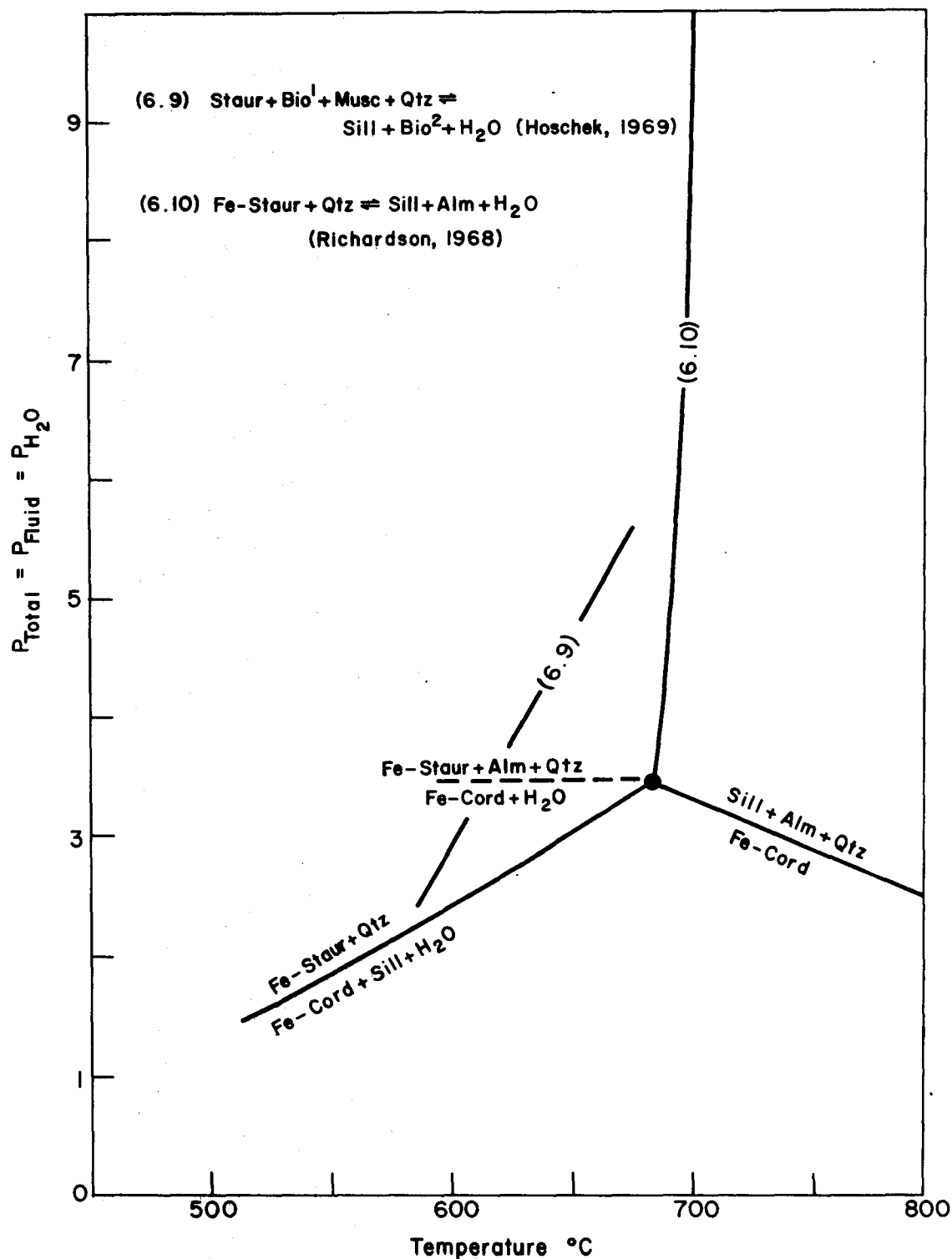
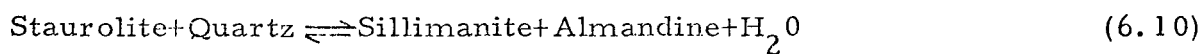


Figure 6.16 Staurolite stability relations after Richardson (1968) and Hoschek (1969). System buffered by the assemblage quartz-fayalite-magnetite. Reactants of (6.9) have $\text{Mg}/\text{Mg}+\text{Fe} = 0.4$.

rocks, the system staurolite+quartz is the simplest system capable of representing the phase relations of staurolite in siliceous rocks and therefore yields the maximum stability field of this assemblage.

Richardson's experimental conditions were such that $P_{\text{Total}} = P_{\text{Fluid}} = P_{\text{H}_2\text{O}}$ thus allowing the maximum positive slopes to the field boundaries in P-T space. The quartz-fayalite-magnetite (QFM) buffer imposed the equilibrium oxygen fugacities on the experimental system and since fayalite is not encountered in common metamorphic assemblages this buffer probably represents the lower limit of f_{O_2} encountered in metamorphic systems containing staurolite. The effect of Mg on the system will probably be to widen slightly the temperature limits of the staurolite+quartz stability field (Richardson, 1968, p. 484). Thus for all practical purposes, the staurolite+quartz stability field shown must cover the reactions involving staurolite discussed above.

Since the natural staurolite assemblages occur in a more complex system, the diagram in Figure 6.16 does not strictly represent any of the equilibria in the study area. Presumably, all these equilibria occur within or across the boundaries of the staurolite+quartz volume in P-T- f_{O_2} space. The reaction relating the phases of assemblage (4) has its analogue in the experimental system wherein:



but because of the additional components in the natural system this equilibrium is probably displaced toward lower temperatures. This is also the case for reaction 6.9 determined experimentally by Hoschek (1969) for experimental conditions identical to those of Richardson in a bulk composition where $Mg/Mg+Fe=0.4$ (Figure 6.16). The position of this equilibrium and that of 6.10 show reasonable agreement between the naturally observed reactions and those determined experimentally.

It should be emphasized that the positions of the reactions considered in the synthetic systems are a function of total pressure, temperature, oxygen fugacity and the degree to which $P_{\text{Total}} = P_{\text{Fluid}} = P_{\text{H}_2\text{O}}$. In the natural systems, bulk composition varies as well. In view of the large number of variables controlling the system, it is not surprising to find several different reactions involving staurolite occurring over a relatively narrow P-T range as is inferred for the study area.

One of the objects of geochemistry is to relate field occurrence with laboratory studies of mineral equilibria with a view toward placing limits on the conditions of formation of the natural assemblages. In this connection the metamorphic grid of Figure 6.17 is useful in the interpretation of the study area. The stability fields of muscovite+quartz (Evans, 1965), common epidote+quartz (Merrin, 1964) and

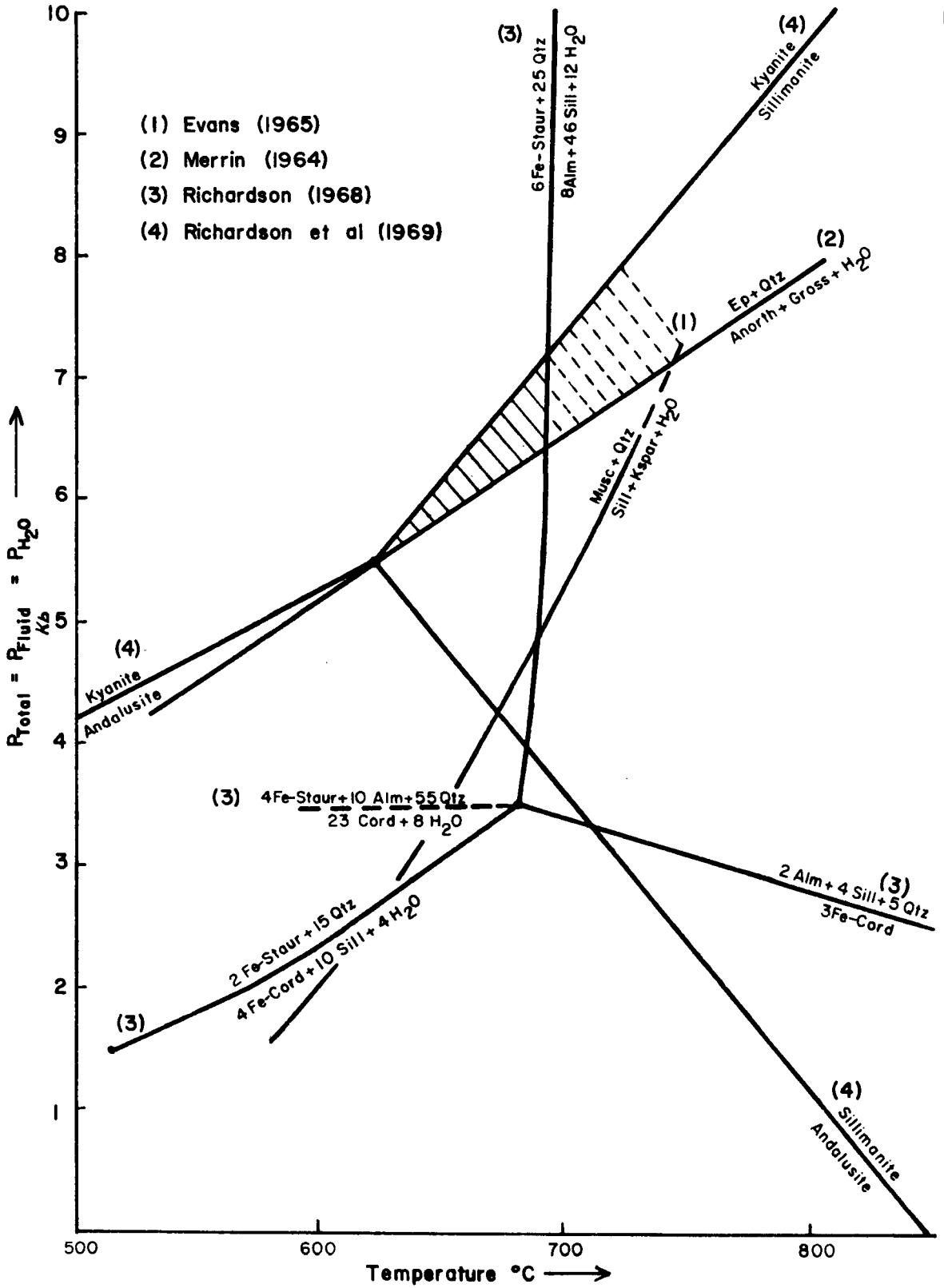


Figure 6.17 Metamorphic Grid for the Study Area

staurolite+quartz (Richardson, 1968) are plotted on this diagram along with the alumino-silicate relations determined by Richardson et al. (1969). Since the condition $P_{\text{Total}} = P_{\text{Fluid}} = P_{\text{H}_2\text{O}}$ was met for all the experimental studies, the stability fields shown represent the maximum area in P-T space over which these mineral pairs and polymorphs can co-exist.

From the diagram, the most probable range of pressure-temperature conditions for the study area is seen to be 5.5 to 7 kilobars total pressure in the temperature interval 625° to 690°C based on the stable coexistence of sillimanite, muscovite+quartz, epidote+quartz and the assumption that all the natural staurolite decomposition reactions occur in the staurolite+quartz stability field. If this assumption is not valid, the upper temperature limit is governed by the muscovite+quartz equilibrium. Since the lower temperature and upper pressure limits are determined by the alumino-silicate triple point, it is worth noting the diversity in location of this point by many experimental studies (Zen, 1969). The diagram of Richardson et al. (1969) constructed for the nearly pure system Al_2SiO_5 with phase transitions reversibly bracketed, agrees well with the work of Newton (1966) and Matsushima et al. (1967) and is preferred for these reasons. Althaus (1967, 1969) has shown that minor amounts of Fe_2O_3 in the system shifts the kyanite-sillimanite univariant to higher pressures at

lower temperatures. Consequently, in rocks of high Fe_2O_3 content the triple point may not occur as shown affecting the above pressure-temperature estimates.

From Table 6.2 and Figure 6.17, the phase assemblages of the quartzo-feldspathic gneisses are those of the amphibolite facies of regional metamorphism. Following the recommendations of Fyfe and Turner (1966) no attempt to categorize these phase assemblages in terms of a sub-facies have been made because:

"it is possible to draw sharp limits only in terms of univariant equilibrium curves for specific reactions"
(Fyfe and Turner, 1966, p. 360.)

Since this approach has been taken in the treatment of the quartzo-feldspathic gneisses, it is perhaps best to consider the map area representative of the upper amphibolite facies in the Bancroft-Madoc sequence.

Leptites

The leptites studied generally have a granoblastic texture with little preferred orientation of the dominant phases, plagioclase, quartz, biotite, K feldspar and oxides. Common additional phases include muscovite, garnet, hornblende and epidote. The characteristic accessories are sphene, minor sulfides and apatite. Biotite shows a range in chemical composition as shown by the pleochroic scheme X = light tan to yellow brown, YZ = medium brown to greenish brown

and very dark brown. Plagioclase compositions fall in the range An₁₅ to An₄₈ with the bulk between An₃₀ and An₄₀. Re-equilibration of plagioclase during retrograde metamorphism has resulted in the production of Na-oligoclase and albite in many examples making the determination of prograde compositions difficult. Plagioclase is most commonly twinned on the albite law but very often twinning is absent. The Fe-Ti oxide minerals are nearly ubiquitous with magnetite and hematite-ilmenite solid solutions the principal phases. Rude compositional banding is sometimes seen on outcrop, hand specimen and thin section scales. This banding is generally imparted by variations in the amounts of biotite and K-feldspar in discreet domains of the rock.

Leptite phase assemblages are summarized in Table 6.3. Figure 6.18 depicts the ACKF compability diagrams for these assemblages. Representative modal analyses are located in Table 5.8. Again, the metamorphic assemblages are those of the upper amphibolite facies. Because of the relative insensitivity of granitic compositions to changing metamorphic conditions no prograde reaction relations have been noted in the course of this investigation. The apparent stable coexistence of muscovite+quartz and common epidote+quartz are in agreement with phase relations found in the quartzo-feldspathic gneisses which imply that conditions of the so-called second sillimanite isograd have not been exceeded on the large scale.

Table 6.3

LEPTITE PHASE ASSEMBLAGES

<u>Rock Type</u>	<u>Characteristic Assemblages</u>
Leptite	Plagioclase-Quartz-Biotite-Oxides
	Plagioclase-Quartz-K-feldspar-Biotite-Oxides*
	Plagioclase-Quartz-K-feldspar-Biotite-Epidote-Oxides
	Plagioclase-Quartz-K-feldspar-Biotite-Garnet-Oxides
	Plagioclase-Quartz-K-feldspar-Biotite-Hornblende-Oxides
	Plagioclase-Quartz-K-feldspar-Biotite-Muscovite-Oxides*
	Plagioclase-Quartz-K-feldspar-Muscovite-Epidote-Oxides
	Plagioclase-Quartz-Biotite-Muscovite-Garnet-Epidote
	Plagioclase-Quartz-Biotite-Garnet-Oxides

* assemblages which when taken together form nearly 75% of leptite phase assemblages

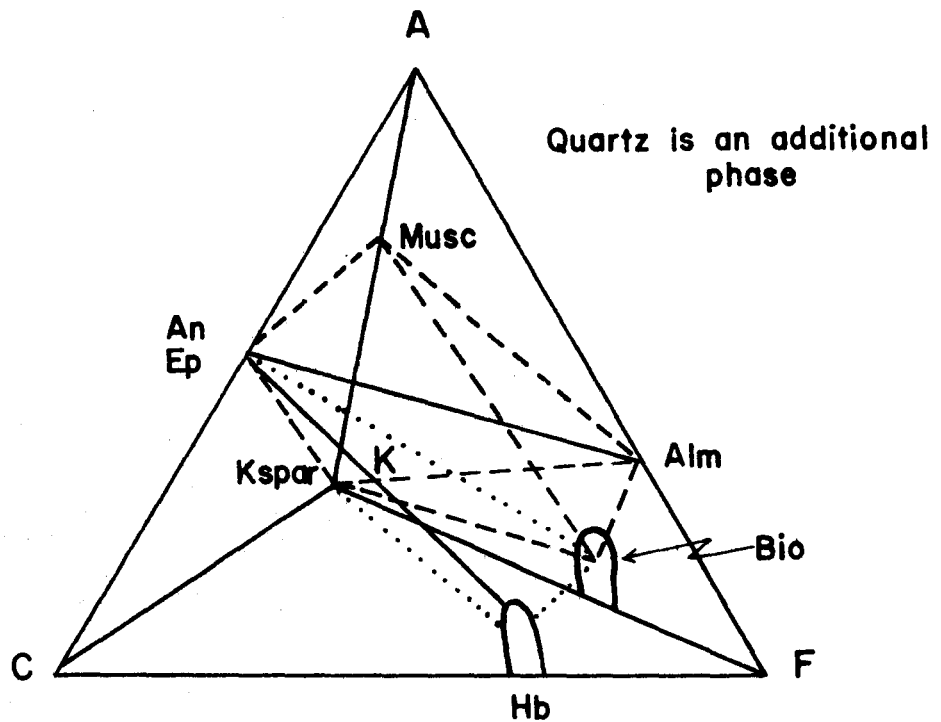


Figure 6.18 ACKF Diagram for Leptites. Note that the lines on the front face of the tetrahedron are shown by solid lines, those on the back three faces by dashed lines and those within the volume by dotted lines.

Carbonate Metasediments

Medium grained carbonate metasediments of the Dungannon formation bound the southeastern margin of the map area. Northwest of the map area another carbonate sequence of unknown stratigraphic position extends to the margin of the Harvey-Cardiff Arch (Hewitt, 1959). Calcitic and dolomitic marbles constitute the dominant lithologies in these units adjacent to the Hermon Group. Included in these marbles are thin feather amphibolites and calc-silicate bands. Because of their restricted bulk composition the relatively pure marbles are of little value in metamorphic phase studies, hence further discussions of phase assemblages will be restricted to those of the inter-banded calc-silicates. Phase assemblages in the marbles are interesting from a geothermometric point of view because of the coexistence of Mg-calcite-dolomite pairs.

Thirty hand specimens of marble were X-rayed by the method of Weber and Smith (1958) in order to identify coexisting Mg-calcite-dolomite pairs. Five such pairs from the carbonate envelope surrounding the Hermon Group rocks were found by this method (Figure 6.19). Petrographic investigation revealed the presence of dolomite lamellae in two of the Mg-calcites (Figure 6.20). The Mg-calcites from these five pairs were separated and analysed by the method of

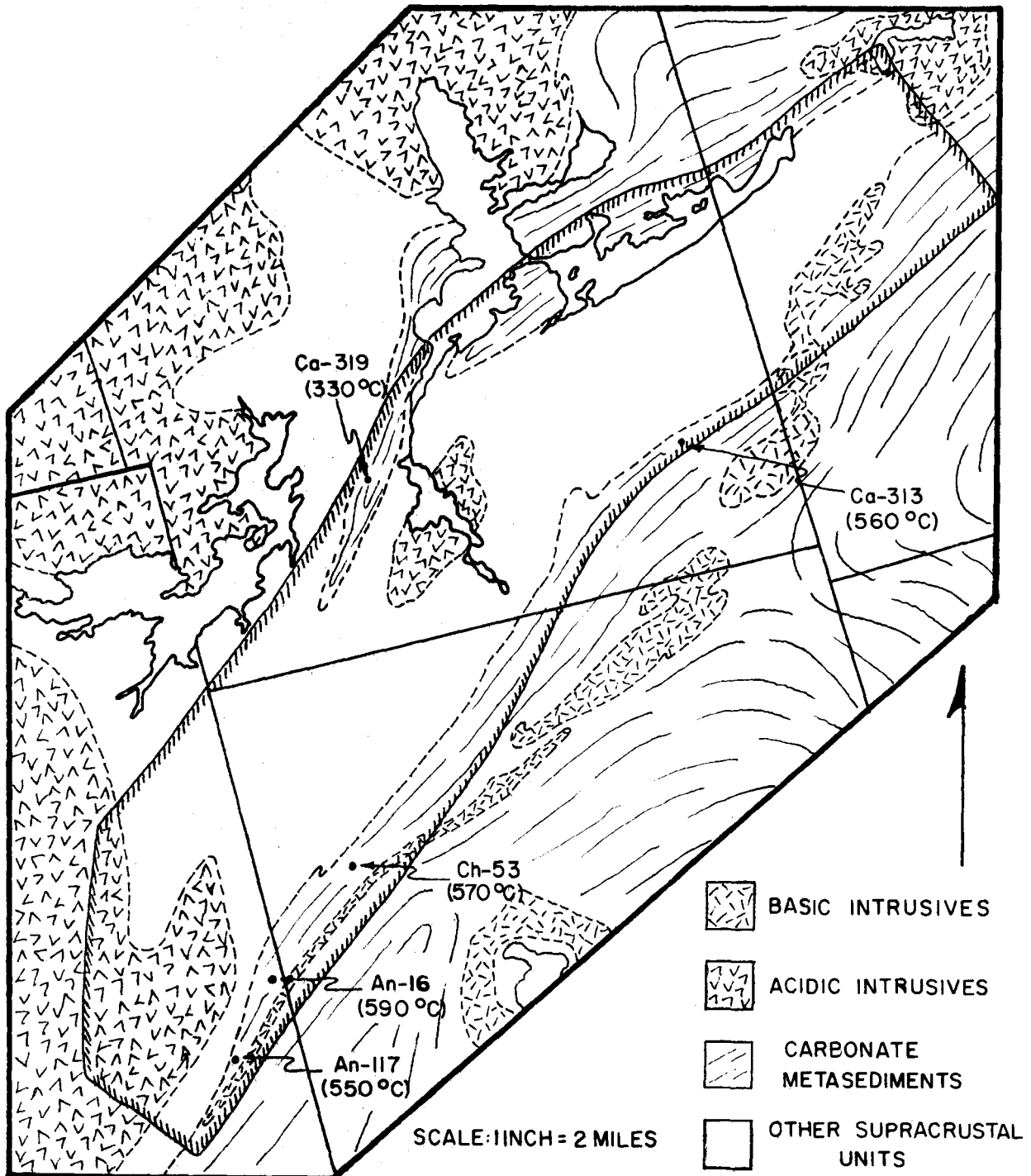


Figure 6.19 Location of analysed Mg-Calcites



Figure 6.20. Dolomite (D) exsolution lamellae in Mg-calcite (C) under crossed nicols. Specimen An-16, 42X.

Jennings and Mitchell (1969) after crude calcite concentrates were obtained by heavy liquid separations. The analytical results are given in Table 6.4.

The solvus temperatures were derived from the Mg-calcite limb of the calcite-dolomite solvus which closely approximates the logarithmic function:

$$\log \text{MgCO}_3 \text{ (Calcite)} = 1.75 \times 10^{-3} T^{\circ}\text{C} - 0.223$$

derived from the experimental data of Goldsmith and Newton (1969). Figure 6.21 relates mole percent MgCO_3 in Mg-calcite to temperature for the range 0 to 1000°C for this function. Since the experimental data only covers temperatures in excess of 400°C an extrapolation must be made for calcites equilibrated with dolomite below this temperature. This extrapolation is shown as a dashed line in Figure 6.21. It should be pointed out that the experimental determinations of the calcite-dolomite solvus (hence the logarithmic curve calculated from it) are polybaric (Graf and Goldsmith, 1955, 1958; Harker and Tuttle, 1955; Goldsmith and Heard, 1961 and Goldsmith and Newton, 1969). Consequently, the amount of Mg in solid solution in calcite is not only a function of temperature but pressure as well. The effect of pressure on this solid solution has been evaluated by Goldsmith and Newton (1969) as approximately 0.12 mole percent MgCO_3 per kilobar. In the present

Table 6.4

PARTIAL ANALYSES OF MG-CALCITES*

Sample	Wgt. % MgO	Wgt. % CaO	Total	Mol. % MgCO ₃	T _s °C [†]
An-16	2.50	52.36	54.86	6.25	590°
An-117	2.18	53.00	55.18	5.45	550°
Ch-53	2.31	51.00	53.31	5.77	570°
Ca-313	2.24	53.15	55.39	5.60	560°
Ca-319	0.89	54.52	55.41	2.22	330°

* D. S. Jennings analyst

† Temperature obtained from Figure 6.21.

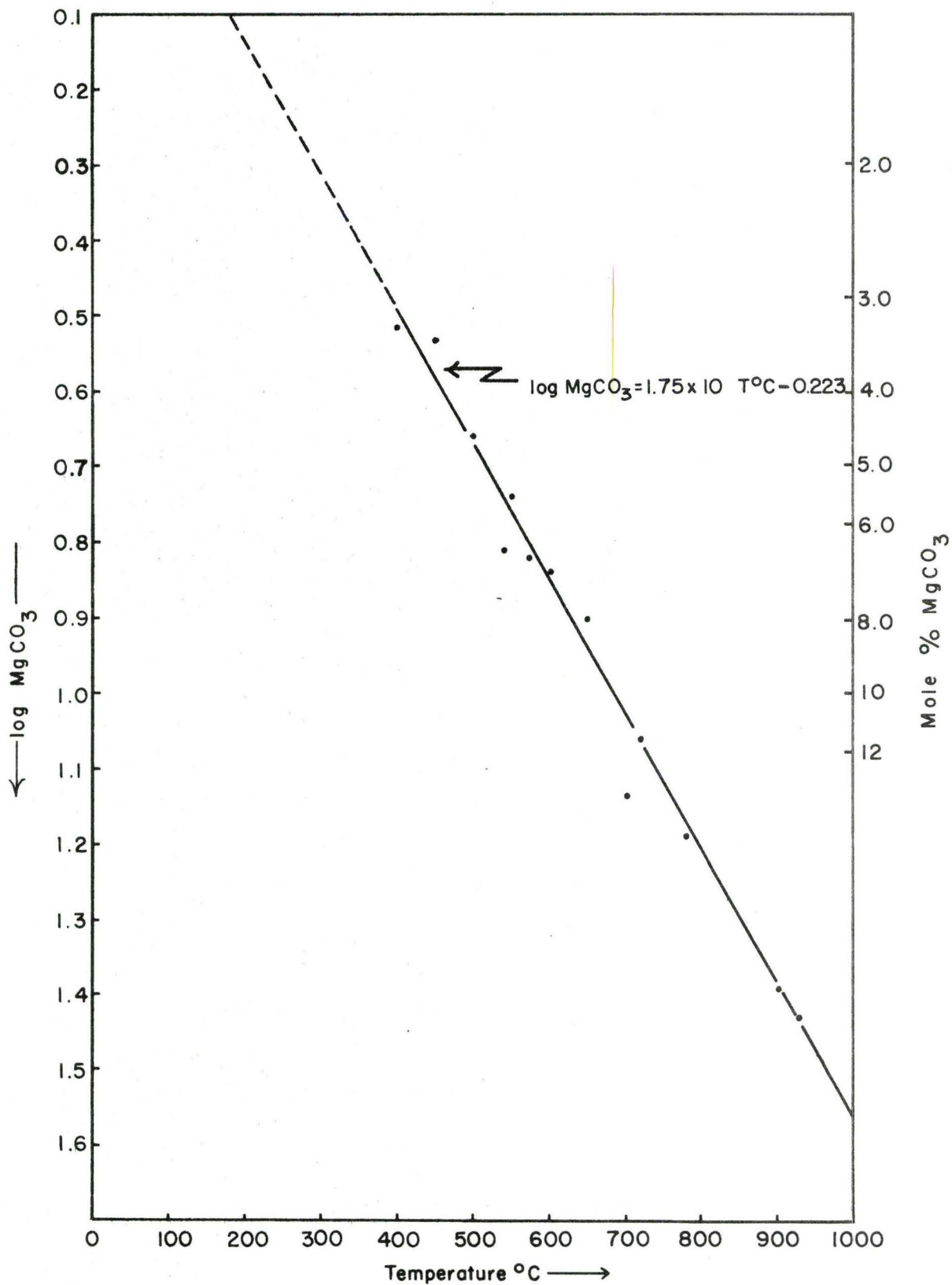


Figure 6.21 The Mg-calcite solvus limb expressed as the function $\log \text{MgCO}_3 = 1.75 \times 10^{-3} T - 0.223$ using data of Goldsmith and Newton (1969)

investigation, no pressure correction has been applied to the raw solvus temperatures for three reasons. Firstly, the total pressure of equilibration of the carbonate pairs is uncertain, probably lying in the range 5.5 to 7 kilobars as shown by Figure 6.17; secondly, it is not certain that the analysed calcites lie exactly on the calcite-dolomite join in the system $\text{CaCO}_3\text{-MgCO}_3$. The substitution of Fe^{+2} , Mn^{+2} , Sr^{+2} and Ba^{+2} for Ca^{+2} or Mg^{+2} may alter slightly the shape of the solvus and any temperatures derived from it. Finally, analytical errors and uncertainty as to the amount of dolomite exsolved upon cooling could lead to temperature uncertainties larger than any introduced by pressure.

That the solvus derived temperatures represent minimal quench temperatures is evident from the exsolution of dolomite from Mg-calcite (Figure 6.20) and the discrepancy between these temperatures and those estimated from Figure 6.17. Nonetheless, the majority of solvus temperatures are not far removed from the postulated maximum range of 625°C to 690°C . Again it should be noted that the position of the triple point in the alumino-silicate system is critical to the estimation of minimal metamorphic temperatures in the map area. The anomalously low solvus temperature given by Ca-319 may either be due to proximity to a minor pegmatite dike approximately 200 stratigraphic feet away or to retrogressive metamorphism. More will be said about

this later. In conclusion, it is puzzling that the calcite-dolomite solvus should record quench temperatures close to those estimated for metamorphic events. The time involved in the cooling off of a metamorphic terrain should be more than sufficient to allow total re-equilibration of the carbonates to low temperature conditions since this is easily achieved in the laboratory in the order of days (Harker and Tuttle, 1955).

Various calc-silicate assemblages occur in the marbles of the map area. These calc-silicates commonly form knots or pods probably representing metamorphosed boudinage structures of more competent interbanded siliceous, dolomitic marbles and slightly ferruginous cherts or orthoquartzites. A summary of calc-silicate assemblages is given in Table 6.5. For convenience, solid solution minerals such as the clinoamphiboles and clinopyroxenes in these assemblages will be referred to by the name of the magnesian end member. In general, the calc-silicate assemblages are iron-poor, but iron-bearing varieties are not uncommon. To a first approximation, these phase assemblages can be represented graphically in the system $\text{CaO-MgO-SiO}_2\text{-CO}_2\text{-H}_2\text{O}$ with phase relations projected on to the plane CaO-MgO-SiO_2 as shown in Figure 6.22. If a fluid phase consisting of a binary $\text{CO}_2\text{-H}_2\text{O}$ mixture is assumed to be present in all assemblages, it can be seen that assemblages (1), (2) and (7) are incompatible. For assemblage (1) the tie lines tremolite-calcite and tremolite-quartz must

Table 6.5

CALC -SILICATE PHASE ASSEMBLAGES

- (1) Tremolite - Diopside - Calcite - Quartz
- (2) Tremolite - Diopside - Calcite - Dolomite
- (3) Tremolite - Calcite - Quartz
- (4) Tremolite - Calcite - Dolomite
- (5) Tremolite - Diopside - Calcite
- (6) Tremolite - Diopside - Dolomite
- (7) Diopside - Dolomite - Quartz
- (8) Diopside - Calcite - Dolomite
- (9) Diopside - Dolomite
- (10) Diopside - Calcite - Grossularite - Clinzoisite - Plagioclase

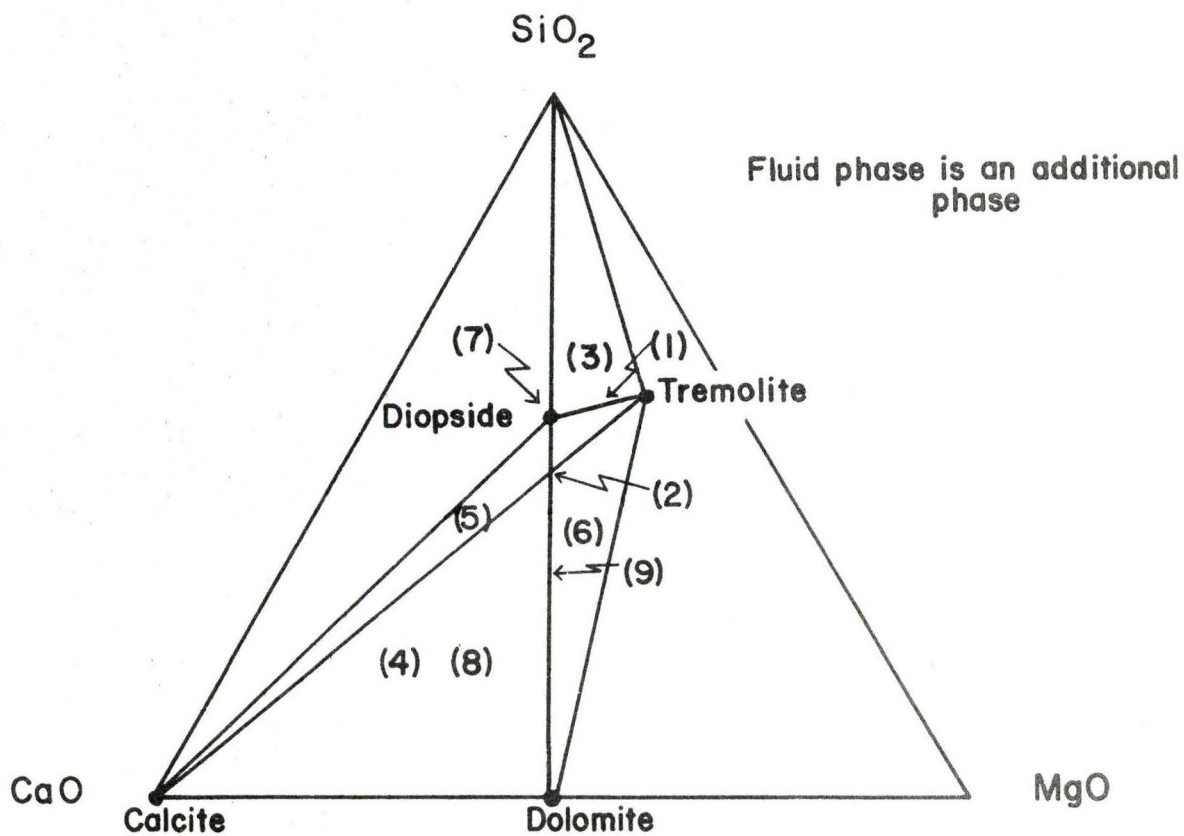


Figure 6.22 Calc-silicate phase relations in CaO-MgO-SiO₂ space. Numbers refer to assemblages in Table 6.5.

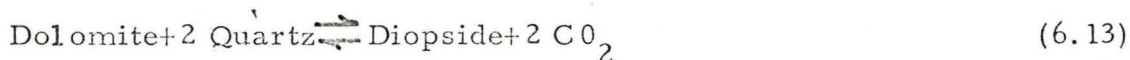
give way to the equivalent tie lines diopside-calcite and diopside-quartz, or vice-versa. The experimental work of Metz (1966) and Metz and Winkler (1964) suggests that with increasing pressure-temperature conditions the assemblage tremolite-calcite-quartz reacts to give diopside according to:



For assemblage (2), the tremolite-calcite tie line breaks to form the tie line diopside-dolomite in Figure 6.22 by the reaction:



in agreement with the predictions of Turner (1967) and Metz and Trommsdorff (1968). Since diopside-dolomite-quartz is degenerate in Figure 6.22, the reaction relating the phases of assemblage (7) in the presence of an anhydrous fluid phase is:



The direction of this reaction is also compatible with the theoretical considerations of Turner (1967) and Metz and Trommsdorff (1968).

The phase incompatibilities just discussed are not in themselves enough to define metamorphic reactions, but there is abundant textural evidence that the three calc-silicate equilibria were operative in the study area. At several locations in Anstruther and Cardiff

townships assemblage (1) occurs with textural relations compatible with reaction 6.11. Both prograde and retrograde examples of this reaction are seen in quartz bearing marbles (Figure 6.23). In silica deficient marbles in Anstruther township assemblage (2) is found with textures implying reaction 6.12. Only retrograde examples of this reaction have been found (Figure 6.24). In Faraday township, zoned dolomite-quartz-diopside pods are found nearly adjacent to bands of coexisting tremolite, calcite and quartz. Where these tremolite-calcite-quartz bands contact dolomitic marble, a reaction rim of diopside has developed separating the two bands. In no case is diopside seen in the three phase band. These relations are illustrated in Figure 6.25 for nearly adjacent compositional bands in the same outcrop. These textures strongly suggest that dolomite and quartz have reacted to form diopside by reaction 6.13, while in contiguous bands tremolite, calcite and quartz have not reacted to form diopside by reaction 6.11.

The coexistence of these assemblages and their reaction relations imply locally buffered $\text{CO}_2\text{-H}_2\text{O}$ systems in nearly adjacent calc-silicate bands. It is apparent that the zoned dolomite-quartz-diopside pods have formed under the influence of an anhydrous fluid phase while the assemblage tremolite-calcite-quartz equilibrated with a hydrous fluid phase. If water had been present in the original dolo-

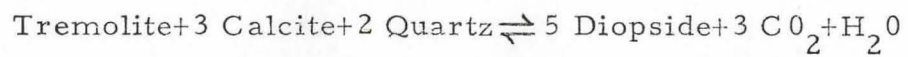


A



B

Figure 6.23. Textures suggestive of the reaction:



A. Prograde direction in specimen An-36.

B. Retrograde direction in specimen An-64.

Abbreviations:

T = tremolite

Q = quartz

C = calcite

D = diopside



Figure 6.24. Texture suggesting the reaction:



Retrograde reaction direction shown: Specimen An-53.

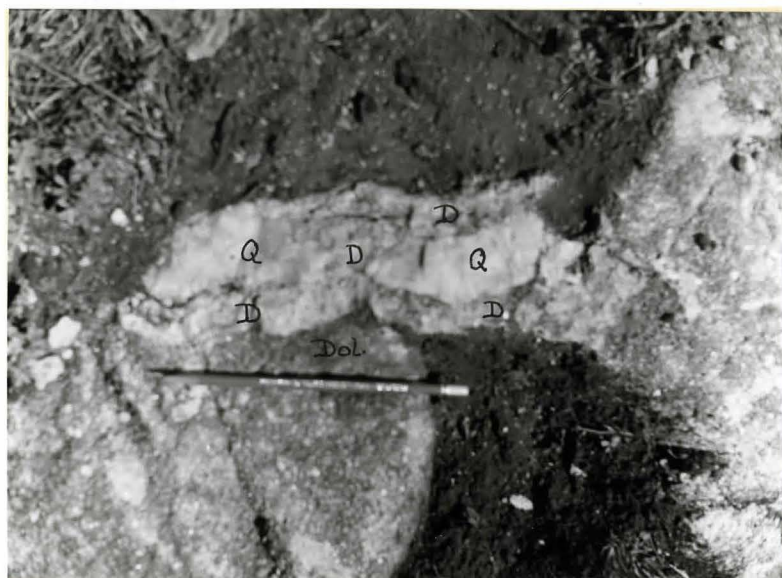
Abbreviations:

T = tremolite

D = diopside

C = calcite

Dol = dolomite



A



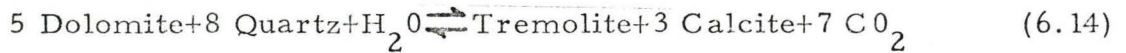
B

Figure 6.25. Relations for assemblages (3) and (7) in the same outcrop, Faraday township.

A. Assemblage (7) showing reaction 6.13.

B. Assemblages (3) and (7). Assemblage (3) not reacting to diopside by reaction 6.11. Assemblage (7) showing reaction 6.13. Specimens Fa-31.

mite and quartz bands now forming the zoned pods, dolomite and quartz would have reacted to form tremolite and calcite under the inferred metamorphic conditions according to:



Since this is not the case, it is reasonable to assume that the nearly adjacent rock volumes containing assemblages (3) and (7) behaved as closed systems across S-surfaces at least with respect to H_2O .

The occurrence of two calc-silicate reactions in the same outcrop deserves further consideration. For such reactions it is reasonable to assume that they have taken place under the same conditions of total pressure and temperature since P-T gradients in an outcrop must necessarily be small or non-existent. If this is the case, the occurrence of reactions 6.11 and 6.12 in the same outcrop and assemblage (3) with reaction 6.13 in another outcrop is due to one or more of the following alternatives:

- (1) Different equilibrium fluid phase compositions governing each reaction in a system where $P_{\text{Total}} = P_{\text{Fluid}}$ (Figure 6.26).
- (2) Identical fluid phase compositions governing the reactions in systems where $P_{\text{Total}} > P_{\text{Fluid}}$ (Figure 6.27).

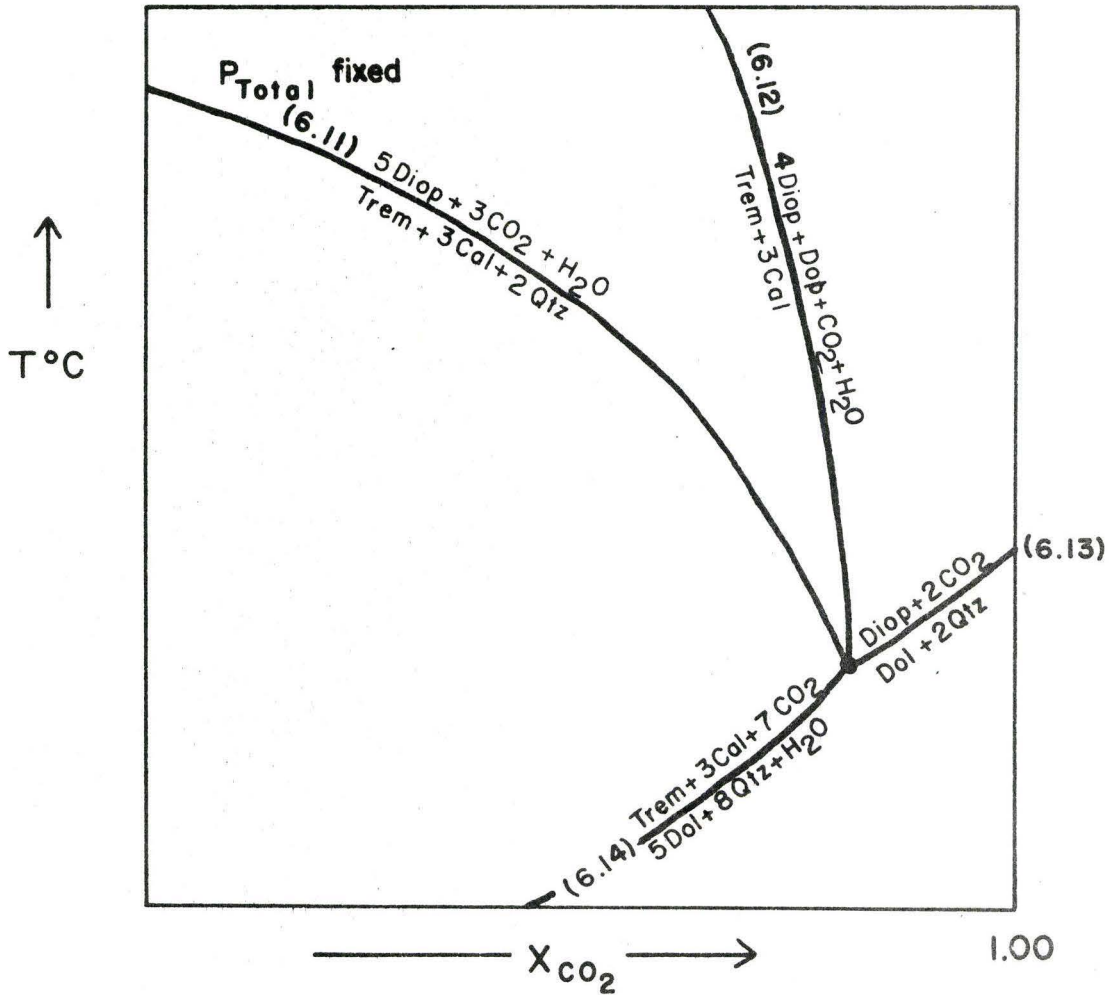


Figure 6.26 Schematic topology of calc-silicate equilibria 6.11, 6.12, 6.13, and 6.14 in $T-X$ space for a fixed total pressure where $P_{\text{Total}} = P_{\text{Fluid}}$ (after Metz and Trommsdorff, 1968, p. 307). X_{CO_2} indicates the mole fraction of CO in a binary $\text{CO}_2\text{-H}_2\text{O}$ fluid phase mixture. For a given T , it can be seen that any two reactions occur at different fluid phase compositions except for the value of T corresponding to the invariant point.

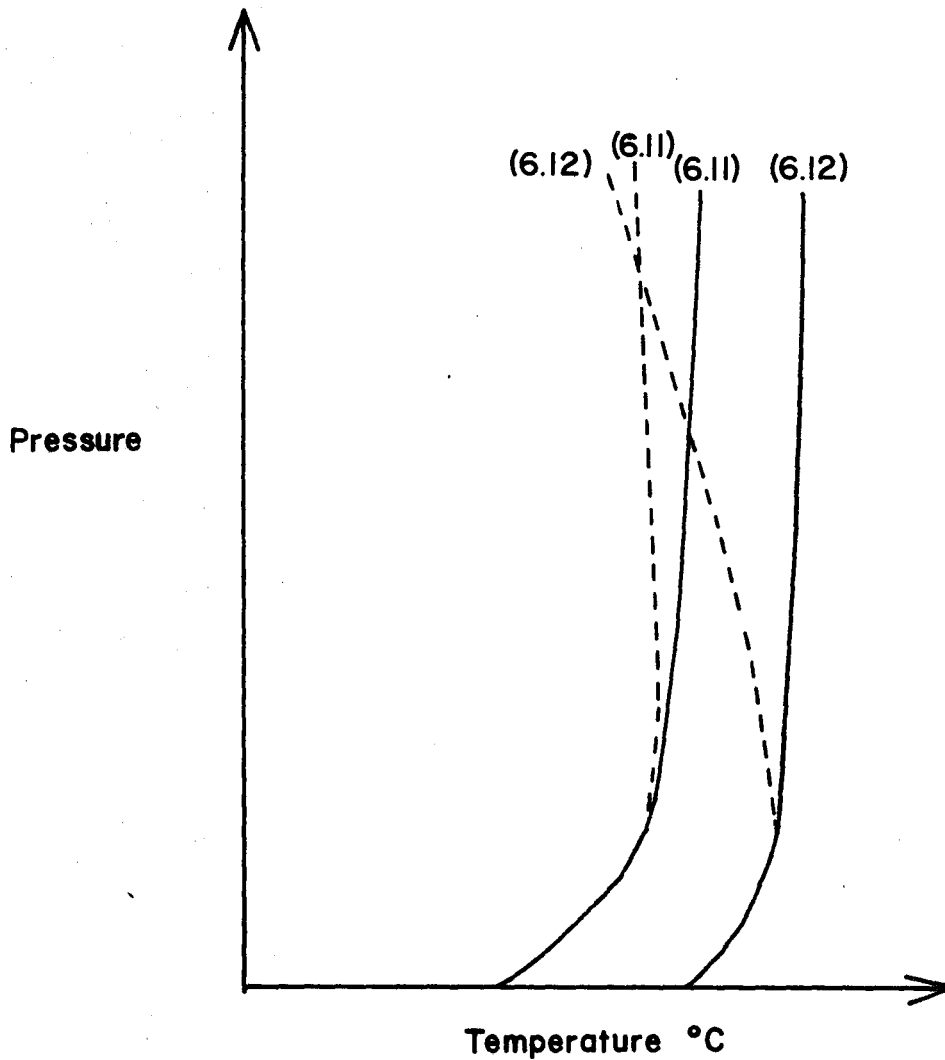


Figure 6.27 Schematic topology of reactions 6.11 and 6.12 in PT space for a fixed fluid phase composition. Solid curves for condition $P_{\text{Total}} = P_{\text{Fluid}}$; dashed curves for condition $P_{\text{Total}} > P_{\text{Fluid}}$. Note that the two reactions can occur at the same P_{Total} and T if $P_{\text{Total}} > P_{\text{Fluid}}$.

- (3) The reactions being governed by different fluid phase compositions in systems where $P_{\text{Total}} > P_{\text{Fluid}}$.

The field and petrographic evidence does not allow us to discriminate between these alternatives conclusively, but as pointed out for some of the Faraday Township examples, different fluid phase compositions seem to influence calc-silicate reactions occurring at the same total pressure and temperature.

6.2.2. Retrograde Metamorphism

Retrograde phase assemblages of the greenschist facies are found in approximately half of the specimens studied. Their mode of occurrence in each rock type is detailed in the subsequent pages and their tectonic significance is inferred.

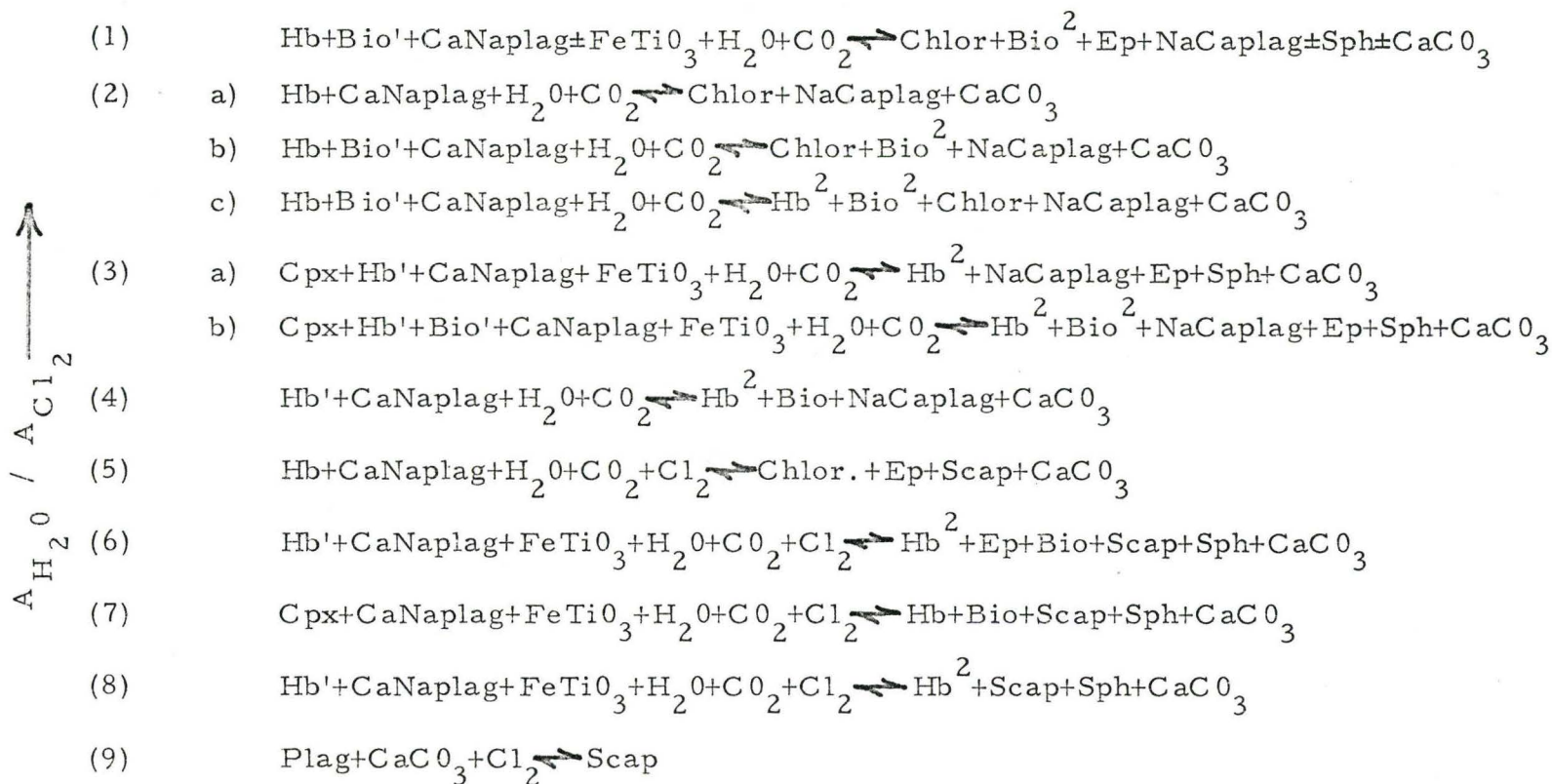
Amphibolites

Amphibolite in general shows the highest degree of retrogression of the rock types encountered in the map area. The principal mineralogic changes include the breakdown of hornblende to chlorite, hornblende recrystallizing to another hornblende (probably actinolite) and clinopyroxene inverting to hornblende. Commonly biotite and plagioclase are recrystallized as well. Large poikiloblastic "feathers" of scapolite replacing plagioclase often cut foliation defined by the prograde assemblage. A detailed summary of retrograde reactions

in the four amphibolite varieties is shown in Table 6.6. These reactions are deduced from textural relations in thin section and are written expressing the general chemical equivalence of reactant and product assemblages. Because of the wide range of possible mineral compositions, no attempt was made to balance the reactions using idealized compositions. The reactions are arranged in order of decreasing A_{H_2O}/A_{Cl_2} (activity of H_2O /activity of Cl_2) of the inferred fluid phase. This ratio is used to give a qualitative notion of the effect of different fluid phase compositions on the retrograde reactions in varying bulk compositions. These reactions have two modes of occurrence (1) in hair line microfractures cutting a hand specimen or thin section and (2) as random occurrences in unfractured compositional bands. The distribution of microfracturing and of reactions with the same or similar A_{H_2O}/A_{Cl_2} ratio is apparently random throughout the map area without being related to mappable shear zones, centers of intrusion or lithologic bands.

While excellent textural criteria exist for each reaction in Table 6.6, only a few representative examples will be depicted in detail. Reaction 2(a), the most common, is suggested by Figure 6.28. Textural evidence for reaction 3 is provided by Figure 6.29 in which the prograde assemblage clinopyroxene-hornblende-plagioclase is seen to recrystallize to a second hornblende and plagioclase, epidote

Table 6.6: RETROGRADE REACTIONS IN AMPHIBOLITE



Abbreviations:

Hb' = prograde hornblende

Hb² = retrograde (actinolitic ?) hornblende

Cpx = clinopyroxene

Bio' = prograde biotite

Bio² = retrograde biotite

Chlor = chlorite

Musc = muscovite

Gar = garnet

Sph = sphene

CaNaplag = calcic plagioclase

NaCaplag = sodic plagioclase

Scap = scapolite

Ep = epidote

Clz = clinozoisite

CaCO₃ = carbonate, probably calcite

Oxide = Fe=Ti oxides

FeTiO₃ = ilmenite component of oxides

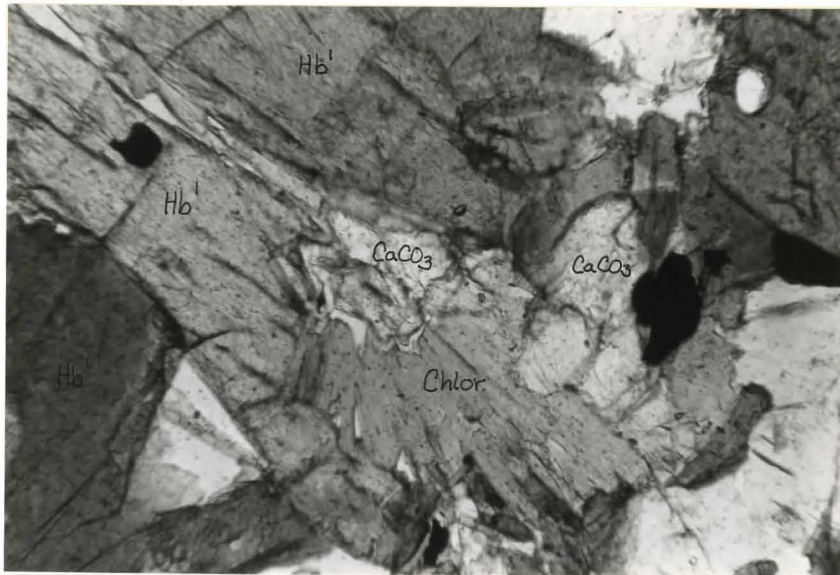


Figure 6.28. Hornblende altering to chlorite by reaction 2(a) of Table 6.6. Ch-43, crossed nicols, 120X.

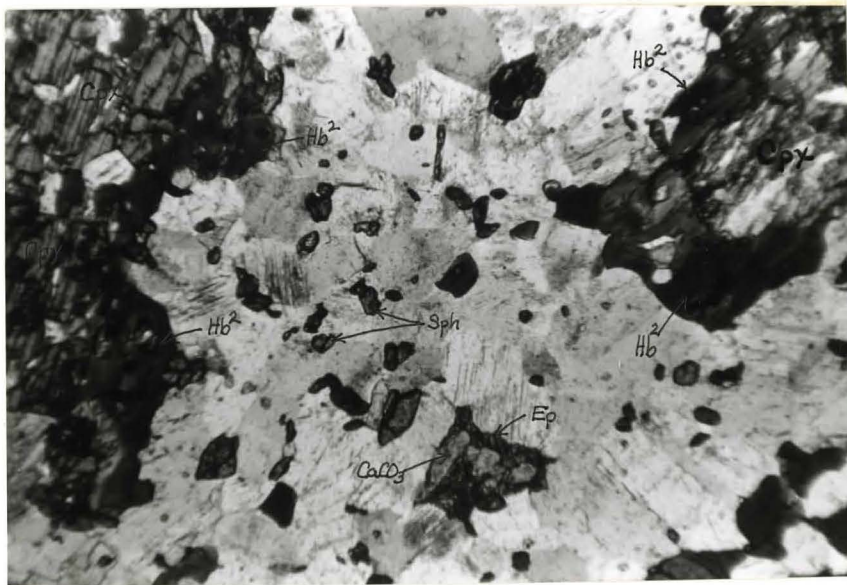


Figure 6.29. Textures supporting reaction 3 of Table 6.6. Specimen 68-74-16, 42X.

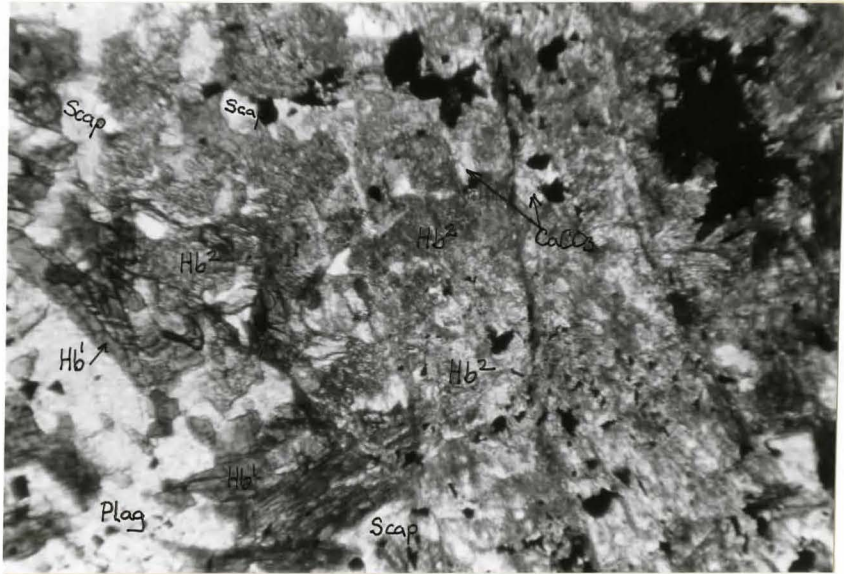


Figure 6.30. Microfractured section showing development of retrograde hornblende by reaction 8 of Table 6.6. Scapolite found only at sites of retrograde reaction. Specimen 2Fa-3, 42X.

and carbonate. Figure 6.30 illustrates a microfractured section in which reaction 8 is localized to points on or adjacent to the fracture. Scapolitization may occur in conjunction with more complex retrograde reactions (e. g. 5 to 8) or it may follow reaction 9. This reaction seems to go in a stepwise fashion with the incipient development of scapolite "dust" on/in plagioclase, followed by the coalescence of this finely crystalline material to form large poikiloblastic grains with included zoned and rounded blebs of plagioclase. This process may eventually result in the production of individual, inclusion-free scapolite grains which are indistinguishable from primary, prograde scapolite. Much of the scapolite encountered in this study appears to be retrograde in origin, a somewhat surprising conclusion.¹

Quartzo-Feldspathic Gneisses

It is convenient to consider the retrogression of this rock type in two parts. Since the retrograde reactions effecting the subaluminous and aluminous gneisses are similar they will be treated together. The hornblende and clinopyroxene gneisses show reactions analogous to those of the amphibolites and will also be treated as a

¹ An occurrence of abundant scapolite "feathers" on a joint surface in amphibolite in eastern Anstruther Township suggests the secondary origin of scapolite on a larger scale.

separate group. Again, as in the case of the amphibolites, the retrograde reactions for each group are deduced from textural evidence and have the same mode of occurrence (i. e. in microfractures or in unfractured bands). Their geographic distribution is also random.

Retrograde reactions applicable to the sub-aluminous and aluminous gneisses are given in Table 6.7 and are arranged in order of decreasing A_{H_2O} . Reactions 2 and 3 in this table are most prevalent. Textures supporting them are shown in Figures 6.31 and 6.32 respectively.

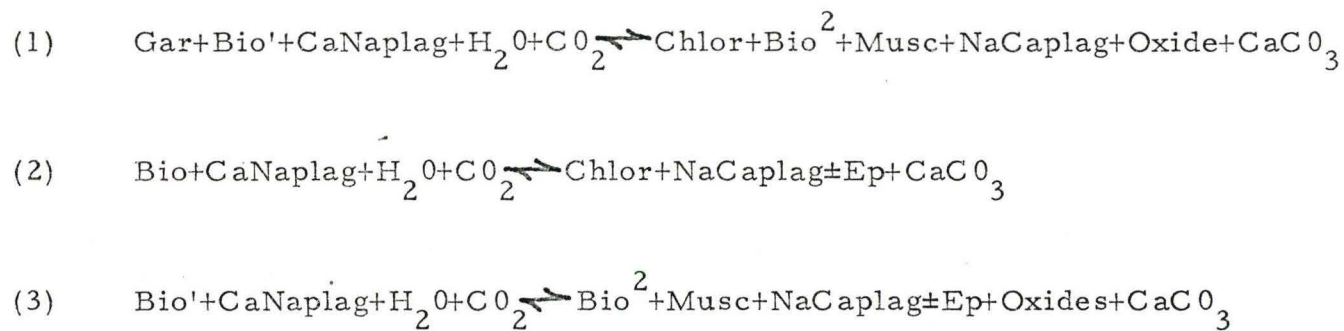
Table 6.8 summarizes the retrograde reactions for the hornblende and clinopyroxene gneisses. Because of their similarity to the reactions in the amphibolites, no textural relations are shown. Scapolite relations in the hornblende and clinopyroxene gneisses are similar to those in the amphibolites as well.

Leptites

The leptites have retrogressed to approximately the same degree as the amphibolites but show a marked decrease in the amount of microfracturing. The retrograde reactions inferred for this rock type are listed in Table 6.9. The textures shown in Figures 6.33 and 6.34 are illustrative of reactions 1 and 4 of this table. Figure 6.32 shows textures identical to those produced by reaction 3.

Table 6.7: RETROGRADE REACTIONS IN SUB-ALUMINOUS AND
ALUMINOUS GNEISSES

A
H₂O



Abbreviations are the same as those used in Table 6.6.



Figure 6.31. Biotite breaking down to chlorite by reaction 2 of Table 6.7. Note different orientation of chlorite. Specimen 2Fb-13, 42X.

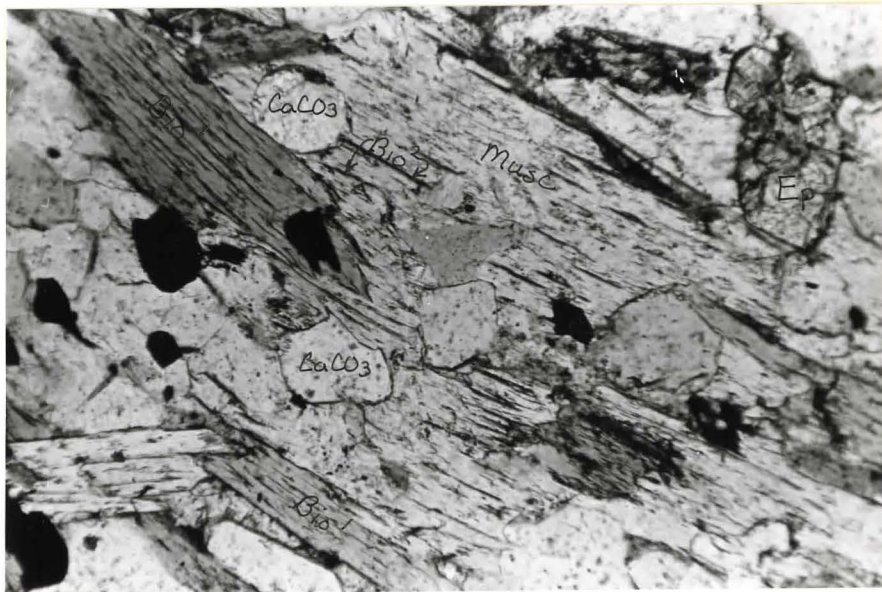
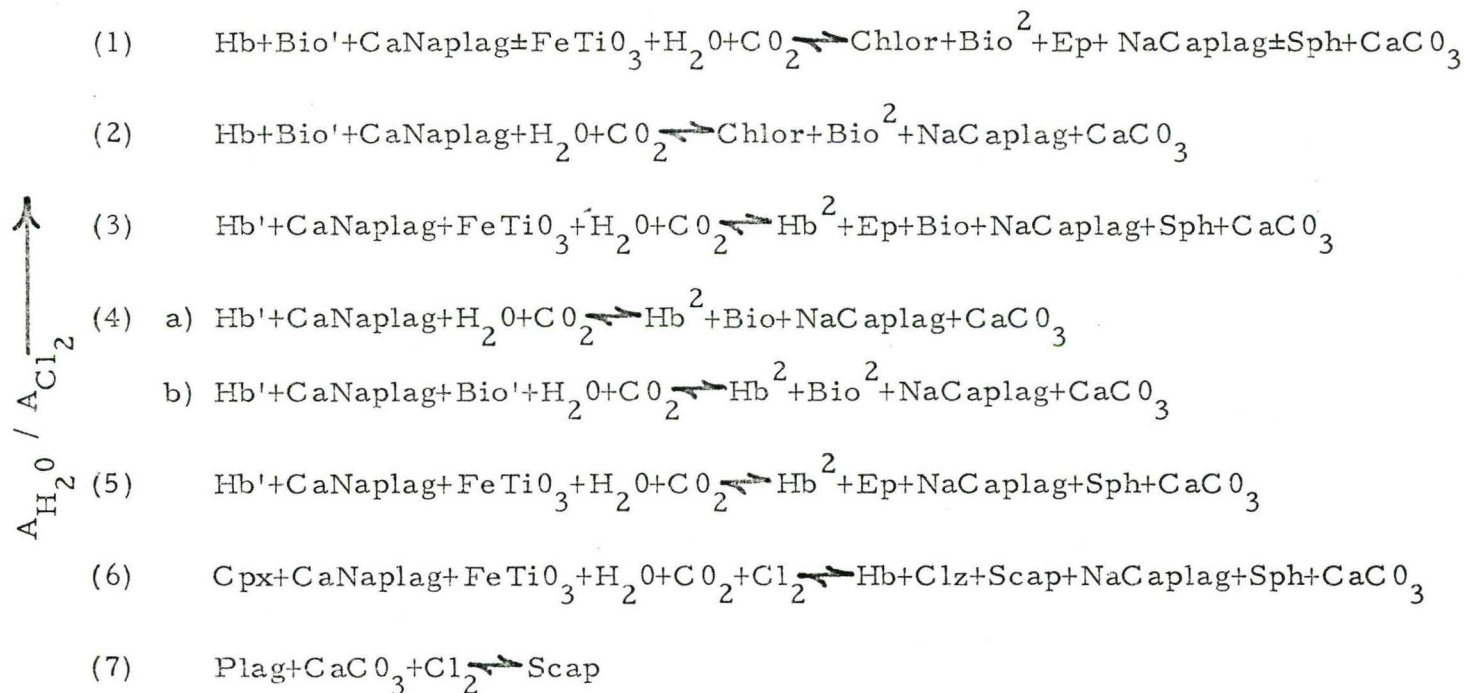


Figure 6.32. Biotite reacting to muscovite and biotite by reaction 3 of Table 6.7. Note different orientation of retrograde muscovite and biotite. Specimen 67-170-4, 120X.

Table 6.8: RETROGRADE REACTIONS IN THE HORNBLENDE AND CLINOPYROXENE GNEISSES



Abbreviations same as those used in Table 6.6.

Table 6.9: RETROGRADE REACTIONS IN LEPTITES

- (1) $\text{Bio} + \text{CaNaplag} + \text{Oxides} + \text{H}_2\text{O} + \text{CO}_2 \rightleftharpoons \text{Chlor} + \text{Musc} + \text{NaCaplag} + \text{CaCO}_3$
- (2) $\text{Bio}' + \text{CaNaplag} + \text{H}_2\text{O} + \text{CO}_2 \rightleftharpoons \text{Bio}^2 + \text{Musc} + \text{NaCaplag} \pm \text{Ep} + \text{Oxides} + \text{CaCO}_3$
- (3) $\text{Bio}' + \text{CaNaplag} + \text{H}_2\text{O} + \text{CO}_2 \rightleftharpoons \text{Bio}^2 + \text{NaCaplag} + \text{Ep} + \text{CaCO}_3$
- (4) $\text{Bio}' + \text{Musc}' \rightleftharpoons \text{Bio}^2 + \text{Musc}^2 + \text{Oxides}$

Abbreviations same as those used in Table 6.6.



Figure 6.33. Chlorite and muscovite forming at the expense of biotite by reaction 1 of Table 6.9. Specimen 2 Fark-10, 120X.



Figure 6.34. Recrystallization of biotite and muscovite by reaction 4 of Table 6.9. Specimen 2 Fark-7, 120X.

Carbonate Metasediments

In the discussion of calc-silicate occurrences it was noted that reactions 6.11 and 6.12 are sometimes frozen in the retrograde sense (Figures 6.23 and 6.24). This coupled with the somewhat low carbonate solvus temperatures (Table 6.4) suggests that retrograde metamorphism in at least the carbonate metasediments was not of long duration. If it had been of long duration, surely all the carbonate pairs would have equilibrated to low temperature conditions and the high temperature assemblages for reactions 6.11, 6.12 and 6.13 would have re-equilibrated leaving little, if any, trace of their former existence. Perhaps sample Ca-319 in Table 6.4 records near equilibrium retrograde thermal conditions.

Interpretation

The two modes of occurrence of the retrograde reactions prompt the following question: Are these reactions controlled intensively by different fluid phase compositions entering the reacting systems along microfractures during retrogression or are they controlled extensively by rock bulk composition? It is probable that the reactions in fractured rocks are intensively controlled if metamorphism and fracturing are contemporaneous. Consider a

rock formed by the prograde event carried to a point in P-T space representative of upper greenschist conditions (e. g. point A on Figure 6.35). As the rock volume is reheated, suppose its bulk composition imposes a fluid pressure of specific magnitude and composition on the potentially reactive prograde assemblage, now out of its stability field. If microfracturing of this potentially reactive prograde system occurs without the introduction of fluid components, the accumulated fluid pressure may be lowered sufficiently to stabilize the high temperature or prograde assemblage as shown in Figure 6.35. Thus for retrograde reactions occurring in and in close association with microfractures, it is likely that the composition of the fluid phase was intensively controlled. The source of these fluids is unknown but they may be released from adjacent compositional bands upon fracturing. Using the same argument, it is probable that the retrograde reactions in unfractured compositional bands are governed by their bulk compositions. The occurrence of two distinct reactions in different compositional bands in the same thin section (as seen in several sections studied) can be cited in support of this.

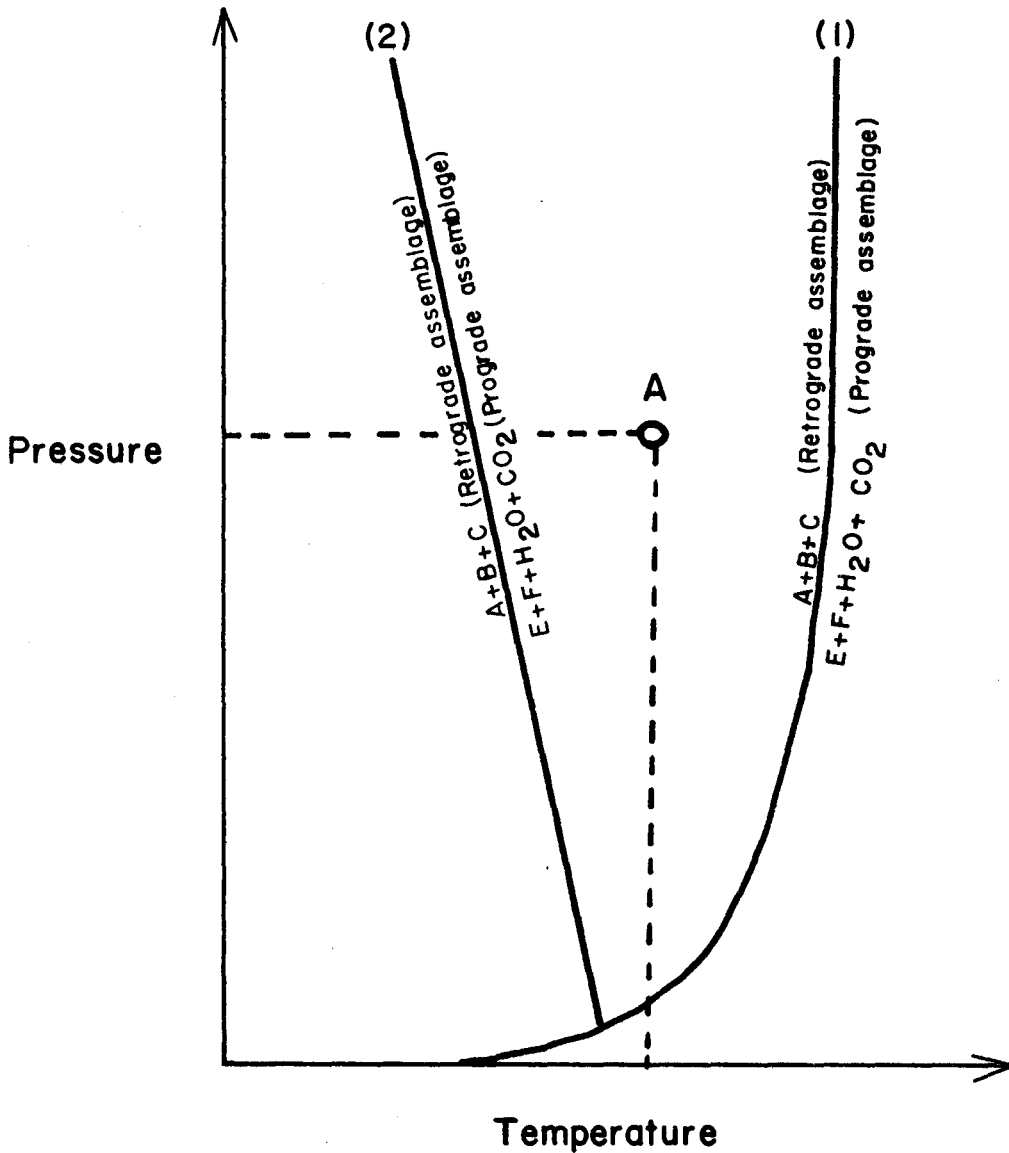


Figure 6.35 Schematic topology of a generalized retrograde reaction illustrating the possible effect of microfracturing on the locus of the reaction. Curve (1) represents the position of the equilibrium before fracturing, curve (2) its position after fracturing. Point A represents greenschist conditions in P-T space.

The retrograde phase assemblages of the supracrustal rocks of the study area are diagnostic of the upper greenschist facies of low to intermediate pressure regional metamorphism (Winkler, 1967, pp. 116-119), or of the albite-epidote amphibolite facies of Fyfe and Turner (1966). More precise assignment must be delayed until the compositions of the retrograde clinoamphiboles are known. If these amphiboles are actinolitic, the upper greenschist facies terminology is preferred (Fyfe and Turner, 1966, pp. 361-362). For the present discussion, the term "greenschist" will be applied to the retrograde metamorphism and its products.

The development of greenschist minerals in microfractures and the prevalence of cold working textures such as bent twin lamellae in plagioclase and undulose extinction in quartz and plagioclase suggests that the retrograde event took place in a brittle deformational episode removed in time from the prograde metamorphism. Preferred orientation of retrograde phases (e. g. Figures 6.31, 6.32 and 6.34) appears to define a fabric distinct from that of the prograde phases implying a different stress field orientation for the retrograde event. Perhaps this event is connected with large scale regional isostatic uplift of the Grenville age province giving rise to the uniformity of K/Ar dates

throughout this immense crustal block. Alternatively, the retrogression may be localized to the map area and may be controlled dominantly by the late stage movement(s) on the large shear zones bounding the area. The resolution of this problem can only come from other detailed studies in the Bancroft-Madoc area and the Grenville in general. Until such studies are concluded, all inferences concerning retrograde metamorphism on the large scale are at best tentative.

6.2.3. Summary

The study area lies geographically within the upper amphibolite facies terrain of the Bancroft-Madoc facies series. Phase assemblages characteristic of the individual zones in this series suggest it to be of the low pressure intermediate type (as defined by Miyashiro, 1962). The most probable age of metamorphism for this terrain is 1125 ± 25 m.y. (Lumbers, 1967a; Silver and Lumbers, 1966).

Phase assemblages from all rock types within the map area are definitive of the upper amphibolite facies of regional metamorphism. Applying the data of experimental petrology to these assemblages, a temperature range of 625° to 690°C in the interval 5.5 to 7 kilobars total pressure seems probable for the prograde event. In general, the bulk of these phase assemblages appear to represent thermodynamic equilibrium because of their conformity

to the phase rule and their chemographic relations in ACKF space.

Evidence of disequilibrium is provided by the four examples of unstable muscovite+quartz, the four staurolite breakdown reactions and the three calc-silicate equilibria studied in detail.

Carbonate solvus temperatures derived from coexisting calcite-dolomite pairs are somewhat removed from the inferred thermal conditions of metamorphism. Clearly, these temperatures reflect postmetamorphic quench conditions in the calcite-dolomite system. Several occurrences of different calc-silicate reactions in the same outcrop imply local buffering of $\text{CO}_2\text{-H}_2\text{O}$ systems in nearly adjacent bands of different bulk composition. It is likely that two reactions in the same outcrop are governed principally by different fluid phase compositions and possibly by deviations of P_{fluid} from P_{total} .

Abundant evidence of retrograde metamorphism of greenschist grade is present in the map area. Retrograde assemblages develop from but do not obliterate the prograde assemblages. These retrograde assemblages may or may not be associated with microfractures. In the former case, it is argued that retrograde metamorphism was governed intensively while it was governed by extensive parameters in the latter case. The cause of this retrograde event is uncertain.

7. TECTONIC SYNTHESIS

7.1. Tectonic History of the Bancroft-Madoc Area

The pattern of tectonic events in the map area becomes more intelligible when referred to Lumbers' (1967a) tectonic synthesis of events in the Bancroft-Madoc area. The earliest recognizable event in this area is the accumulation of the Tudor metavolcanics dated by U-Pb methods at 1310 ± 15 m. y. (Silver and Lumbers, 1966). Between this data and 1250 ± 25 m. y. the remaining units in a large part of the supracrustal prism accumulated in a volcano-sedimentary series as outlined in Chapter 3. The date of 1250 ± 25 m. y. marks the culmination of the earliest deformational, metamorphic and plutonic episode in the region. At this time the biotite-diorite series (e. g. plutons of the Elzevir-Ashby Dome) was intruded into the supracrustal prism concomitant with the development of the plagioclase isograds and the greenschist and lower amphibolite terrains (Figure 6.1) within this prism (Lumbers, 1967a). A period of emplacement of mafic sills and dikes followed by larger scale late gabbro, diorite and nepheline syenite intrusives separates this event from the most intense meta-

morphic event dated at 1125 ± 25 m. y. (Silver and Lumbers, 1966). This event produced the general northeast-southwest trend to fold structures as well as the sillimanite isograd and upper amphibolite terrain and appears to have obliterated most of the effects of the 1250 m. y. event in the older and lower grade amphibolite facies terrain (Lumbers, 1967a). It is this event that the name Grenville is commonly associated with. It is instructive to note that the earlier greenschist terrain centered on Grimsthorpe and Tudor townships was not appreciably affected by this event (Lumbers, 1967a). Plutonic rocks of the quartz monzonite group (e. g. the Loon Lake Complex) in this portion of the Lowlands were also intruded at this time (Lumbers, 1967a) possibly creating some of the broad, open folding and cross folding found throughout this region. An aerielly extensive period of intrusion of pegmatites and calcite-fluorite-apatite veins followed this metamorphic episode at approximately 1050 ± 20 m. y. (Silver and Lumbers, 1966; Lumbers, 1967a). The rather uniform K-Ar dates of 1000 to 800 m. y. for the Grenville Province as a whole (Wanless *et al.*, 1967) might best be explained as a "quench" age following broad regional uplift and dynamothermal metamorphism in this time interval. A summary of tectonic events in the Bancroft-Madoc area after Lumbers (1967a) is given in Figure 7.1.

DECREASING TIME →

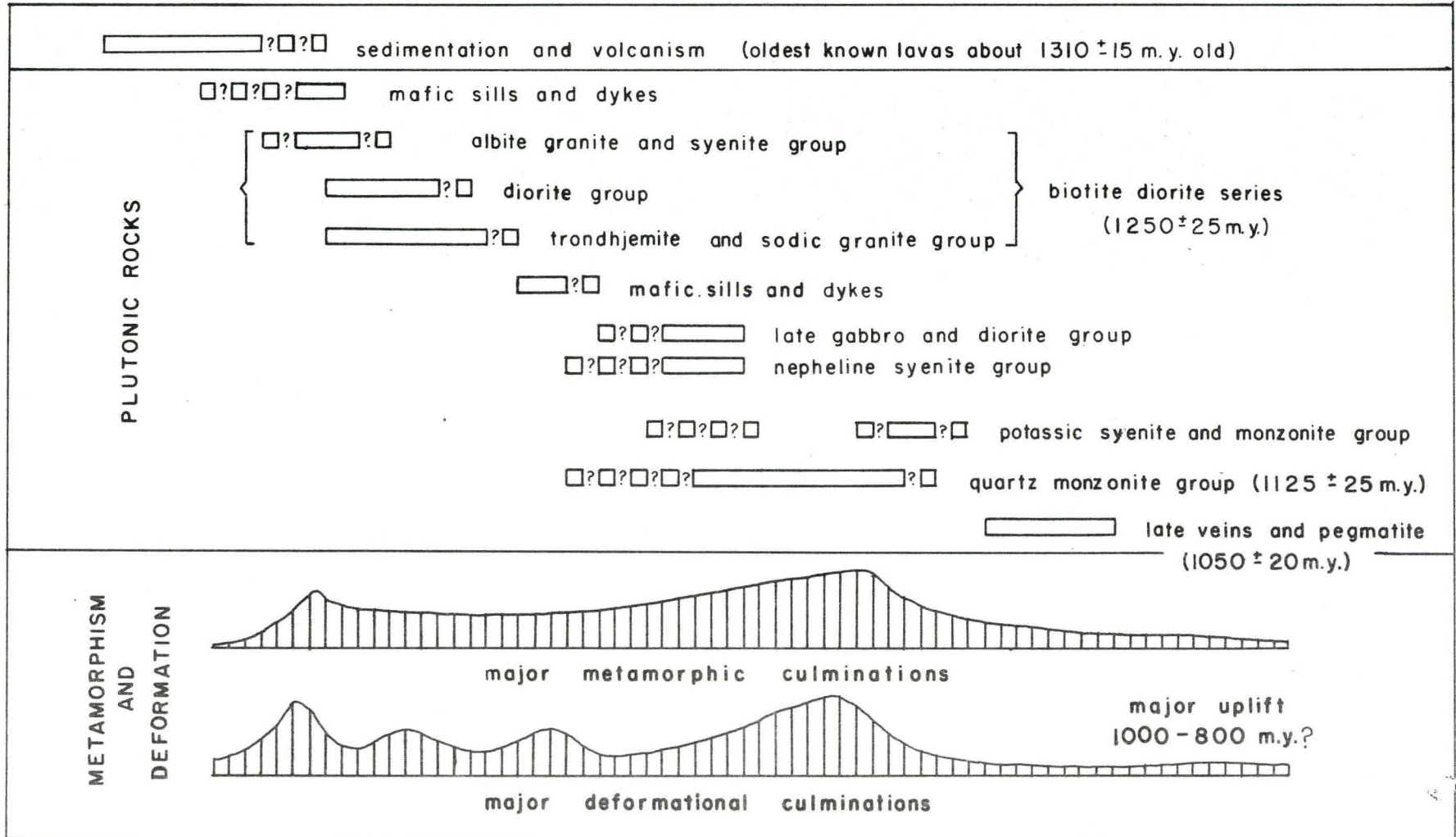


Figure 7.1: Summary of Tectonic Events in the Bancroft-Madoc Area

(After Lumbers, 1967b)

7.2. Tectonic History of the Mapped Area

The most logical point to begin a discussion on the geological evolution of the study area is a model of accumulation for the Hermon Group rocks. On the basis of their correlation with the Hermon Group to the east, crude estimates can be made of their period of deposition. The 1310 ± 15 m. y. age on the Tudor metavolcanics (the oldest formation of the Hermon Group) and 1250 ± 25 m. y. ages on the biotite-diorite series cutting the Hermon Group establish lower and upper age limits respectively for the Hermon Group (Silver and Lumbers, 1966). It is probable that the bulk of the Hermon Group rocks in the map area accumulated within this interval. It remains to deduce a satisfactory model of accumulation for these rocks using the available stratigraphic, structural and chemical data.

If the rocks in the map area are correlative with the Hermon Group elsewhere in the Bancroft-Madoc area, it is logical to assume a common history for both groups as a first approximation. Thus, the model of accumulation proposed by Lumbers (1967a) as reviewed in Chapter 3 should be applicable in large part to the study area. The gross stratigraphic similarities between this area and the eastern portion of the Bancroft-Madoc area suggest similar modes of origin. However, distinct differences exist between these areas which necessitate minor modifications of Lumbers' interpretation of the depositional history of the supracrustal prism in the map area.

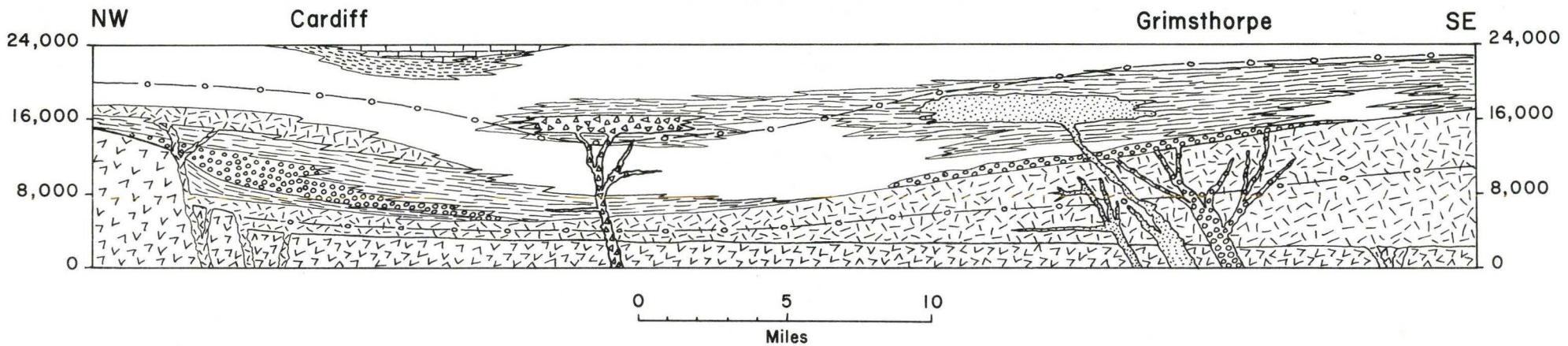
Inspection of Figure 3.1 reveals a greater abundance of leptite or Oak Lake lithologies in the northwestern portion of the Bancroft-Madoc area than in the southeastern portion. In the map area, these leptites have been shown to be meta-arkoses intercalated with pelitic clastic units, while Lumbers interprets them as rhyolitic volcanics interbanded with clastic debris derived from the weathering of volcanic piles. Lumbers' model is very probably accurate for the acidic supracrustal rocks in the southeastern portion of the Bancroft-Madoc area west of the Elzevir-Ashby Dome, but the presence of large amounts of clastic debris in the study area suggests its proximity to a granitic foreland. It is suggested that this foreland formed a margin of the basin of accumulation near the map area providing a ready source of immature, clastic debris. Unfortunately, insufficient data are available to evaluate whether this postulated foreland represents a structural high in a geosynclinal downwarp or whether it coincides with the margin of a subsiding volcano-tectonic depression. Lumbers (1967a) invokes a geosynclinal model for the deposition of the Upper Proterozoic supracrustal remnants throughout the Grenville Age Province, but at the same time, the Bancroft-Madoc area resembles the volcano-tectonic depressions of the Superior Age Province described by Goodwin and Shklanka (1967). A great deal of structural, stratigraphic

and geochronologic data on many more Grenville supracrustal remnants is needed before these alternatives can be evaluated.

Regardless of the regional depositional mechanism, outpourings of basaltic lavas from a shield volcanic complex in the southeastern portion of the Bancroft-Madoc area (Lumbers, 1967a) and probably from vents near the map area margins resulted in isostatic subsidence of the entire Bancroft-Madoc portion of the depositional basin. This subsidence in turn resulted in tectonic instability of the basin margins near the map area with the production of arkosic and pelitic wedges into the basin overlying the basal basaltic flows. Renewed basaltic activity, presumably from vents in the map area, contemporaneous with carbonate sedimentation and minor volcanic activity in the basin can account for the observed stratigraphic relationships in the study area and in the Bancroft-Madoc area as summarized in Figure 7.2. From their inferred, original disposition in this figure and their present disposition (Figure 2.1), it is apparent that the study area affords a cross sectional view of the Hermon Group rocks while an approximate plan view is found along the western flanks of the Elzevir-Ashby Dome.

Following the accumulation of the Hermon Group in the map area between 1310 ± 15 and 1250 ± 25 m. y. , the chronologic relations between 1250 ± 25 and 1125 ± 25 m. y. are unclear. It is not certain whether

Cross Section Showing Inferred, Original Stratigraphic Relations in the Bancroft—Madoc Area



-  Burnt Lake Formation
-  Turriff Metavolcanics
-  Vansickle Formation
(Hermon Group Quartzo-Feldspathic Gneisses in NW)
-  Oak Lake Formation
(Hermon Group Leptites in NW)
-  Tudor Metavolcanics
(Hermon Group Amphibolites in NW)

-  Lasswade Marble
-  Apsley Formation
-  Dungannon Formation
-  Hypothetical Isochronous Lines
-  Basement Complex

Figure 7.2

or to what extent the metamorphism associated with the 1250 m. y. event affected the rocks of the study area. From the available structural information, there is no suggestion of two or more periods of folding within this area.

To the northeast in an adjoining area south of Bancroft, Best (1966) has found two distinct fold generations present in the Dungannon, Apsley and Lasswade formations of the Mayo Group. In rocks obviously equivalent to the sequence under investigation he finds structural relations similar to those of the writer, i. e. only one distinct fold generation. Perhaps the earlier more open period of folding found by Best is related to the 1250 m. y. event, while the tighter folds of the second generation obliterate or tighten the earlier generation (Best, 1966) and are related to the more intense 1125 m. y. event. This interpretation is speculative and may be subject to revision upon further study. The foliated nature and phase assemblages of the Tallan Lake sill along the southeastern edge of the map area suggest intrusion of this body prior to the culmination of upper almandine amphibolite facies metamorphism dated at 1125 ± 25 m. y. It is likely that this event produced the tight isoclinal folding and mineral growth commonly referred to as "Grenville metamorphism" in this area. Toward the waning stages of this event, the Anstruther-Burleigh batho-

lith, dated at 1103 ± 39 m. y. (Krogh, 1964), was intruded into the supracrustal sequence. The Silent Lake stock very probably postdates the 1125 m. y. event but structural data, as yet, are insufficient to confirm this. The relation of the Silent Lake stock to the major granitic plutons of the Harvey-Cardiff Arch or Hastings Highlands is uncertain as well. Regional uplift between 1000 m. y. and 800 m. y. (possibly along fault systems such as those paralleling the Highland boundary and trending across the northwestern portion of the map area) perhaps was responsible for "quenching" the K-Ar "clocks" and inducing the retrograde metamorphism noted in the study area. A summary of events in this area is presented in Figure 7.3. Because of the various inadequacies of the data, the conclusions of this chapter must be treated solely as working hypotheses for further study.

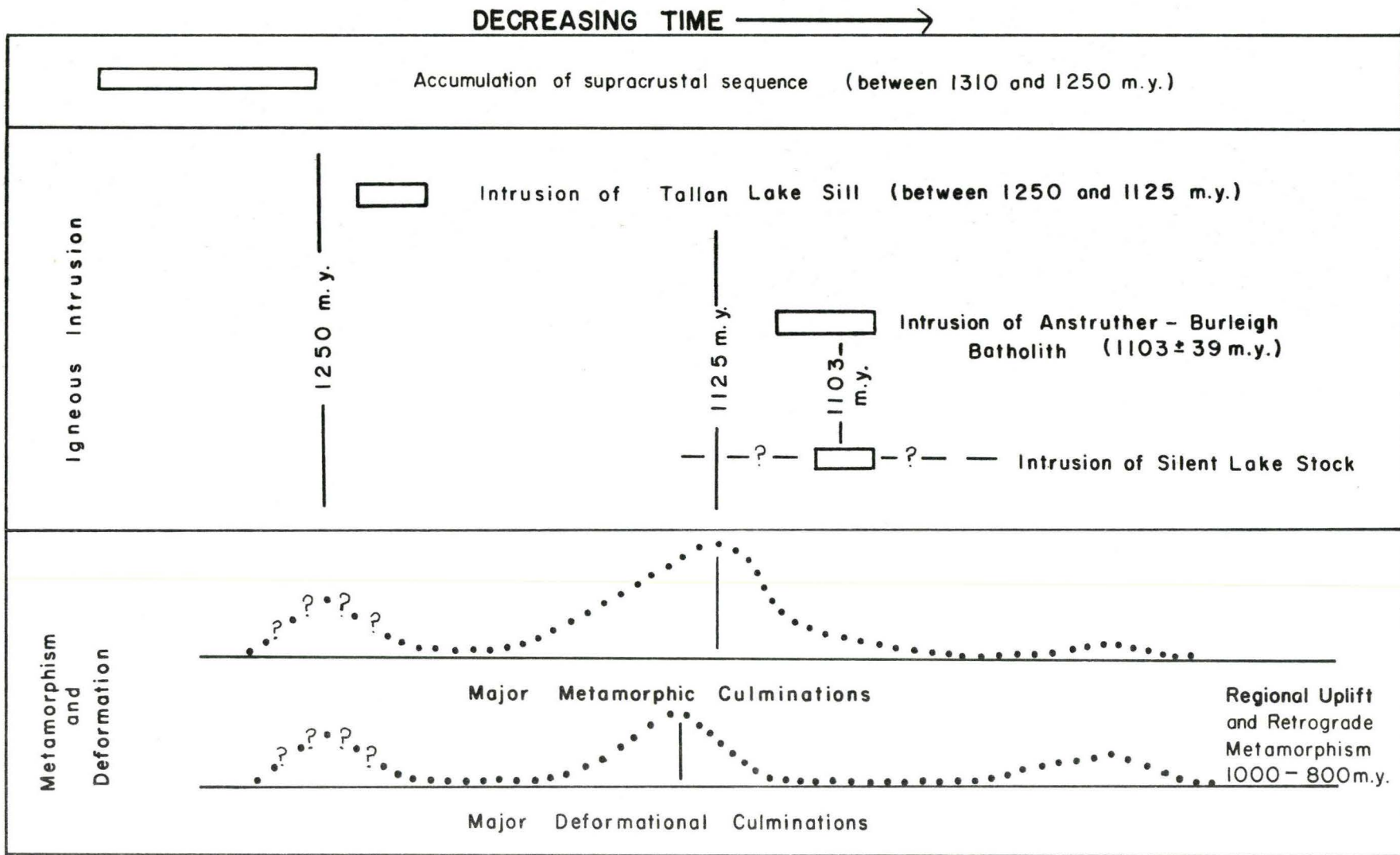


Figure 7.3: Summary of Tectonic Events in the Map Area

BIBLIOGRAPHY

- Adams, F.D. and Barlow, A.E. (1910) Geology of the Haliburton and Bancroft areas province of Ontario: Geol. Surv. Can., Mem. 6, 419 p.
- Althaus, E. (1967) The triple point andalusite-sillimanite-kyanite: Contrib. Mineral. and Petrol., 16, 29-44.
- _____ (1969) Experimental evidence that the reaction of kyanite to form sillimanite is at least bivariant: Amer. Jour. Sci., 267, 273-277.
- Asklund, B. (1923) Petrological studies in the neighborhood of Stavsjø, at Kolmorden. Granites and associated basic rocks of the Stavsjø area: Svenig. Geol. Unders. Afh., Ser. C, 324: 1-122.
- Best, M.G. (1966) Structural geology of precambrian rocks south of Bancroft, Ontario: Can. Jour. Earth Sci., 3, 441-455.
- Brew, D.A. and Muffler, L.J.P. (1965) Upper Triassic undevitrified volcanic glass from Hound Island, Keku Strait, southeastern Alaska: U.S. Geol. Surv. Prof. Paper 525-C, 38-43.

- Buddington, A. F. and Chapin, T. (1929) Geology and mineral deposits of southeastern Alaska: U.S. Geol. Surv., Bull. 800, 398 p.
- _____ and Leonard, B. F. (1962) Regional geology of the St. Lawrence County magnetite district, northwest Adirondacks, New York: U.S. Geol. Surv., Prof. Paper 376.
- Carlisle, D. (1963) Pillow breccias and their aquagene tuffs, Quadra island, British Columbia: Jour. Geol., 71, 48-71.
- Carmichael, D. M. (1968) Structure and progressive metamorphism in the Whetstone Lake area, Ontario, with emphasis on the mechanism of prograde metamorphic reactions: Unpublished Ph. D. thesis, Univ. of California, Berkeley.
- _____ (1969) On the mechanism of prograde metamorphic reactions in quartz-bearing pelitic rocks: Contr. Mineral. and Petrol., 20, 244-267.
- Chesworth, W. (1967) The origin of certain granitic rocks occurring in Glamorgan township, southeastern Ontario: Unpublished Ph. D. thesis, McMaster Univ., Hamilton.
- Chinner, G. A. (1960) Pelitic gneisses with varying ferrous/ferric ratios from Glen Clova, Angus, Scotland: Jour. Petrol., 1, 178-217.
- _____ (1965) The kyanite isograd in Glen Cova, Angus, Scotland: Min. Mag., 34, 132-143.

- Condie, K. C. (1967) Geochemistry of early Precambrian graywackes from Wyoming: *Geochim. et Cosmochim. Acta*, 31, 2135-2149.
- Eade, K. E., Fahrig, W. F. and Maxwell, J. A. (1966) Composition of crystalline shield rocks and fractionating effects of regional metamorphism: *Nature*, 211, 1245-1249.
- Eckelmann, F. D. and Poldervaart, A. (1957) Geologic evolution of the Beartooth Mountains, Montana and Wyoming, Pt. I: Archean history of the Quad Creek area: *Geol. Soc. Amer. Bull.*, 68, 1225-1262.
- Elliot, R. B. and Morton, R. D. () The nodular metamorphic rocks from the environs of Kragerø, south coast of Norway: *Norsk Geol. Tidsskr.*, 45, 1-20.
- Engel, A. E. J. and Engel, C. G. (1951) Origin and evolution of hornblende-andesine amphibolites and kindred facies: *Geol. Soc. Amer. Bull.*, 62, 1435-1436 (abs.).
- _____ and _____ (1953) Grenville series in the northwest Adirondack Mountains, New York: *Geol. Soc. Amer. Bull.*, 64, 1013-1097.
- _____ and _____ (1962) Progressive metamorphism of amphibolite, northwest Adirondack Mountains, New York: *Geol. Soc. Amer. Bull.*, Buddington volume, 37-82.

- Engel, A. E. J., Engel, C. G. and Havens, R. G. (1965) Chemical characteristics of oceanic basalts and the upper mantle: Geol. Soc. Amer. Bull., 76, 719-734.
- Evans, A. M. (1964) Geology of Ashby and Denbigh townships: Ontario Dept. Mines, Geol. Rpt. No. 26, 1-39.
- Evans, B. W. (1965) Application of a reaction-rate method to the breakdown equilibria of muscovite and muscovite plus quartz: Amer. Jour. Sci., 263, 647-667.
- _____ and Leake, B. E. (1960) The composition and origin of the striped amphibolites of Connemara, Ireland: Jour. Petrol., 1, 337-363.
- Eskola, P. (1950) Paragenesis of cummingtonite and hornblende from Muuruvesi, Finland: Amer. Min., 35, 728-734.
- Faure, G. and Hurley, P. M. (1963) The isotopic composition of strontium on oceanic and continental basalts: Application to the origin of igneous rocks: Jour. Petrol., 4, 31-50.
- Fiske, R. S. (1963) Subaqueous pyroclastic flows in the Ohanapecosh formation, Washington: Geol. Soc. Amer. Bull., 74, 391-406.
- _____, Clifford, A. H. and Waters, A. C. (1963) Geology of Mount Rainier National Park, Washington: U. S. Geol. Surv. Prof. Paper 444, 93 p.

- Fiske, R.S. and Matsuda (1964) Submarine equivalents of ash flows in the Tokiwa formation, Japan: *Amer. Jour. Sci.*, 262, 76-106.
- Flawn, P. T. (1950) Sedimentary amphibolites in the Van Horn Mountains, Texas: *Geol. Soc. Amer. Bull.*, 61, 1460 (abs.).
- Fleuty, M. J. (1964) The description of folds: *Proc. Geol. Assoc.* 75, 461-492.
- Francis, G.H. (1958) The amphibolite of Doir 'a' Chatha (Durcha), Sutherland: *Geol. Mag.*, 95, 25-40.
- Fyfe, W.S. and Turner, F.J. (1966) Reappraisal of the metamorphic facies concept: *Contrib. Mineral. and Petrol.*, 12, 354-364.
- Goldsmith, J.R. and Heard, H.C. (1961) Subsolidus phase relations in the system CaCO_3 - MgCO_3 . *Jour. Geol.*, 69, 45-74.
- _____ and Newton, R.C. (1969) P-T-X relations in the system CaCO_3 - MgCO_3 at high temperatures and pressures: *Amer. Jour. Sci.*, 267-A, 160-190.
- Goodwin, A.M. and Shklanka, R. (1967) Archean volcano-tectonic basins: form and pattern: *Can. Jour. Earth Sci.*, 4, 777-795.
- Graf, D.L. and Goldsmith, J.R. (1955) Dolomite-magnesian calcite relations at elevated temperatures and CO_2 pressures: *Geochim. et Cosmochim. Acta*, 7, 109-128.

- Graf, D. L. and Goldsmith, J. R. (1958) The solid solubility of MgCO_3 in CaCO_3 . A revision: *Geochim. et Cosmochim. Acta*, 13, 218-219.
- Hague, J. M., Baum, J. L., Herrmann, L. A. and Pickering, R. J. (1956) Geology and structure of the Franklin-Sterling area, New Jersey: *Geol. Soc. Amer. Bull.*, 67, 435-474.
- Harker, R. I. and Tuttle, O. F. (1955) Studies in the system CaO-MgO-CO_2 : Part 2. Limits of solid solution along the binary join $\text{CaCO}_3\text{-MgCO}_3$: *Amer. Jour. Sci.*, 253, 274-282.
- Haskin, L. A., Frey, F. A., Schmitt, R. A. and Smith, R. H. (1966) Meteoritic, solar and terrestrial rare-earth distributions: *Phys. and Chem. of the Earth*, 7, 167-321.
- Hermann, A. G. (in press) Yttrium and the Lanthanides in *Handbook of Geochemistry*, 2, New York, Springer-Verlag, Chap. 39.
- Hewitt, D. F. (1959) *Geology of Cardiff and Faraday townships*: Ontario Dept. Mines, LXVI, 3, 81 p.
- _____ (1961) *Nepheline syenite deposits of southern Ontario*: Ontario Dept. Mines, 69, 194 p.
- _____ and James, W. (1956) *Geology of Dungannon and Mayo Townships*: Ontario Dept. Mines, 64, 65 p.
- _____ and Satterly, J. (1957) *Haliburton-Bancroft area*: Ontario Dept. Mines, Map No. 1957b.

- Hietanen, Anna (1967) On the facies series in various types of metamorphism: *Jour. Geol.*, 75, 187-214.
- Hoover, L. (1963) Geology of the Anlauf and Drain quadrangles, Douglas and Lane counties, Oregon: U.S. Geol. Surv. Bull., 1122-D, 62 p.
- Horn, D.R., Delach, M.N. and Horn, B.M. (1969) Distribution of volcanic ash layers and turbidites in the North Pacific: *Geol. Soc. Amer. Bull.*, 80, 1715-1724.
- Hoschek, G. (1969) The stability of staurolite and chloritoid and their significance in metamorphism of pelitic rocks: *Contr. Mineral. and Petrol.*, 22, 208-232.
- Jaffe, H.W., Robinson, P. and Klein, C. (1968) Exsolution lamellae and optic orientation of clinoamphiboles: *Science*, 160, 776-778.
- Jennings, D.S. and Mitchell, R.H. (1969) An estimate of the temperature of intrusion of carbonatite at the Fen complex, S. Norway: *Lithos*, 167-169.
- van de Kamp, P.C. (1964) Geochemistry and classification of amphibolites and related rocks: Unpublished M.Sc. thesis, McMaster Univ., Hamilton.
- _____ (1968) Geochemistry and origin of metasediments in the Haliburton-Madoc area, southeastern Ontario: *Can. Jour. Earth Sci.*, 5, 1337-1372.

- Klein, C. (1968) Coexisting amphiboles: *Jour. Petrology*, 9, 281-330.
- Köhler, A. and Raaz, F. (1951) Über eine neue Berechnung und graphische Darstellung von Gesteinsanalysen: *Neues Jahrbuch f. Min. Monatshefte*, 247-263.
- Krogh, T. E. (1964) Strontium isotopic variation and whole rock isochron studies in the Grenville province of Ontario: *Twelfth Ann. Prog. Rpt. for 1964: Dept. of Geol. and Geophys., M. I. T.* 73-124.
- Kudo, A. M. (1962) The discriminant function used in classifying some amphibolites: Unpublished M. Sc. thesis, McMaster Univ., Hamilton.
- Lal, R. K. and Moorhouse, W. W. (1969) Cordierite-gedrite rocks and associated gneisses of Fishtail Lake, Harcourt township, Ontario: *Can. Jour. Earth Sci.*, 6, 145-165.
- Leake, B. E. (1964) On the distinction of ortho- and para-amphibolites: *Jour. Petrol.*, 5, 238-254.
- Lumbers, S. B. (1964) Preliminary report on the relationship of mineral deposits to intrusive rocks and metamorphism in part of the Grenville province of southeastern Ontario: *Ontario Dept. Mines, P. R.* 1964-4.

Lumbers, S. B. (1967a) Stratigraphy, plutonism and metamorphism in the Ottawa River remnant in the Bancroft-Madoc area of the Grenville province of southeastern Ontario, Canada: Unpublished Ph. D. thesis; Princeton Univ., Princeton.

_____ (1967b) "Geology and mineral deposits of the Bancroft-Madoc area" in Geology of parts of eastern Ontario and western Quebec, GAC-MAC Guidebook, Kingston, 1967, 13-29.

Luth, W. C., Jahns, R. H., Tuttle, O. F. (1964) The granite system at pressures of 4 to 10 kilobars: Jour. Geophys. Res., 69, 759-773.

Magnusson, N. H. (1936) The evolution of the Lower Archaean rocks in central Sweden and their iron, manganese and sulphide ores: Quart. Jour. Geol. Soc. London, XVII, 332-359.

Manson, V. (1968) Geochemistry of basalts: Major elements, in H. H. Hess and A. Poldervaart, eds. Basalts: The Poldervaart Treatise on Rocks of Basaltic Composition, 1, New York, John Wiley and Sons, 217-246.

Matsushima, S., Kennedy, G. C., Akella, J. and Haygarth, J. (1967) A study of equilibrium relations in the systems Al_2O_3 - SiO_2 - H_2O and Al_2O_3 - H_2O : Amer. Jour. Sci., 265, 28-44.

- Merrin, S. (1964) Experimental investigations of epidote paragenesis:
Unpublished Ph.D. thesis, The Pennsylvania State Univ.,
University Park.
- Metz, P. (1966) Untersuchung eines heterogenen bivalenten Gleichgewichts mit CO_2 und H_2O als fluider Phase bei hohem Druck:
Ber. Bunsenges. Physik. Chemie, 7, 1043-1045.
- _____ and Trommsdorff, V. (1968) On phase equilibria in metamorphosed siliceous dolomites: Contr. Mineral. and Petrol., 18, 305-309.
- _____ and Winkler, H.G.F. (1964) Experimentelle Untersuchung der Diopsidbildung aus Tremolit, Calcit und Quarz: Z. Naturwiss., 19, 460-462.
- Middleton, G.V. (1960) Chemical compositions of sandstones: Geol. Soc. Amer. Bull., 71, 1011-1026.
- Miyashiro, A. (1958) Regional metamorphism of the Gosaisyo-Takanuki district in the central Abukuma plateau: Jour. Fac. Sci., Univ. Tokyo, XI, 219-272.
- Moine, B. et de la Roche, H. (1968) Nouvelle approche du problème de l'origine des amphibolites à partir de leur composition chimique: C.R. Acad. Sc. Paris, t. 267, Serie D, 2084-87.
- Nayudu, Y.R. (1964) Volcanic ash deposits in the Gulf of Alaska and problems of correlation of deep-sea ash deposits:
Marine Geol., 1, 194-212.

- Newton, R.C. (1966) Kyanite-sillimanite equilibrium at 750°C:
Science, 151, 1222-1225.
- Nockolds, S.R. (1954) Average chemical compositions of some igneous
rocks: Geol. Soc. Amer. Bull., 65, 1007-1032.
- Orville, P.M. (1969) A model for metamorphic differentiation origin
of thin-layered amphibolites: Amer. Jour. Sci., 267,
64-86.
- Peck, D.L., Griggs, A.B., Schlicker, H.G., Wells, F.G. and Dole,
H.M. (1964) Geology of the central and northern parts of
the western Cascade Range in Oregon: U.S. Geol. Surv.,
Prof. Paper 449, 56 p.
- Pettijohn, F.J. (1963) Chemical composition of sandstones-excluding
carbonate and volcanic sands: U.S. Geol. Surv., Prof.
Paper 440-S, 21 p.
- _____ (1957) Sedimentary rocks: 2nd ed., Harper and Bros., New
York.
- Poldervaart, A. (1955) Chemistry of the earth's crust: Geol. Soc.
Amer. Spec. Paper, 62, 119-144.
- Prinz, M. (1968) Geochemistry of basalts: Trace elements, in H.H.
Hess and A. Poldervaart, eds., Basalts: The Poldervaart
Treatise on Rocks of Basaltic Composition, 1, New York,
John Wiley and Sons, 265-289.

- Richardson, S.W. (1968) Staurolite stability in a part of the system Fe-Al-Si-O-H: *Jour. Petrol.*, 9, 467-488.
- _____, Gilbert, M.C. and Bell, P.M. (1969) Experimental determination of andalusite-sillimanite equilibria; the aluminum silicate triple point: *Amer. Jour. Sci.*, 267, 259-272.
- Rogers, J.W. (1965) Geochemical significance of the source rocks of some graywackes from western Oregon and Washington: Vice Presidential Address, *Texas Acad. Sci.*
- Ross, M., Papike, J.J. and Weiblen, P.W. (1968) Exsolution in clin amphiboles: *Science*, 159, 1099-1102.
- Schwarcz, H.P. and Clayton, R.N. (1965) Oxygen isotope studies of amphibolites: *Can. Jour. Earth Sci.*, 2, 72-84.
- Shaw, D.M. (1956) Geochemistry of pelitic rocks. Part III: Major elements and general geochemistry: *Geol. Soc. Amer. Bull.*, 67, 919-934.
- _____(1957) Some recommendations regarding metamorphic nomenclature: *Proc. Geol. Assoc. Canada*, 9, 69-81.
- _____(1962) Geology of Chandos township: Ontario Dept. Mines, *Geol. Report No. 11*, 1-28.
- _____(1968) A review of K-Rb fractionation trends by covariance analysis: *Geochim. et Cosmochim. Acta*, 32, 573-601.

- Shaw, D.M. and Kudo, A.M. (1965) A test of discriminant function in the amphibolite problem: *Min. Mag.*, 34, 423-435.
- _____, Reilly, G.A., Muysson, J.R., Pattenden, G.E. and Campbell, F.E. (1967) An estimate of the chemical composition of the Canadian precambrian shield: *Can. Jour. Earth Sci.*, 4, 829-853.
- Shido, F. (1958) Plutonic and metamorphic rocks of the Nakosa and Iritono districts in the central Abukuma plateau: *Jour. Fac. Sci., Univ. Tokyo*, 11, 131-217.
- Silver, L.T. and Lumbers, S.B. (1966) Geochronologic studies in the Bancroft-Madoc area of the Grenville Province, Ontario, Canada: (Abs.) *Geol. Soc. Amer., Spec. Publ. No. 87*, 156.
- Simony, P.S. (1960) Origin of the Apsley paragneiss: Unpublished M. Sc. Thesis, McMaster Univ., Hamilton.
- Snavely, P.D., Jr. and Wagner, H.C. (1964) Geologic sketch of northwestern Oregon: *Geol. Surv. Bull.* 1181-M, 17 p.
- Taylor, S.R. (1964) Abundance of chemical elements in the continental crust: a new table: *Geochim. et Cosmochim. Acta*, 28, 1273-2185.

- Taylor, S.R. and White, A.J.R. (1966) Trace element abundances in andesites: *Bull. Volcanologique*, t. 29, 177-194.
- Thompson, J.B., Jr. (1957) The graphical analysis of mineral assemblages in pelitic schists: *Amer. Min.*, 42, 842-858.
- Turekian, K.K. and Kulp, J.L. (1956) The geochemistry of strontium: *Geochim. et Cosmochim. Acta*, 10, 245-296.
- _____ and Wedepohl, K.H. (1961) Distribution of the elements in some major units of the earth's crust: *Geol. Soc. Amer. Bull.* 72, 175-192.
- Turner, F.J. (1967) Thermodynamic appraisal of steps in progressive metamorphism of siliceous dolomitic limestones: *N. Jb. Miner. Mh.*, 1, 1-22.
- _____ and Verhoogan, J. (1960) *Igneous and metamorphic petrology*: 2nd ed., McGraw Hill, New York.
- Tuttle, O.F. and Bowen, N.L. (1958) Origin of granite in the light of experimental studies in the system $\text{NaAlSi}_3\text{O}_8$ - KAlSi_3O_8 - SiO_2 - H_2O : *Geol. Soc. Amer.*, Mem. 74, 153 p.
- Vernon, R.H. (1962) Co-existing cummingtonite and hornblende in an amphibolite from Duchess, Queensland, Australia: *Amer. Min.*, 47, 360-370.

- Vinogradov, A.P. (1956) Regularity of distribution of chemical elements in the Earth's crust: *Geochemistry*, 1, 1-43.
- _____ (1962) Average contents of chemical elements in the principal types of igneous rocks of the earth's crust: *Geochemistry*, 7, 641-664.
- Walker, K.R., Joplin, G.A., Lovering, J.F. and Green, R. (1960) Metamorphic and metasomatic convergence of basic igneous rocks and lime-magnesia sediments of the Precambrian of northwestern Queensland: *Jour. Geol. Soc. Aust.*, 6, 149-178.
- Wanless, R.K., Stevens, R.D., Lachance, G.R. and Edmonds, C.M. (1967) Age determinations and geological studies K-Ar Isotopic Ages, Rpt. 7: *Geol. Surv. Can.*, Paper 66-17, 120 p.
- Watters, W.A. (1959) An association of hornblende and cummingtonite from Ringaringa, Stewart Island, New Zealand: *N. Z. Jour. Geol. Geophys.* 2, 248-256.
- Weber, J.N. and Middleton, G.V. (1961) Geochemistry of the turbidites of the Normanskill and Charny formations - I and II: *Geochim. et Cosmochim. Acta*, 22, 200-288.

- Weber, J. N. and Smith, F. G. (1961) Rapid determination of calcite-dolomite ratios in sedimentary rocks: Jour. Sed. Pet., 31, 130-131.
- Whetten, J. T. (1966) Sediments from the Lower Columbia River and origin of graywacke: Science, 152, 1057-1058.
- Wilcox, R. E. and Poldervaart, A. (1958) Metadolerite dike swarm in Bakersville-Roan mountain area, North Carolina: Geol. Soc. Amer. Bull., 69, 1323-1368.
- Winkler, H. G. F. (1967) Petrogenesis of metamorphic rocks: New York, Springer-Verlag New York Inc., 237 p.
- Yoder, H. S. Jr. and Tilley, C. E. (1962) Origin of basalt magmas: An experimental study of natural and synthetic rock systems: Jour. Petrol., 3, 342-532.
- Zen, E. (1969) The stability relations of the polymorphs of aluminum silicate: a survey and some comments: Amer. Jour. Sci., 267, 297-309.

APPENDIX

I. ANALYTICAL METHODS

Major Element Analysis

The majority (30) of the major element analyses were performed by Mr. Kenneth Ramlal using the analytical facilities of the Geology Department at the University of Manitoba. A summary of his methods is given below. Four additional amphibolite analyses were contributed by Dr. Peter C. van de Kamp then of the University of Bristol and one amphibolite analysis by Mr. J.R. Muysson of McMaster University was taken from an unpublished master's thesis (Kudo, 1962). The reader is referred to van de Kamp and Kudo (1962) for details of their respective analytical procedures.

<u>Element</u>	<u>Method</u>
Si	X-ray fluorescence spectrometry. Weighed sample plus $\text{Li}_2\text{B}_4\text{O}_7$ and La_2O_3 heated in graphite crucible at 1050°C for one half hour. Resulting glass bead ground to -200 mesh with HBO_3 (Total weight 2.1000 gms.) and then compressed to pellet form at 50,000 p. s. i. Elements simultaneously analysed on multi-channel ARL X-ray spectrometer.
Al	
Fe(Total)	
Mg	
Ca	
K	
Ti	
Mn	
Zr	

Na₂O, Atomic absorption spectrophotometry. Sample dissolved
 Cu, Ni, Co, with HF, H₂SO₄, HNO₃ in platinum crucibles. Solution
 Cr, Pb, Zn, analysed on Perkin Elmer 303 A. A. S.
 and trace
 metals

P₂O₅ Colorimetry using solution as for Na₂O above. The
 absorption at 430 mμ of molybdivanado-phosphoric acid
 complex on a Coleman spectrophotometer.

FeO Rock decomposed with HF and 1:4 H₂SO₄ solution and
 titrated with K₂Cr₂O₇ using sodium diphenylamine sul-
 fonate as indicator.

H₂O⁻ Determined by heating the sample to constant weight at
 110°C.

H₂O(Total) Determined by a modification of the Penfield method using
 Pbo as a flux for minerals which decompose only at high
 temperatures.

H₂O⁺ H₂O(Total) - H₂O⁻.

S Determined by heating samples in an induction furnace
 with O₂ flowing through the combustion chamber. SO₂
 evolved is then titrated. Leco induction furnace and
 automatic titrator are used.

Cl Sample decomposed by HCl and heat. The CO₂ evolved is
 passed through a drying train and is collected on Ascarite.

An estimation of precision and accuracy of these methods follows:

Constituent	Concentration(%)	Instrument	Accuracy of
		Precision	Replicates
		σ	Std. Dev.
			σ
SiO ₂	60.0	0.12	0.20
Al ₂ O ₃	9.0	0.05	0.13
Fe ₂ O ₃ (Total)	10.0	0.017	0.03
MgO	4.0	0.04	0.10
CaO	10.0	0.02	0.07
K ₂ O	2.6	0.01	0.01
MnO	0.41	0.01	0.01
TiO ₂	0.48	0.02	0.02
Na ₂ O	4.20	0.01	0.05
H ₂ O (Total)			
CO ₂	1.15	0.05	0.12
P ₂ O ₅	0.20	0.01	0.01

Trace Element Analysis

Optical spectrographic techniques of analysis were used to determine trace element concentrations in the bulk of the rocks studied. Mrs. F. E. Campbell, Mrs. D. Jordan and Mr. P. Fletcher of McMaster University performed the analyses by the procedure outlined below.

A buffer mixture utilizing a palladium internal standard was prepared by mixing 3.0% PdCl_2 and 97.0% graphite by weight. This mixture was diluted by a factor of 10 with graphite to yield a mixture of 0.3% PdCl_2 and 99.7% graphite. 100 mg. of this mixture combined with 500 mg. of graphite and 600 mg. Cs_2CO_3 yielded a final buffer mixture containing 0.025% PdCl_2 , 49.975% graphite and 50.000% Cs_2CO_3 . The weighing of dry Cs_2CO_3 was performed as quickly as possible to minimize problems of deliquescence. Samples to be analysed were mixed by grinding under acetone in 1:1 proportions with the final buffer and loaded into six, cratered anode electrodes. Approximately 200 mg. of sample plus buffer is adequate for the filling of these electrodes. Prior to arcing, the filled electrodes were dried in a sandbath in excess of one hour and heated with a direct bunsen flame for one minute immediately before ignition.

Instrumental and procedural data are as follows:

Spectrograph:	Jarrell-Ash 21 foot grating, Wadsworth mount, first order dispersion of 5.2 Angstroms per mm.
Condensing Optics:	25 cm. focal length cylindrical lens on horizontal axis at the slit, 6.7 cm. focal length cylindrical lens on vertical axis at 16.1 cm. from slit, 5 mm. diaphragm at 27.5 cm. from slit, 72.5 cm. arc-slit distance.
Intensity Control:	7 step rotating sector at slit; log. intensity ratio 0.2; two wire mesh screens used for the range 2400-4800 \AA ; yellow filter in sector for the range 5700-8300 \AA , no wire mesh screens.

- Slit: 30 microns in length, 8 mm. in width.
- Arc Gap: 4 mm.
- Electrode Stand: ARL arc-spark stand, water cooled jaws.
- Jet: Stallwood jet used with a mixture of 80% argon and 20% oxygen for the range 2400-4800 \AA , or air stream for the range 5700-8300 \AA at 18 SC HF.
- Exposure: To completion, between 60 and 120 seconds.
- Electrodes: Anode-Ultra Carbon Corp. performed 1/8" diameter rod, plain crater 1/16" x 3/8"
Cathode-National Carbon Co. special graphite, 1/8" diameter rod.
- Photographic Plates: Eastman Kodak SA-1, range (2200-3500 \AA)
" " IIIF, " (3500-4800 \AA)
" " 1-N, " (5700-8300 \AA)
- Voltage and Amperage: 225 volts DC open circuit, 9.5 amps.
- Development: 3 minutes in Kodak D-19 developer at 20°C, one half minute wash in distilled water, 5 minutes in Amfix solution, at least 10 minutes wash in cold running water, rinse in distilled water and dry.
- Densitometry: ARL photodensitometer, three steps measured, background correction applied.

Standard and Analysis Lines

Standard Line	Analysis Line
Pd 3242.7	Ga 2943.6
	Be 3130.4
	V 3183.9
	Cu 3274.0
	Y 3327.8
	Zr 3391.9
	Ni 3414.8
Pd 3609.5	Sc 3911.8
	Mn 4034.4
	Mn 4041.3
	Cr 4254.3
Cs 4555.4	Ba 4554.0
	Sr 4607.3
Cs 6723.2	Li 6103.6
	Ba 6141.7
	Li 6707.8
Cs 7609.0	Rb 7800.2

REGIONAL STRUCTURE AND LITHOSTRATIGRAPHY BANCROFT-MADOC AREA



Modified after Lumbers (1964)

EXPLANATION

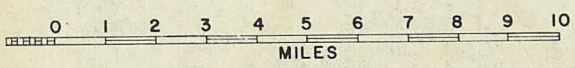
- | | | | |
|------------------------|------------------------------|---------------------------|-----------------------|
| Paleozoic Rocks | | Plutonic Rocks | |
| □ | Middle Ordovician Limestones | □ | Basic Dikes and Sills |
| □ | Potassic Granite Group | □ | Sodic Granite Group |
| □ | Syenitic Group | □ | Diorite-Gabbro Group |
| □ | Nepheline Syenite Group | Supracrustal Rocks | |
| Hermon Group | | Mayo Group | |
| ■ | Burnt Lake Formation | □ | Lasswade Marble |
| ■ | Turriff Metavolcanics | □ | Apsley Formation |
| ■ | Vansickle Formation | □ | Dungannon Formation |
| ■ | Oak Lake Formation | | |
| ■ | Tudor Metavolcanics | | |

SYMBOLS

- | | |
|-------|---|
| ▲ | Top direction in metavolcanics |
| ~ | Fault or lineament |
| — | Geologic boundary defined |
| - - - | Geologic boundary inferred |
| □ | Unmapped area or absence of exposure |
| ↗ | Anticlinical fold, plunge in direction of arrow |
| ↘ | Synclinal fold, plunge in direction of arrow |
| ● | Town, population over 1,000 |
| ○ | Village, population under 1,000 |
| — | Line of cross section |
| □ | Map area |



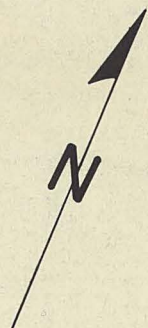
LOCATION MAP



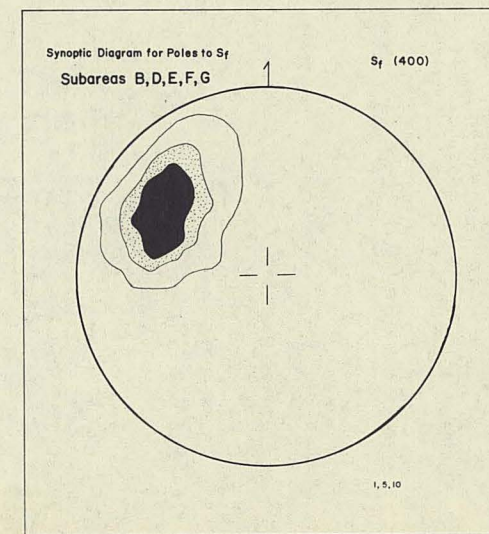
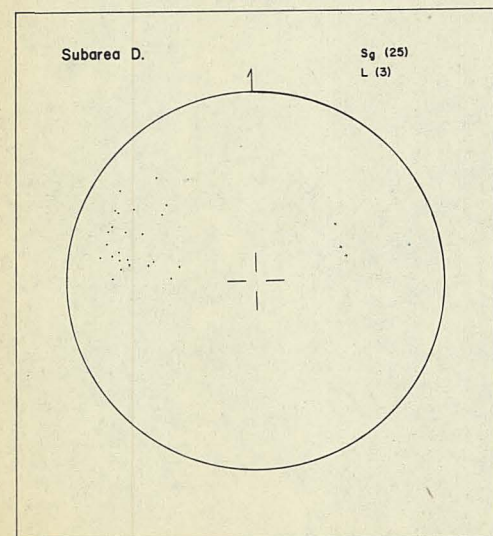
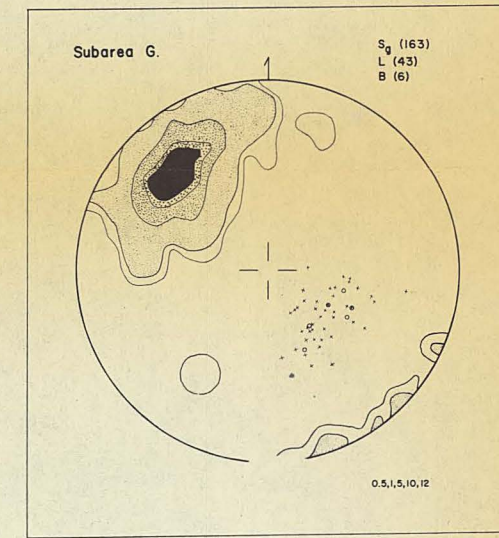
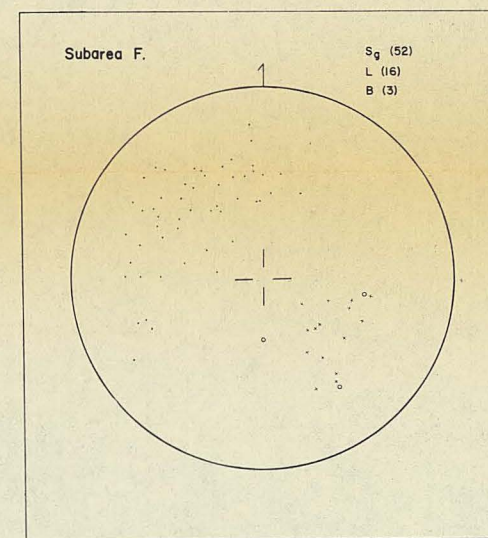
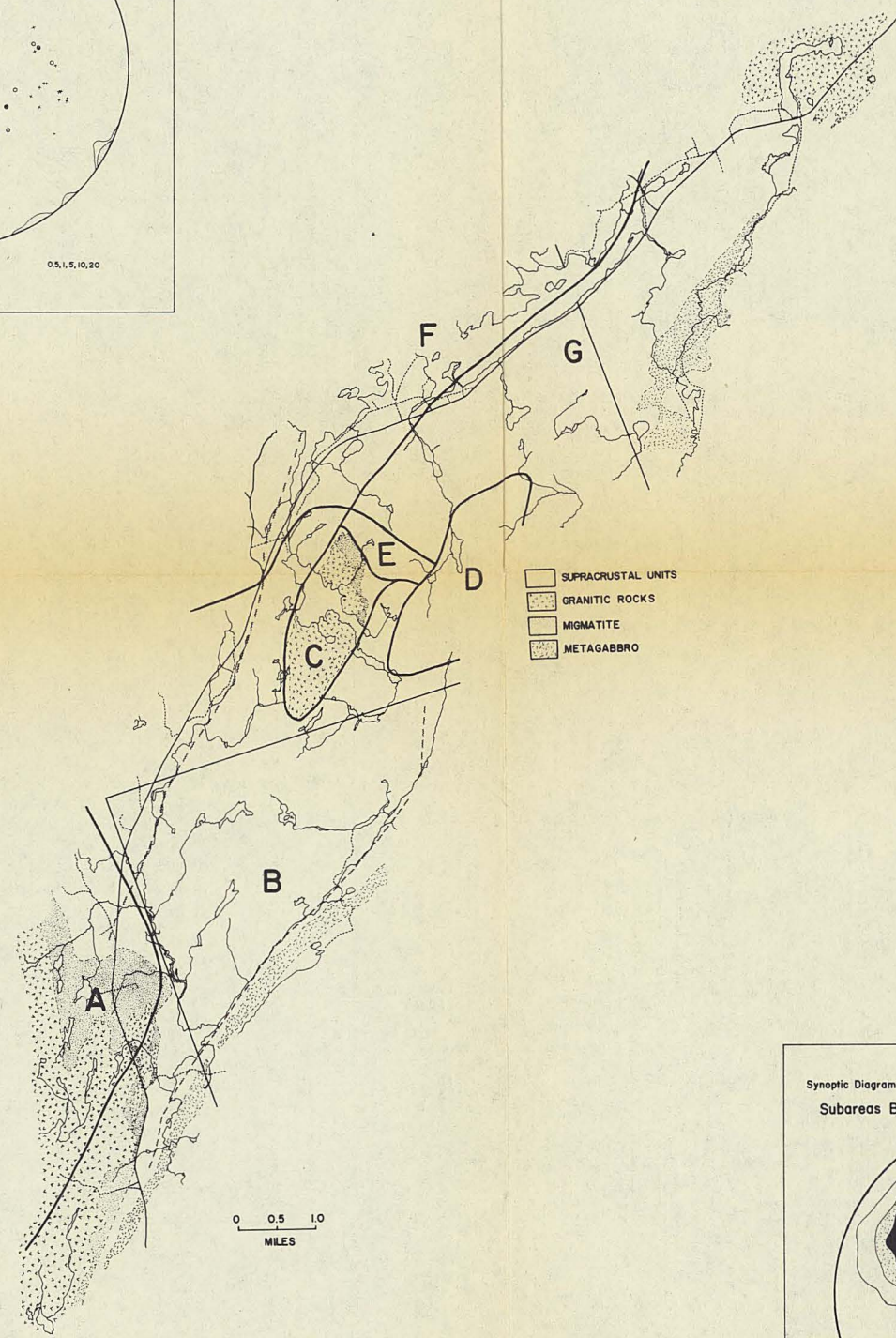
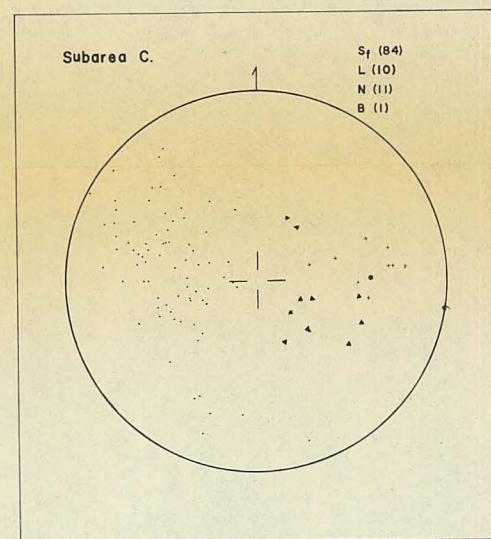
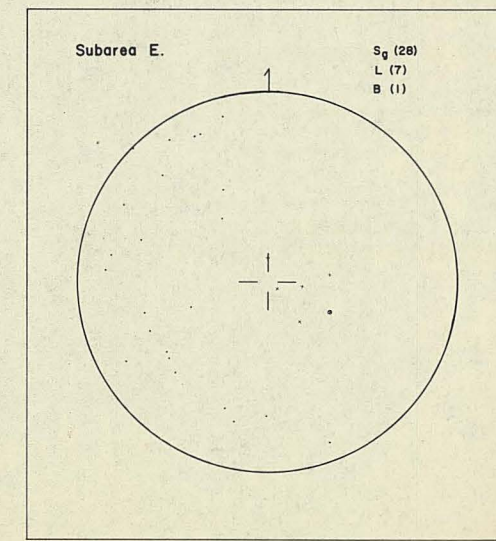
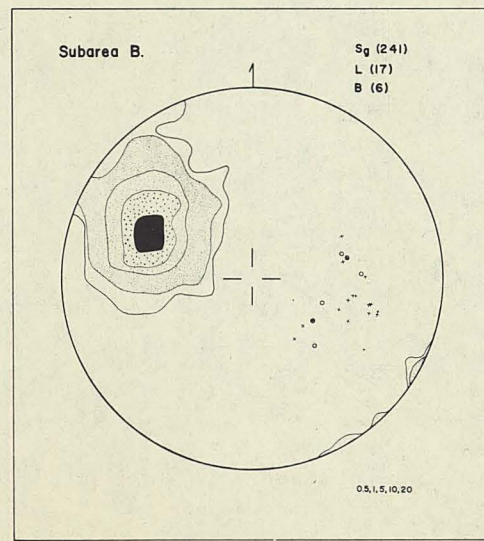
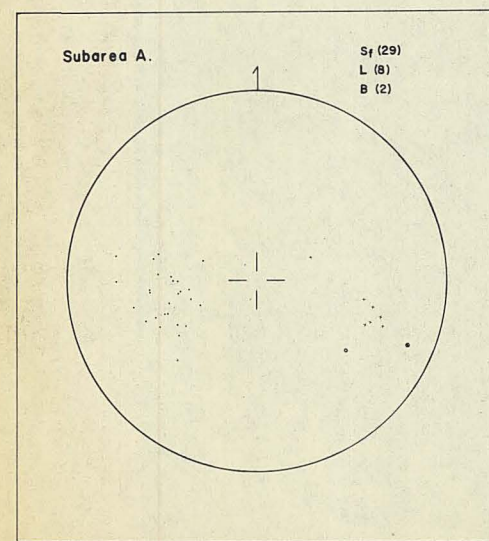
1 Inch = 2 Miles

Township Index Map

CARDIFF	FARADAY	DUNGANNON	MAYO	ASHBY
CHANDOS	WOLLASTON	LIMERICK	CASHEL	EFFINGHAM
METHUEN	LAKE	TUDOR	GRIMSTHORPE	ANGLESEA



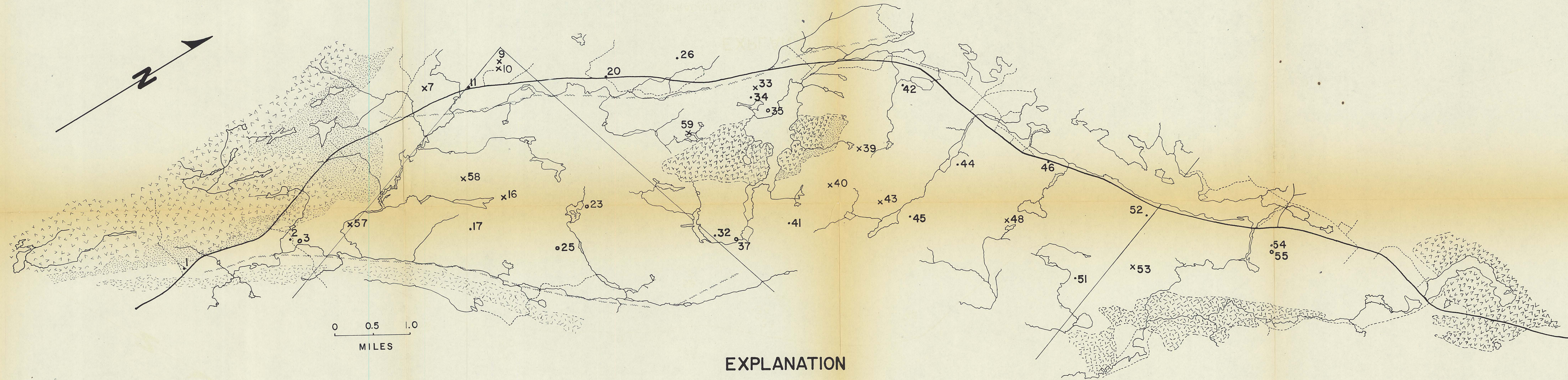
PETROFABRIC DIAGRAMS



EXPLANATION OF MACROSCOPIC FABRIC DIAGRAMS SUBAREAS A-G

- ↑ NORTH ARROW
- S_g (163) NUMBER OF S_g POLES PLOTTED
- S_f (84) NUMBER OF S_f POLES PLOTTED
- L (43) NUMBER OF LINEATIONS PLOTTED
- B (6) NUMBER OF FOLD AXES PLOTTED
- 0.5, 1, 5, 10, 12 CONTOUR LINES (% PER 1% AREA)

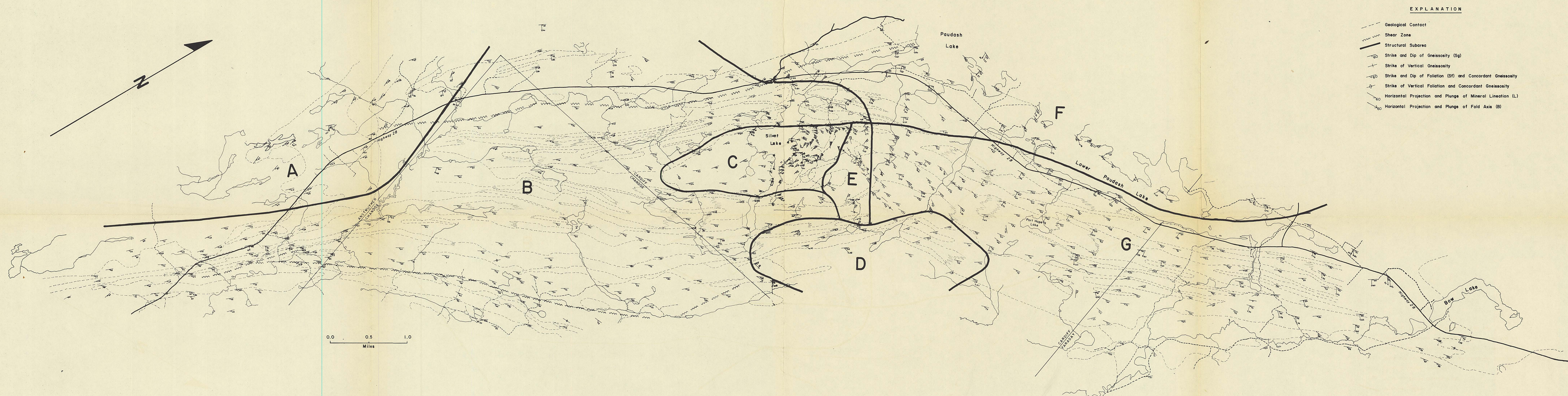
NOTE: POLES TO S PLANES ARE CONTOURED WHERE MORE THAN 100 POINTS ARE PLOTTED; LINEAR FABRIC ELEMENTS ARE NOT CONTOURED; •• S PLANE POLE
-- LINEATION, •• FOLD AXIS



EXPLANATION

- | | | | |
|---|--------------------|---|----------------------------|
|  | SUPRACRUSTAL UNITS |  | AMPHIBOLITE |
|  | GRANITIC ROCKS |  | QUARTZO-FELDSPATHIC GNEISS |
|  | MIGMATITE |  | LEPTITE |
|  | METAGABBRO | | |

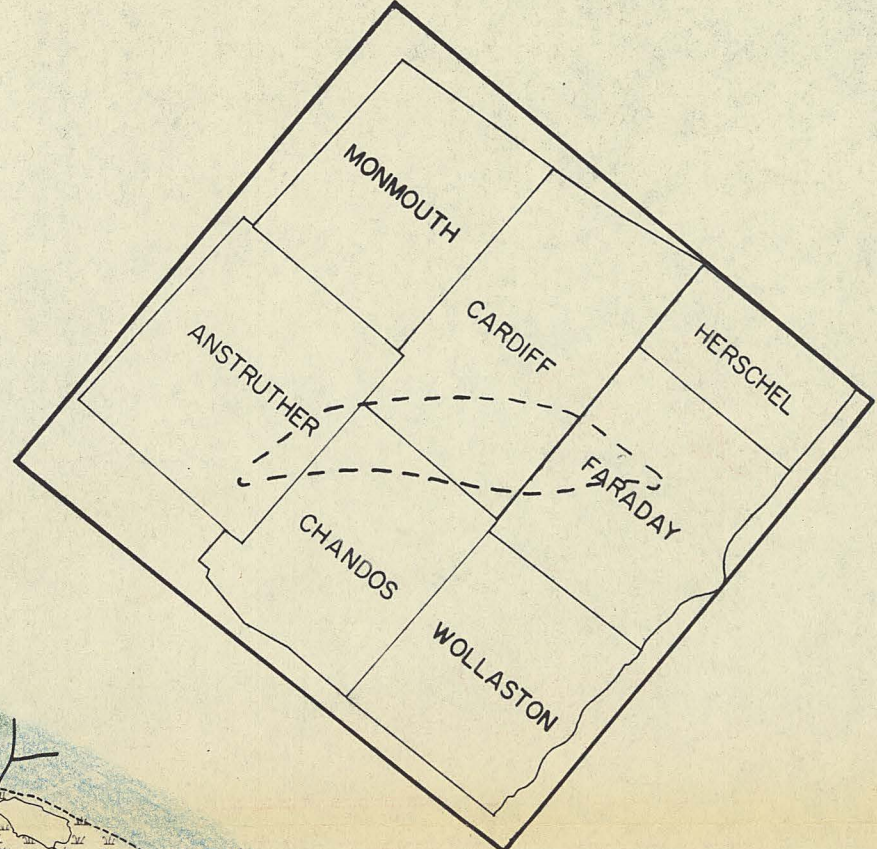
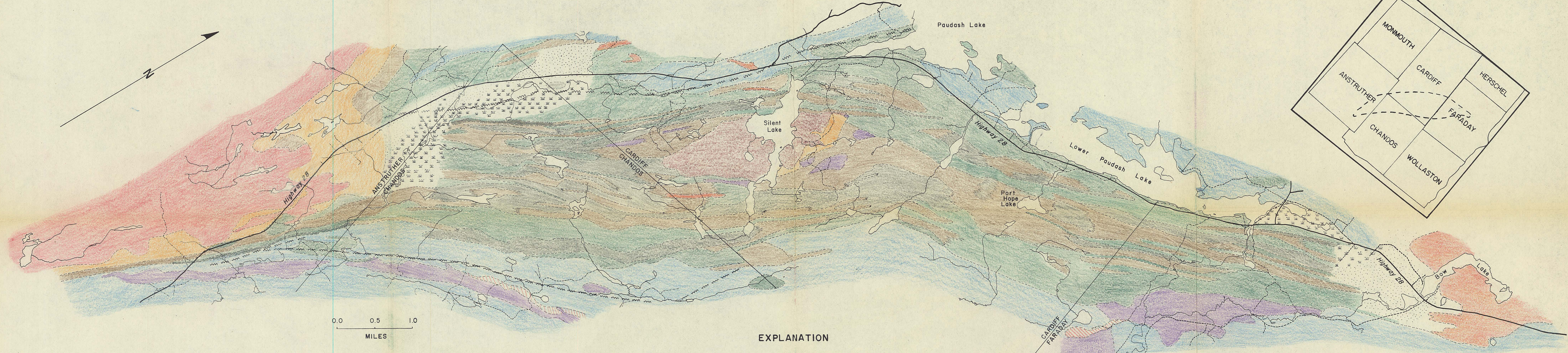
STRUCTURAL COMPILATION MAP



EXPLANATION

- Geological Contact
- Shear Zone
- Structural Subarea
- Strike and Dip of Gneissosity (Sg)
- Strike of Vertical Gneissosity
- Strike and Dip of Foliation (Sf) and Concordant Gneissosity
- Strike of Vertical Foliation and Concordant Gneissosity
- Horizontal Projection and Plunge of Mineral Lineation (L)
- Horizontal Projection and Plunge of Fold Axis (B)

LITHOLOGIC MAP



- SYMBOLS**
- Geological Contact
 - - - Shear Zone
 - ≡≡≡ Swamp
 - ⋯ Sand Plain

0.0 0.5 1.0
MILES

EXPLANATION

- INTRUSIVE ROCKS**
- Anstruther-Burleigh Granite and Granite Gneiss (Granite and Biotite Granite with Abundant Gneissic Inclusions)
 - Silent Lake Granite (Granite, Biotite Granite, Quartz Monzonite with Quartz-Sillimanite-Plagioclase Nodules and Veins)
 - Bow Lake Granite and Minor Pegmatite Bodies (Granite and Pegmatite)
 - Migmatite (Maximum Extent of Granitic Material in Country Rocks)
 - Tallan Lake Sill and Minor Metagabbro Bodies (Acidic Differentiates Hachured)

- SUPRACRUSTAL ROCKS**
- Amphibolite (Includes Normal, Biotite, Cummingtonite, and Clinopyroxene Varieties)
 - Quartzo-Feldspathic Gneiss (Includes Non-Aluminous, Aluminous, Hornblende and Clinopyroxene Varieties)
 - Leptite
 - Carbonate Metasediments (Includes Marbles, Feather Amphibolites and Calc-Silicate Bands)

Jim